Assessing the impact of extreme rainfall on land cover changes in New Caledonia using remote sensing

Julia Eliesabeth Levermann
May, 2013

Assessing the impact of extreme rainfall on land cover changes in New Caledonia using remote sensing

by

Julia Eliesabeth Levermann

Thesis submitted to the University of Southampton in partial fulfilment of the requirements for the degree of Master of Science in Geo-information Science and Earth Observation with a specialisation in environmental modelling and management.

Project supervisors

Dr. Emma Tompkins
Dr. Gareth Roberts

UNIVERSITY OF Southampton

Disclaimer

This document describes work undertaken as part of a programme of study at the University of Southampton, United Kingdom. All views and opinions expressed therein remain the sole responsibility of the author, and do not necessarily represent those of the institute.

Abstract

New Caledonia, a French overseas territory located in the southwest Pacific Ocean, faces major environmental concerns because of soil erosion. The island provides favourable conditions for erosion with its steep slopes, extreme rainfall events and vulnerable soils. The process is accelerated by anthropogenic-induced land cover changes, which cause serious degradations of the fragile environment. Susceptibility to erosion is particularly strong during the beginning of the wet season due to the frequent occurrence of tropical depressions and cyclones. These events generate intense precipitation, which often leads to flooding and the disruption of vegetation cover. Areas affected by resulting land cover changes, such as the reduction of vegetation cover, are especially prone to erosion. The main objective of this research was to assess changes in land cover after an extreme rainfall event using high resolution satellite imagery, and to model potential soil erodibility to better understand resulting impacts on the environment.

In this study, land cover situations of October 2011 and January 2012, framing a tropical depression, were mapped and temporal changes over this period were evaluated. Additionally, potential soil erodibility was modelled, and the results compared to the observed changes in land cover.

Land cover was successfully mapped and the overall accuracy of the image classification resulted in 92.25 % and 93.06 % for 2011 and 2012, respectively. All land cover classes were affected by change, while sparse vegetation experienced a reduction by 0.38 km², bare soil increased by 0.39 km². Areas where soils of high silt contents coincide with sparse vegetation cover and steep slopes are highly erodible.

Optical remote sensing is helpful to extract information on land cover, it poses however an inadequate approach for detecting changes in land cover across seasons due to the influence of external factors. Soil erodibility can successfully be modelled and provides preliminary understanding of which areas might potentially be affected by erosion. Due to uncertainties concerning the data sources, it is difficult to estimate how reliable these results are. Consequently, no final statement can be made whether soil erodibility contributed to land cover changes.

Key words: Land cover, change detection, remote sensing, soil erodibility, New Caledonia

Acknowledgements

First of all, I would like to thank my supervisors Dr. Emma Tompkins and Dr. Gareth Roberts for their valuable advice and support. During my time in New Caledonia, Emma and Gareth always found time for Skype meetings, which was not easy with a time difference of 11 hours. Back in Southampton, their doors were always open for me.

I would also like to thank the Institut de Recherche pour le Développement, Nouméa in New Caledonia for the opportunity of doing an internship with them. This research would not have been possible without the support of Marc Despinoy, Morgan Mangeas and Florian de Boissieu. Merci!

Thank you to all my ITC and GEM friends for the great moments we shared in Enschede, NL and Southampton, UK over the last 22 month.

Finally, I would like to thank my parents and my brothers for their encouragement and support.

Table of Contents

List of figures

List of tables

Abbreviations and acronyms

ANN	Artificial Neutral Network
CART	Classification and Regression Tree
CNRT	Centre National de Recherche Technologique
CVA	Change Vector Analysis
DT	Decision Tree
DTSI	Direction des Technologies et Services de l’Information
ETM+	Enhanced Thematic Mapper Plus
GIS	Geographic Information System
GPS	Global Positioning System
IRD	Institut de Recherche pour le Développement, Research Institute for Development
ISODATA	Iterative Self-Organizing Data Analysis Technique
MLC	Maximum Likelihood Classifier
MODIS	Moderate-resolution Imaging Spectroradiometer
NDVI	Normalised Difference Vegetation Index
OEIL	Observatoire de l’Environnement Nouvelle-Calédonie, Environmental Observatory of New Caledonia
PCA	Principal Component Analysis
UNESCO	United Nations Educational, Scientific and Cultural Organization
SMA	Spectral Mixture Analysis
SPOT5	Système pour l’Observation de la Terre
SPREP	Secretariat of the Pacific Regional Environment Programme
SVT	Support Vector Machine
UK	United Kingdom
USLE	Universal Soil Loss Equation
RUSLE	Revised Universal Soil Loss Equation
VID	Vegetation Index Differencing

1 Introduction

1.1 Background

New Caledonia is a French overseas territory located in the southwest Pacific Ocean. It has an exceptionally rich terrestrial and marine ecosystem, with one of the highest rates of endemic[1] species in the world. The archipelago is thus considered as a global biodiversity hotspot[2] (SPREP, 2012). The main island, Grande Terre, is furthermore surrounded by the second longest double-barrier coral reef in the world, which has been listed on the World Heritage List of UNESCO[3] in 2008 (David et al., 2010; Ministère des Outre-Mer, 2012). The protection of this fragile environment is consequently extremely important.

Soil erosion is a major problem on the island, causing significant environmental degradations. On one hand, conditions on the island make it susceptible for erosion due to natural pressures, such as extreme rainfall events during the wet season, vulnerable soils and steep slopes (Université de la Nouvelle-Calédonie, 2010). On the other hand, anthropogenic pressures, such as forest fires, exploitation of natural resources, unsustainable agricultural practices and urbanisation, accelerate the erosion process (Dumas et al., 2010; Rouet et al., 2009).

The archipelago holds about 25% of the global nickel ore reserves, thus mining has been the major driver of the island's economy for over a century. Nickel ore is being extracted by surface mining, which requires the removal of vegetation, and therefore makes an area more prone to erosion. In their search for copper and nickel, which has been mined since 1872, prospectors burned away vegetation to gain better access to the countryside. This has consequently resulted in a drastic modification of the original landscape. The native flora and fauna were damaged in such a way that the impacts are still evident today (Chabanet et al., 2010; David et al., 2010; SPREP, 2012; United Nations, 2003).

---

[1] Native or restricted to a certain place (Oxford University Press, 2012)

[2] Biodiversity hotspot are areas "that (a) feature exceptional concentrations of species with high levels of endism, and (b) face exceptional threats of destruction" (Meyers, 1990: 243).

[3] The United Nations Organization for Education, Science and Culture

Today, “over 40 watersheds throughout New Caledonia and, indirectly, the downstream estuaries and reefs, are affected by various levels of mining activities” (David et al., 2010: 328). Most of the damage observed, results from old and abandoned mines, due to the mining techniques, which were applied during the time of the “nickel boom” until the 1970s, and the lack of legislation protecting the environment until the 1980s. During these times, mining companies usually had poor management concerning surface runoff, and the storage of mining tailings was quite common (Tranap, 2004; Université de la Nouvelle-Calédonie, 2012a). Therefore, water management is not only a major challenge for new mining projects but also for rehabilitation sites, as well as exploited and abandoned mines (Université de la Nouvelle-Calédonie, 2012a).

Rainfall is considered as the driving force of soil erosion in tropical climates. Rainfall rates often follow a seasonal pattern (Dumas et al., 2010; Morgan, 2005). During the early stage of the wet season, November and December, the erosive force of rainfall is particularly strong due to the occurrence of tropical depressions and cyclones. In addition, the vegetation cover is not yet sufficient enough to protect the soil (Vrieling, 2006). “In an era of increasing tropical storms, the phenomenon of erosion is the foremost cause of coastal, fringe reef and lagoon deterioration, particularly on the east coast” of New Caledonia (SPREP, 2012: 112).

Vegetation cover protects the soil from erosion and surface runoff. Once this cover is removed, for example due to extreme rainfall or because of the strip mining process, the lateritic soils are extremely vulnerable (Morgan, 2005; Savy, 2011). Intense precipitation strips particles from sensitive soils, leading to increased soil erosion and transportation of excavated waste materials to the catchment (Rouet et al., 2009). Soil removed by rainfall-runoff can result in major sediment inputs in the watersheds, with immediate and recurrent impacts on the environment and the local population. When sediments are carried to the rivers and coastal zones, they cause serious degradation of the littoral system, e.g. damages of coastal flora and fauna. Furthermore, they contribute to increased risk of flooding due to rising of waterbeds, resulting in damages of agricultural areas and marine habitats as well as hyper-sedimentation. Hyper-sedimentation[4], seen in Figure 1, may lead to coral bleaching due to increased water turbidity (David et al., 2010; Dumas et al., 2010; Rouet, 2009).

[4] Severe water turbidity caused by suspended sediments

Figure 1: Bay of Poro, a mining village on the east coast, after intense rainfall on April 16th, 2011.

Many New Caledonians, mostly the indigenous habitants of the island, the Kanak, still live a traditional way of life, which is largely based on subsistence agriculture and fishing. Accordingly, “any threat to the marine and terrestrial ecosystems could have grave and widespread consequences” (Ali, 2006: 373). It is essential to address the problem of erosion immediately to minimize and prevent the consequences on the population and environment (Université de la Nouvelle-Calédonie, 2012a).

1.2 Problem statement

In a context, where not only human but also natural drivers play a role in contributing to erosion, it is necessary to characterize the pressures on watersheds in mining areas to better assess the environmental impacts on coastal zones. In order for mitigation actions to become effective in minimising erosion impacts on the environment, the key components of the erosion process have to be determined and areas affected by erosion and sedimentation need to be identified (Rouet et al., 2009; Université de la Nouvelle-Calédonie, 2012b).

Figure 2presents the causal framework of the problem. As mentioned, the erosive force of rainfall is particularly strong towards the beginning of the wet season due to the combination of frequent occurrences of extreme rainfall events, dry soils and sparse vegetation cover (Morgan, 2005). According to Terry et al. (2008), tropical depressions and cyclones cause intense precipitation, which often result in flooding and the disruption of vegetation and the landscape. Areas affected by land cover changes, such as the reduction of vegetation cover, are especially prone to erosion (Morgan, 2005). It is consequently necessary to identify areas affected by land cover change after extreme rainfall.

New Caledonia was affected by an exceptional rainfall event over Christmas 2011. The tropical depression, which affected the entire island, had been particularly intense on the east coast. In Houaïlou, 528.5 mm of rainfall was measured in approximately 26 hours, this is about half of the annual average rainfall Southampton, UK receives (Met Office, 2013). Rainfall has been measured since 1952, but this event has been exceptional as the equivalent of more than a quarter of the average annual amount of precipitation (1914.2 mm) fell within 24 hours. The amount of rainfall is furthermore equivalent to more than three times the amount of rain that usually falls in the month of December (Méteo France, 2011).

The present study aims at contribute to the project "Fonctionnement des petits bassins versants miniers"[5], implemented by the “Centre National de Recherche Technologique”[6] (CNRT) in New Caleodnia. Spatial information about land cover and its changes after the extreme rainfall event of December 2011 are obtained by applying an image classification and change detection using remotely sensed data. Furthermore, spatial information on soil erodibility in a small watershed is provided by applying an erosion model. This shall contribute to a better understanding of the impact of rainfall on land cover changes and its consequences on the environment.

[5] Functioning of small ‘mining’ watersheds
[6] National centre for technological research

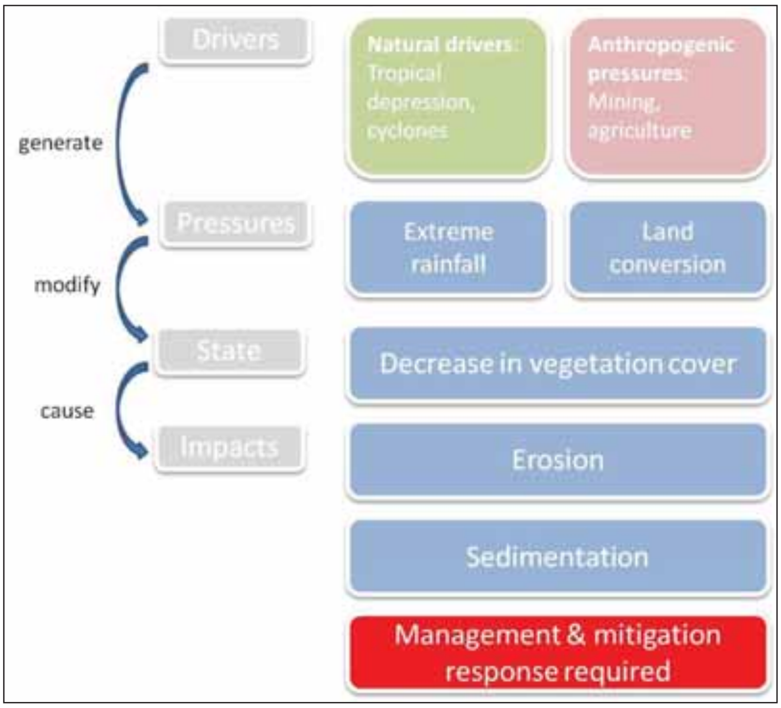

Figure 2: Casual framework of the problem.

1.3 Project: "Fonctionnement des petits bassins versants miniers"

This study was conducted as part of an internship with the "Institut de recherche pour le développement"[7] (IRD) in Nouméa, New Caledonia, under the framework of the project "Fonctionnement des petits bassins versants miniers". The project, which was implemented in 2010, aims to improve water management in mining areas by improving the understanding of functions and mechanism of small watersheds in New Caledonia, and quantifying the upstream flows for minimizing the impact of sediment transport in the downstream areas (CNRT, 2009).

[7] Research institute for development

1.4 Objectives and research questions

1.4.1 General objective

The overall aim of this research is to assess changes in land cover after an extreme rainfall event, and to model potential soil erodibility in a small watershed, which contains mining activities, in Poro, New Caledonia, to better understand resulting impacts on the environment.

1.4.2 Specific objectives

1. To map the land cover situations of October 20th 2011 and January 18th 2012 for the study area based on high-resolution satellite imagery.

2. To quantify land cover changes over the period of October 2011 to January 2012, framing a strong rainfall event in December 2011.

3. To model potential soil erodibility in a small watershed in the study area.

4. To compare areas with high soil erodibility to areas of land cover change.

1.4.3 Research questions

Objective 1

- Can land cover be assessed based on the available satellite imagery?
- How are the different land cover classes distributed over the study area?

Objective 2

- Can land cover changes be assessed based on multi-temporal satellite imagery?
- Did land cover changes occur in Poro between October 2011 and January 2012?
- If so, where did these changes occur and to what extent?

Objective 3

- Is it possible to model soil erodibility in a small watershed in Poro?
- Which areas are affected by soil erodibility?

Objective 4

- Did soil erodibility contribute to land cover changes?

The research matrix, shown in Table 1, highlights the connections between the specific research objectives and the research questions. Additionally, it indicates what methods will be used to complete the objective and answers the research questions, along with the source of the data that will be used.

Objectives	Research questions	Methods	Data source
To map the land cover situations of October 2011 and January 2012 in the study area based on multi-temporal high-resolution satellite imagery.	➢ Can land cover be assessed based on the available satellite imagery? ➢ How are the different land cover classes distributed over the study area?	Supervised image classification	High resolution satellite imagery (RapidEye, 5m) October 2011 January 2012
To quantify land cover changes over the period of October 2011 to January 2012, framing a strong rainfall event in December 2011.	➢ Can land cover changes be assessed based on multi-temporal satellite imagery? ➢ Did land cover changes occur in Poro between October 2011 and January 2012? ➢ If so, where did these changes occur and to what extent?	Post-classification change detection	Image classifications of October 2011 and January 2012
To model potential soil erodibility in a watershed in the study area.	➢ Is it possible to model soil erodibility in a small watershed in Poro? ➢ Which areas are affected by soil erodibility?	Revised Universal Soil Loss Equation	- Land cover classification of 2011 -Digital elevation model (DEM) -Soil maps
To compare areas with high soil erodibility to areas of land cover change.	➢ Did soil erodibility contribute to changes in land cover?	Visual assessment	Results of the change detection process and the erodibility modelling

Table 1: Research matrix

2 Literature review

2.1 Remote sensing

“Remote sensing (RS) is the science and art of obtaining information about an object, area or phenomenon through the analysis of data acquired by a device that is not in contact with the object, area, or phenomenon under investigation” (Lillesand and Kiefer, 1994: 1). To obtain this information, sensors[8], mounted on airplanes or satellites and, collect image data by using electromagnetic radiation, which is emitted and / or reflected by the target on the ground. Sensors can be divided into two groups: active and passive systems. Active remote sensing systems, such as radar, send out radio waves and record the returning wavelength, while passive remote sensing records natural radiation. The sun is the most common source of radiation for passive RS (Liew, 2001; Vrieling, 2006).

Passive remote sensing can be distinguished into optical, thermal and microwave remote sensing. This study uses optical remote sensing, which operates in the visible, near infrared, middle infrared and short wave infrared range of the electromagnetic spectrum. Materials differ in their reflection and absorption, consequently, targets, such as different land covers, can be distinguished based on their spectral properties.

Optical remote sensing sensors can broadly be classified into panchromatic, multispectral and hyperspectral imaging systems. Panchromatic sensors, such as IKONOS PAN, only record black and white images, while multispectral imagine systems capture data across the electromagnetic spectrum. Earth observation satellites, such as SPOT HRV-XS and Landsat TM, are multispectral platforms[9] and are often used to map land cover. Hyperspectral satellites, such as NASA’s Hyperion record several hundred spectral bands and consequently collects very detailed spectral information (Liew, 2001).

Advantages of remote sensing are the rapid data collection over large or inaccessible areas. It furthermore replaces time consuming and expensive field data collection. Remote sensing represents one of the most powerful tools to map and extract key information on land cover. Its consistent and regular data acquisition allows for the

---

[8] Device which records satellite image

[9] Satellite or airplane which carries the sensor

extraction, analysis and monitoring of changes in a timely and cost effective manner (Cihlar, 2000; Lu and Weng, 2007; Mas, 1999).

2.2 Land cover classification techniques

The term land cover describes the (bio) physical coverage, both natural and artificial, of the Earth's surface. However it does not consider information about it how it is being used by humans (Food and Agricultural Organisation, 2000). There is a growing need for information on land cover, as changes in land cover affect ecosystem services, contribute to climate change, and are regarded as the primary source of soil degradation. For a better understanding of environmental changes, successful natural resource management and policy development, the detection and analysis of such changes is required (Dash et al., 2007; Lambin et al., 2001; Srivastava et al., 2012).

The most common approach to map land cover is digital image classification, which is "the process used to produce thematic maps from imagery" (Schowengerdt, 2006: 387). Based on their spectral properties pixels in the images are assigned to different land cover categories according to their values (Lunetta, 1998). As mentioned, materials can be distinguished based on their spectral signature as they reflect and absorb differently. Depending on the aim of the study and the available information, either a supervised or unsupervised classification approach is selected. When selecting an unsupervised approach, the image is mechanically classified based on spectral properties. Supervised classification on the other hand requires prior knowledge and more user interaction. Once information about land cover classes exists, the supervised classification approach should be the method of choice. But this information may not always be available, especially over large areas. A hybrid approach is considered when these two classifications are combined (Dash et al., 2007; Lillesand and Kiefer, 2004; Lu and Weng, 2007).

Factors, such as the complexity of landscapes, the selected remote sensing data, image pre-processing as well as the classification process pose a challenge when classifying data into a thematic map, and can influence the overall classification result. Performing an accuracy assessment provides information about the amount of correctly classified ground truth pixels (Cihlar et al., 1998; Lillesand and Kiefer, 2004; Lu and Weng, 2007). Several image classification techniques were developed (Foody, 1996; Gallego, 2004; Gong and Howarth, 1990; Pal and Mather, 2003; San Miguel-Ayanz and Biging, 1997), however currently only one comprehensive review of these classification approaches exists by Lu and Weng (2007). A short description of unsupervised and supervised classification approaches will be provided in the following sections.

Unsupervised pixel based classification techniques
In an unsupervised classification approach no a priori information on land cover and its distribution is required. A clustering-based algorithm is applied to classify the image into natural groupings by assigning image pixels with similar spectral properties into a particular category. These categories then need to be labelled and merged by the analyst. Advantages of this approach are that the minimum user interaction minimizes human error (Cihlar, 2000; Lillesand and Kiefer, 2004; Ramsey, 2008). The proposed categories are however not always logical, thus merging them into meaningful land cover classes is not always easy. Furthermore, it is not possible to improve the overall results by including expert knowledge about the study area into the process (Jain et al., 2000). The most common unsupervised classification approaches are the iterative self-organizing data analysis (ISODATA) and K-means clustering algorithm (Lu and Weng, 2007).

Several studies have successfully implemented unsupervised classifications to map and monitor land cover and forest changes (Bruzzone et al., 2002; Huiping et al., 2011; van Lier et al., 2011). In other studies, Manyatsi and Ntshangase (2008) used an unsupervised classification approach on Landsat images to map land cover and analyse soil erosion in Swaziland. Saadat et al. (2011) applied a hybrid approach to map land use and land cover in Iran in order to help soil erosion control efforts.

Supervised pixel based classification techniques
The supervised classification approach is more complex than the unsupervised classification and requires prior knowledge about land cover types that are to be classified and mapped (Cihlar, 2000). Knowledge can be obtained from maps, aerial photography or field work. This method can be divided into three stages: training, classification and testing. Training samples characterize the spectral properties of each feature class in an area with known properties. Before selecting training samples, the analyst has to determine the land cover classes into which the image should be classified. Once these are determined, points in areas of known land cover are selected to define training samples and then applied for the training of the classifier in order to classify the spectral data in a thematic map (Lillesand and Kiefer, 2004; Lu and Weng, 2007). Because classifications are prone to errors, the overall accuracy of the

classifier needs to be assessed in the final step, based on ground truth data[10]. Advantages of the supervised approach are the control over the selected class and the detection of possible classification errors with the help of accuracy assessments. The selection and definition of training data is however time consuming, costly and not always representative throughout the whole study area. Furthermore, the analyst applies a structure to the data, which does not always correspond with reality (Cihlar, 2000; Lillesand and Kiefer, 2004).

The maximum likelihood classification (MLC) is one of the most common applied supervised techniques. It is known for its ability to establish good separation between classes, improving the accuracy of classifications. However, it is highly dependent on having strong training data and that the datasets follows a normal distribution. It applies an algorithm which is based on Bayes' theorem of decision making and assumes multivariate normal distribution of a class sample (Lillesand and Kiefer, 2004; Richards and Jia, 2006; Srivastava et al., 2012). Maximum likelihood algorithms were successfully used on multi-date data to monitor land cover changes in Central Chile (Schulz et al., 2008), and to map land cover in order to derive input parameters for soil erosion prediction (Baban and Yusof, 2001; Beskow et al., 2009; Cyr et al., 1995; Meusburger et al., 2010a).

More advanced classification algorithms are artificial neural network (ANN), support vector machine (SVM) and decision trees (DT). These are considered learning algorithms since they can be trained by the user to detect and analyse specific patterns (Otukei and Blaschke, 2010). Several studies suggested that ANN is superior to traditional approaches, such as MLC, because it does not rely on the assumption of normally distributed data, its learning function is based on training samples (Shao and Lunetta, 2012; Szuster et al., 2011). Its logical rules are however not always easy to comprehend, why it is often referred to as a 'black-box' (Kotsiantis, 2013; Szuster et al., 2011).

SVM are a type of "theoretically superior machine learning algorithms, [which] employ optimization algorithms to locate the optimal boundaries between classes" (Huang, 2002: 726). Shao and Lunetta (2012) compared SVM with neural networks (NN), and classification and regression trees (CART) by using MODIS time-series data to classify land cover with limited training point data. They concluded that SVM performed superior to the other two, especially when working with a limited number of training samples.

[10] Actual field measurements

Decision tree classifiers (DT), a non-parametric classifiers, require no prior assumption about the distribution of the dataset (Otukei and Blaschke, 2010). Advantages of DTs are that their logical rules are easier to comprehend than the ones in artificial neural networks (Kotsiantis, 2013), expert knowledge is however often necessary in order to define decision boundaries (Otukei and Blaschke, 2010). Otukei and Blaschke (2010) assessed the potential DTs, SVM and MLC algorithms for land cover mapping, and conclude that DTs performed better than the other two applied techniques.

Pal and Mather (2003) tested the effectiveness of DTs, MLC and ANNs classifiers using multispectral Landsat ETM+ and hyperspectral DAIS[11] imagery, and conclude that "the ML algorithm is preferred unless there are particular reasons for believing the data do not follow a Gaussian (or, at least, a unimodal) distribution" (Pal and Mather, 2003: 564).

The results of a classification process depend on several factors, such as the image quality or the analyst's skills. It is thus not possible to conclude that a certain classifier will always lead to good results. In order to determine the most suitable one for a particular study, the most common approach is to compare different classifiers and select the one, with the best results (Lu and Weng, 2007).

In previous research, land cover in New Caledonia was mapped over the period of 2003 to 2008 using SPOT5 images. A membership function was applied to the images, classifying them into 19 different land cover classes with an overall accuracy of 75.5 % (Direction des Technologies et Services de l'Information, 2008). Additionally, land cover of the years 1998, 2002, 2006 and 2010 was mapped, partly based on RapidEye images. The results are used for land cover maps and change detection applications within the national geo-portal by the Observatoire de l'Environnement Nouvelle-Calédonie (OEIL).

2.3 Change detection techniques

Change detection can be defined as "the process of identifying differences in the state of an object or phenomenon by observing it at different times" (Singh, 1989: 989), which requires reliable and frequent data acquisition (Lu et al., 2004b). For successfully managing natural resources, land cover changes, a key driver of global environmental change, need to be mapped, quantified and monitored (Lambin and Strahler, 1994). Conventional approaches for collecting environmental data, such as field survey, are "time

[11] Digital Airborne Imaging Spectrometer

consuming and often ineffective at delivering the required information in a cost and time efficient manner" (Hirata et al., 2001: 508).

Data acquired from satellites, radar and aerial photography are the major data sources for identifying and analysing spatio-temporal patterns of land cover changes. Their repetitive coverage at short intervals and consistent image quality, as well as the availability of historical images, allows the extraction of landscape information, that can help to successfully monitor land cover transformations (Coppin et al., 2004; Lu et al., 2004b; Théau, 2012). The launch of the first series of Landsat Satellites in 1972 guaranteed the regular acquisition of data in multispectral bands (Coppin and Bauer, 1996). From then on, it was possible obtain consistent data for monitoring changes over large areas with a spatio-temporal resolution of 15-60 m every 16 days (NASA, 2013). Due to the continuity of the Landsat missions, and the development of new sensors and platforms, great progress was made in the field of remote sensing and the development of change detection techniques (Coppin and Bauer, 1996; Lambin and Strahler, 1994; Mas, 1999; Singh, 1989).

Changes can be distinguished into abrupt and gradual changes. To detect gradual changes, which result from changes over time, a series of multi-date images are required. For the detection of abrupt changes, two sets of images, that surround the event causing the change, are sufficient (Coppin and Bauer, 1996; Théau, 2012). Furthermore, changes in land cover can be distinguished into two types, "land cover conversion" and "land cover modification" (Coppin et al., 2004). The first type represents a complete conversion from one land cover class into another, typically induced by human land-use activities (deforestation or urban growth for example). While land cover modifications reflect landscape alterations within one class, due to natural processes, such as different phenological conditions, or climatic changes (Coppin et al., 2004; Coppin and Bauer, 1996; Lunetta et al., 2006).

A successful change detection analysis should provide information about whether a change has occurred and identify its nature, measure the extent of the occurring change and finally assess its spatial pattern. Identifying the optimal method for this is however a difficult process and it is often best to test and compare different techniques and then select the most suitable one. The selection should be based on the results of an accuracy or a qualitative assessment (MacLeod and Congalton, 1998).

According to Singh (1989), "the basic premise in using remote sensing data for change detection is that changes in land cover must result in changes in radiance values [,] and changes in radiance due to land cover change must be large with respect to radiance changes caused by other factors". These 'other' factors concern (1) the remote sensing system, (2) the environmental characteristics and (3) the method of image processing. Data selection and image pre-processing consequently pose major steps when implementing a change detection, otherwise inherent noise might create erroneous change phenomena and hereby lead to a falsification of the results (Lu et al., 2004b).

By selecting appropriate data, the influence of external factors can partially be reduced. Acquiring data of anniversary dates[12] for example minimises the impact of phenological changes and sun angle effects (Coppin and Bauer, 1996). Once appropriate remotely sensed data has been acquired, it is necessary to pre-process these images in order to remove data acquisition errors and image noise. The main pre-processing steps include: geometrical rectification[13] radiometric correction[14], and if necessary the masking of clouds, water bodies and other irrelevant features Without a reliable radiometric calibration, spatial and temporal changes might occur due to differences in the sensor calibration, atmosphere, and / or sun angle (Coppin and Bauer, 1996; Jensen, 1996; Lu et al., 2004b).

Assessing the accuracy of the image classifications and the change detection analysis is a crucial step for accurately understanding and estimating the changes in land cover. Several factors, such as the image quality, pre-processing, image classification, applied change detection algorithm, availability and quality of ground truth data, as well as the interpreter's knowledge and skills in working with remote sensing data can influence the accuracy of the result (Coppin et al., 2004; Jianya et al., 2008; Lu et al., 2004b). According to Lu et al. (2004b) the combination of different change detection techniques can help improve the change detection accuracy. The most common accuracy assessment elements include: overall accuracy, producer's accuracy, user's accuracy and Kappa coefficient.

The last element to consider before implementing a change detection concerns the definition of change and change direction. While some change detection techniques only provide change and no-change

[12] Images acquired during the same month but in different years
[13] Process of correcting spatial distortions within the image
[14] Process of correcting distortions due to illumination variations, viewing geometry, etc. within the image

information, such as image differencing, other techniques, such as post-classification comparison, provide information about from-to changes in a matrix (Lu et al., 2004b).

Several methods to detect land cover changes have been developed by Singh (1989), Lambin and Ehrlich (1997), and Mas (1999), and been reviewed among others by Jensen (1996), Lunetta et al. (2006), Coppin et al. (2004) and Lu et al. (2004b).

Singh (1989) believes digital change detection methods can be characterized based on (1) data transformation procedures, and (2) the analysis techniques used to delimit areas of significant changes. He furthermore distinguishes two approaches, namely "comparative analysis of independently produced classifications", also known as post-classification comparison, and "simultaneous analysis of multi-temporal data", also referred to as pre-classification spectral change detection. Lunetta et al. (2006) and Coppin et al. (2004) drew similar conclusions in their reviews, and classified change detection methods in pre-classification and post-classification as well.

The post-classification method is a straight forward approach, in which two multi-temporal images are independently classified and then used to detect detailed "from-to" changes (Singh, 1989). Common techniques include the post-classification comparison, change vector analysis (CVA) and hybrid change detection. According to Lu et al. (2004b) the advantage of these techniques is the compensation of impacts of atmospheric and sensor differences, as well as phenological conditions between multi-temporal images. Additionally, they can provide a complete change detection matrix. This approach does however have its limitations. The individual image classifications can be very time consuming and require knowledge in the classification process. Errors could occur during the two initial classifications and affect the final accuracy (Coppin et al., 2004; Lu et al., 2004b; Mas, 1999; Singh, 1989). Additionally, changes within land cover classes cannot be determined by comparing different land cover classifications (Lambin and Strahler, 1994).

Pre-classification is a widely used approach, which includes techniques such as image differencing, image rationing, principal component analysis (PCA), and vegetation index differencing (VID) (Coppin et al., 2004; Lu et al., 2004b; Singh, 1989). Singh (1989) suggests that image differencing is the most common pre-classification method, which involves the subtraction of the oldest image from the newest. Lu et al. (2004b) concludes that image differencing is easy to implement and interpret. However it can only be used to detect binary changes and cannot provide a detailed change matrix. According to studies by Weismiller et al. (1977), Jensen and Toll (1982), and Coppin and Bauer (1996) image differencing performs better than the other pre-classification methods and produces excellent results. But they also conclude that the techniques may be too simplistic to adequately describe many of the surface changes and that the selection of threshold values of change and no-change in the resulting images might pose a challenge.

Coppin et al. (2004) groups the different change detection methods based on temporal characteristics in two broad categories: bi-temporal change detection and temporal trajectory analysis. The bi-temporal method examines the changes between two fixed dates, while time-trajectories also considers “the progress of the change over the period” (Jianya et al., 2008: 759). Jianya et al. (2008) adopted the distinction proposed by Coppin et al. (2004) but builds on this by dividing the “bi-temporal” category into (1) direct comparison, (2) post-analysis comparison and (3) uniform modelling.

Additional classifications of change detection techniques were proposed by Deer (1995) and Mas (1999), who both define the approaches into three categories. Deer (1995) categorizes the approaches into (1) pixel based, (2) feature based[15], and (3) object based, while Mas (1999) groups them into (1) image enhancement, (2) multi-date classification and (3) the comparison of two independent land cover classification. Lu et al. (2004b) discuss seven different types of change detection methods: (1) algebra, (2) transformation, (3) classification comparison, (4) advanced models, (5) Geographical Information Systems (GIS) approaches, (6) visual analysis and (7) other approaches. Lu et al. (2004b) conclude that image differencing, principal component analysis (PCA) and post-classification comparison are the most commonly used methods. They furthermore state that spectral mixture analysis (SMA), artificial neural networks (ANN) as well as the integration of geographical information system and remote sensing data have become important techniques for change detection applications.

In the last few years, interest in change detection techniques applying time series analysis, as artificial intelligence or knowledge-based expert systems, has grown. According to Coppin et al. (2004) artificial intelligence and knowledge-based approaches pose advantages because it is possible to overcome some of the limitations of the traditional statistical classifiers by integrating additional

[15] Features, such as shape, colour and texture

aspects of vegetative cover categories other than merely relying on its spectral change.

Dhakal et al. (2002) compared four change detection techniques, including (1) Spectral Image Differencing (SID), (2) Tasseled Cap Brightness Image Differencing (TCBID), (3) Principal Component Analysis (PVA), and (4) Spectral Change Vector Analysis (SCVA), for their effectiveness in detecting areas associated with flood and erosion caused by heavy rainfall. SCVA was found to be the most accurate for detecting affected areas. Prenzel and Treitz (2004) successfully tested a “hybrid” change method for extracting thematic land surface change information in a watershed in Indonesia. El-Kawy et al. (2011) and Shalaby and Tateishi (2007) both concluded that their approach of integrating visual interpretation with a supervised classification of satellite imagery is an effective method to detect land use and land cover changes in Egypt. Zanotta and Haertel (2012) proposed a new approach to detect land cover changes using multi-temporal image data, in which they defined change “in terms of degrees of membership to the class change [instead of] allocating pixels to one of two disjoint classes (change, no-change)” *(Zanotta and Haertel, 2012: 2927)*. Their results indicated the soundness of the proposed methodology, there are however circumstances, in which this approach may not be the most adequate one, such as monitoring the changes in the vegetation cover as well as other environmental problems.

Most techniques discussed and reviewed above, focus on bi-temporal based change detection approaches, such as “the single analysis of a combined dataset of two or more dates, or the comparative analysis of images obtained at different moments after previous independent classification” (Mas, 1999: 143). Only little attention is paid to temporal trajectory analysis, such as time series analysis. By collecting data throughout the growing season, approaches based on time series analysis have the advantage of resolving issues, such as the influence of phenology on the change detection results (Coppin et al., 2004). Up to now, only a few studies focus on land cover monitoring on a continuous basis. In order to establish time profiles, high temporal resolution data is required, which can only be derived from coarse (AVHRR) and moderate (MODIS) spatial-resolution sensors. The application of this data however poses a serious disadvantage, the loss of spatial details makes auto-classification difficult and “limits the change categories that can be detection and monitored” (Coppin et al., 2004: 1569), making the temporal trajectory analysis a limited approach (Jianya et al., 2008).

Despite the amount of change detection reviews, there is no consensus about the optimal or most effective technique (Jianya et al., 2008; MacLeod and Congalton, 1998). Numerous studies, which addressed the problem of accurately monitoring land cover changes, commonly agreed that change detection is a complicated process (Coppin et al., 2004; Lu et al., 2004b; Mas, 1999; Singh, 1989). An algorithm, which led to reliable results in one study, is not necessarily the best choice in a similar study. Selecting a suitable change detection algorithm is therefore of great significance, and deserves careful consideration(Coppin et al., 2004).

To date no previous research has been found on land cover changes in New Caledonia.

2.4 Soil erosion and erosion modelling

Erosion refers to the three stage process of detachment, transport and deposition of soil particles by erosive agents. It can be distinguished into wind, and rainfall and runoff erosion, based on the agents inducing the degradation process (Aksoy and Kavvas, 2005; Vrieling, 2006). This phenomenon affects all types of landscapes, however areas with steep slopes and erodible soils are especially susceptible, particularly when sparse vegetation cover coincides with high intensity rainfalls (Vrieling et al., 2008).

Natural erosion, also known as geologic erosion, is the natural soil-forming process, which occurs in all soil types and is not influenced by anthropogenic activities. Once the natural equilibrium between soil properties and soil profile is disturbed and a certain threshold level is exceeded, it is considered as accelerated erosion and can become a major environmental concern. This kind of erosion is usually triggered by human activities, such as deforestation, unsustainable agriculture, anthropogenic climate change and intensive land use. These processes lead to a reduction of vegetative cover, expose soils and consequently make them vulnerable to rainfall-runoff (Blanco-Canqui and Lal, 2008; Shrestha, 2011; Toy et al., 2002).

Soil erosion by water can be distinguished into three types: sheet, rill and gully erosion. Sheet erosion is regarded to be the least severe type, while gully erosion can lead severe environmental damages (Toy et al., 2002). Water erosion, one of the most important causes of land degradation worldwide (Eswaran et al., 2001), is a complex process, which occurs as a direct result of rainfall. It responds to the rainfall amount, the differences in rainfall intensity are however the determining factor (Nearing et al., 2005). The effect of rainfall on erosion differs with factors as soil type, relief and predominant vegetation type. According to Morgan (2005) the erosivity of rain, the erodibility of soils, the slope of the terrain and the nature of plant cover are the four most important ones for soil erosion.

Soil properties, such as soil texture, organic matter content, soil structure and infiltration, influence the erodibility of soils, its resistance to detachment and transport (Cebecauer and Hofierka, 2008: 191). Soils containing clay are less prone to erosion than soils with large amounts of silt-sized particles. Clay binds particles better together and thereby increases its physical resistance to erosion. Furthermore, soils containing high levels of organic materials are more resistant to erosion because organic materials create a stronger structure, increase infiltration, and thereby reduce surface runoff (Blanco-Canqui and Lal, 2008; Lal, 1994; Morgan, 2005).

The erosivity of rainfall is determined by the climate. Frequent and intensive rainfalls cause saturated soils, which reduces the rate of rainfall infiltrating the soil, and results in higher levels of surface runoff. The impact of rainfall hitting the exposed and saturated soils causes the detachment of soil particles from the Earth's surface, which are then transported by water flow and deposited once the flow velocity is no longer sufficient to transport the particles (Lal, 1994; Morgan, 2005; Pimentel et al., 1995). But rainfall duration also poses another important factor, long durations with low intensity rainfall can lead to increased soil moisture, resulting in more surface runoff (Blanco-Canqui and Lal, 2008; Lal, 1994; Morgan, 2005).

Effect of vegetation cover on soil erosion

Vegetation cover decreases potential soil erosion by protecting the soil from rainfall. Above ground cover, such as canopy cover, reduces the speed of rainfall and prevents it from directly hitting the surface (Meusburger et al., 2010a). The effect of vegetation on the erosion process does not only depend on its density, but also on the type and structure of vegetation. Once the process of erosion has started and the topsoil, the most nutrient rich layer, is being removed, plant growth is reduced, resulting in more erosion (Morgan, 2005; Pimentel et al., 1995; Shrestha, 2011). Terrain conditions play another important role in the process. Erosion risk increases with slope steepness and slope length because of a higher velocity in surface runoff (Morgan, 2005; Wischmeier and Smith, 1978).

Erosion is recognized as a worldwide problem leading to environmental degradation (Vrieling, 2006). It not only causes severe environmental impacts, but also leads to high economic costs due to its effects on agricultural productions and water quality (Lal, 1994;

Pimentel et al., 1995). Environmental impacts of accelerated erosion are, among others, the degradation of arable land and soil productivity, the pollution of water by sediments and an increased risk of flooding (FAO, 1977; Lal, 2004). According to Nearing et al. (2005), climate change leads to an increase in rainfall amounts, and their erosive power results to higher soil erosion rates. Erosion on the other hand results in the emission of soil organic carbon, in form of CO_2 and CH_4, which in return contributes to global warming (Nearing et al., 2005; O'Neal et al., 2005).

Erosion modelling

For a better understanding of erosion and its causes, it is necessary to monitor and model its process (Blanco-Canqui and Lal, 2008; Ouyang et al., 2010). According to the Food and Agriculture Organization of the United Nations (FAO, 1977), a clear understanding of the effects of soil erosion is fundamental for controlling and modelling the process. The number of different factors involved in the process however poses a challenge when modelling erosion. Vrieling (2006) stated that remote sensing presents a reliable source because it provides homogeneous data over larger areas with a regular revisit capability, and can therefore successfully contributes to the assessment of erosion.

Several erosion and sediment transport models, such as the Universal Soil Loss Equation (USLE), the Revised Universal Soil Loss Equation (RUSLE), the Limburg Soil Erosion Model (LISEM) and the Areal Non-point Source Watershed Environment Response Simulation (ANSWERS), were developed to estimate soil erosion on different temporal and spatial scales and to detect affected areas (Jetten et al., 2003; Morgan et al., 1998; Renard et al., 1997; Wischmeier and Smith, 1978). Erosion models can be distinguished as empirical, conceptual and physically based models, and differ in complexity and input parameter requirements. Empirical models are primarily based on empirical observations, while physically based models aim at representing each individual process of the overall natural processes and then combine them into a complex model. Conceptual models on the other hand are a combination of empirical and physically based models (Aksoy and Kavvas, 2005; Merritt et al., 2003; Nearing et al., 2005). Most of these models were developed for a certain environment and scale. Therefore, their application in other regions or scales may cause errors in results, leading to a constant development of new models and the modification of existing techniques (Jetten et al., 1999; Jetten et al., 2003; Vrieling, 2006).

According to Vrieling (2006), USLE and its revised version, RUSLE, which both predict average annual soil loss from hill slopes due to sheet and rill erosion, are the most widely applied method for agricultural land and forest watersheds. Both approaches calculate soil loss by multiplying the following factors: rainfall and runoff (R) in USLE, erosivity (R) in RUSLE, soil erodiblity (K), slope-length (L) and slope steepness (S), land cover (C) as well as support practices (P) (Merritt et al., 2003; Wischmeier and Smith, 1978). These models are often applied due to their simplicity and the option of combining them with remotely sensed data and Geographic Information Systems (GIS). They have however a number of limitations, it is for example not event-based and therefore “cannot identify events most likely to result in large-scale erosion” (Merritt et al., 2003: 774). Additionally, it does not consider gully erosion and mass movements (Beskow et al., 2009).

Soil erodibility modelling using the Universal Soil Loss Equation

According to Nearing et al. (1994), adapting USLE to a new environment is a time-consuming and cumbersome process. The model requires long term data on soil and rainfall, which are not always available. Detailed information about the input parameters for different regions is scarce, especially in data-poor environments (Morgan, 1995), therefore it is often required to develop a new database in order to run the model in a new region (Nearing et al., 1994). Due to these limitations, a variety of modifications and revisions of the basic USLE model have been proposed, such as the revised USLE (RUSLE) (Renard et al., 1997; Renard and Freimund, 1993) and the modified USLE (M-USLE) (Kinnell and Risse, 1998).

A key factor influencing the vulnerability of an area to erosion is land cover (Cebecauer and Hofierka, 2008; Meusburger et al., 2010a). Several researchers concluded that an increase of vegetation cover is the most effective method to reduce and control soil erosion risk (Cyr et al., 1995; Huiping et al., 2011; Marques et al., 2007; Xu et al., 2005; Zhongming et al., 2010; Zhou et al., 2008). Within the USLE model, the factor C depends on the type of vegetation, as well as the management and fractional vegetation cover (Meusburger et al., 2010a). This factor is however also considered as one of the most difficult parameters to estimate, therefore several approaches exist (De Asis and Omasa, 2007).

Traditionally, C-factor values, which range between 0 and 1 depending on the vegetation density, are simply derived from literature and field data, and then assigned to the different vegetation types in a classified map (De Asis and Omasa, 2007; Morgan, 2005). Cebecauer and Hofierka (2008) used the CORINE land cover database to define the C-factor by assigned values for each vegetation type based on rough estimates using available literature. For the prediction of potential soil loss in a watershed in Brazil, Beskow et al. (2009) used Landsat images for the classification of land cover, and assigned values to the C-factor based on previous studies carried out in different parts of Brazil with similar land use and cover. Mati et al. (2000) developed a land cover map for a basin in Kenya, based on visual interpretation of multispectral SPOT image and field surveys, and estimated C-factor values using USLE guide tables.

Assigning C-factor values based on literature however leads to relatively constant C-factor values over large areas, and does not accurately reflect the variation in vegetation cover (Wang et al., 2002). Additionally, classification errors are often transferred into C-factor maps (De Asis and Omasa, 2007). The application of direct linear and non-linear regression models between image bands and ratios can help to increase the spatial variability and decrease the influence of classification errors (De Asis and Omasa, 2007; Vrieling, 2006; Zhongming et al., 2010). Another approach for deriving information on vegetation cover is to apply spectral indices and spectral unmixing (Meusburger et al., 2010a; Vrieling, 2006). Liu et al. (2004), Thiam (2003), Gay et al. (2002) and Goel et al. (2002) used spectral indices, such as the normalized difference vegetation index (NDVI), as an indicator for the mapping of vegetation cover. Ouyang et al. (2010) explored the relationship between NDVI with corresponding soil erosion and sediment yield in the Yellow River Basin and stated that vegetation has a significant impact on sediment formation and transport. NDVI is considered to be the most commonly method for assessing vegetation cover by using remote sensing (Cyr et al., 1995). De Jong (1994) and De Jong et al. (1999) however concluded that Landsat derived vegetation indices, such as NDVI, have a low correlation with the C-factor. Reasons are the sensitivity to the vegetation's vitality as its condition does not necessarily relate to its function of protecting the soil, well as the effect of soil reflectance (De Asis and Omasa, 2007). NDVI starts to saturate once the vegetation cover exceeds 50%, furthermore it is not sensitive to greenness of lower vegetation, leading to underestimates in vegetation cover for certain areas (Zhongming et al., 2010). De Asis and Omasa (2007) concluded that traditional methods for extracting of vegetation information from remote sensing data were found to be inaccurate.

According to Meusburger et al. (2010a), the problem of low correlation between NDVI and C-factor can be avoided by applying linear spectral unmixing (LSU). This method is however mainly applicable in (semi-) arid environments (Vrieling, 2006). Another approach to overcome the problem of low correlation is the application of soil adjusted vegetation indices, such as TSAVI. Cyr et al. (1995) compared four different vegetation indices (NDVI, PVI, SAVI and TSAVI) and concluded that TSAVI performed better for vegetation assessment than NDVI. They furthermore concluded that, when estimating ground cover, it is important to carefully select a vegetation index, which can successfully discriminate vegetation from bare soil.

De Asis and Omasa (2007) proposed a new approach based on Spectral Mixture Analysis (SMA) of Landsat ETM data to map the C-factor for modelling soil erosion. The linear SMA proved to be superior to NDVI when deriving and mapping the C-factor. Zhou et al. (2008) used the non-parametric k-nearest neighbour technique (k-NN) in order to estimate vegetation cover in a mountainous watershed. Furthermore, the performance of predictions to those by NDVI and multivariate regression were tested. The study concluded that the k-NN method proved to map vegetation cover more accurately. Meusburger et al. (2010a) stated that the availability of high-resolution satellites such as IKONOS and QuickBird increased the options for mapping of vegetation parameters. In their approach they explored how high resolution maps of fractional vegetation cover (FVC) and land cover improve soil erosion risk mapping using USLE and the Pan-European Soil Erosion Risk Assessment model (PESERA) in an alpine catchment. High resolution maps of land cover and FVC were obtained from image classification and linear spectral unmixing analysis (Meusburger et al., 2010a).

According to De Asis and Omasa (2007) the research on improving ways to estimate the C-factor with remotely sensed data is important because reliable vegetation cover plays an essential role in accurately identifying and estimating soil erosion.

Erosion research in New Caledonia

Erosion research in New Caledonia has been conducted among others by Dumas et al. (2010) and Rouet et al. (2009). Rouet et al. (2009) compared different approaches for soil erosion mapping and hazard assessment in data poor regions, such as New Caledonia. Both approaches, the erosion mapping and the data mining approach, showed potential in contributing to the erosion and hazard assessment on the island, improvements on the methods are however required.

Dumas et al. (2010) mapped areas prone to erosion on the west coast of the island by applying a multi-criteria evaluation model and the Universal Soil Loss Equation (USLE). The results can be considered as “an initial step towards a more accurate estimation of the terrigenous discharge into the lagoon”. Printemps (2007) and Bui-Duyet (2011) also conducted research on soil erosion using the USLE model. All studies concluded that the combination of areas of bare soils, steep slopes and high precipitation make an area especially vulnerable to erosion.Dumas et al. (2010) A major drawback on the application of USLE in New Caledonia is however the missing validation of the results.

3 Study area and data description

3.1 Study area

New Caledonia is an archipelago located in the Southwest Pacific Ocean (21°30'S–165°30'E) about 1200 km east of Australia, as shown in Figure 3. It was considered an overseas territory of France until 1998 when it became a special collectivity of France. The territory has an area of 18,575 km² and comprises the main island Grande-Terre with the capital Nouméa, the four Loyalty Islands in the east (Ouvéa, Lifou, Tiga and Maré), the Isle of Pines in the south, as well as numerous smaller islands. The estimated population was 252,000 in 2009 (Haut-commissariat de la République en Nouvelle-Calédonie, 2011; Ministère des Outre-Mer, 2012).

Geography

Grande Terre, which is elongated northwest-southeast, is the largest island with an area of 16,000 km². Its length of 400 km is dominated by a high mountain range, the "Chaîne Centrale". These mountains, of which some are over 1500 m high, influence the rainfall patterns and thus divide the island into two distinct regions. The east coast, which is exposed to southeast trade winds, receives high amounts of precipitation and is covered by dense vegetation, such as primeval rain forests. The west coast on the contrary is protected from the trade winds by the mountain chain, resulting in a drier climate within the rain shadow. This part of the island is dominated by large savannahs and sclerophyll forest (Dumas et al., 2010; Ministère des Outre-Mer, 2012).

Ultramafic rocks cover about 30 % of Grande Terre. These rocks are mainly composed of a ferruginous crust, a very erodible layer of laterites underneath, a layer of serpentinite and the parent rock, peridotite, as seen in Figure 4. Under the wet and hot climate, a weathering process forms lateritic nickel ore deposits from ultramafic rocks, which are the major source in the nickel mining process (Guillon and Lawrence, 1973; L'Huillier et al., 2010; Proctor, 2003).

The New Caledonian Lagoon, which has been designated on the World Heritage List of UNESCO since 2008, is one of the largest lagoons in the world, with a total area of 24,000 km². Furthermore, the island has the second largest barrier reef in the world. The New Caledonia Barrier Reef, which has a length of 1,500 km, surrounds Grande-

Terre, the Isle of Pines and a few smaller island (Chabanet et al., 2010).

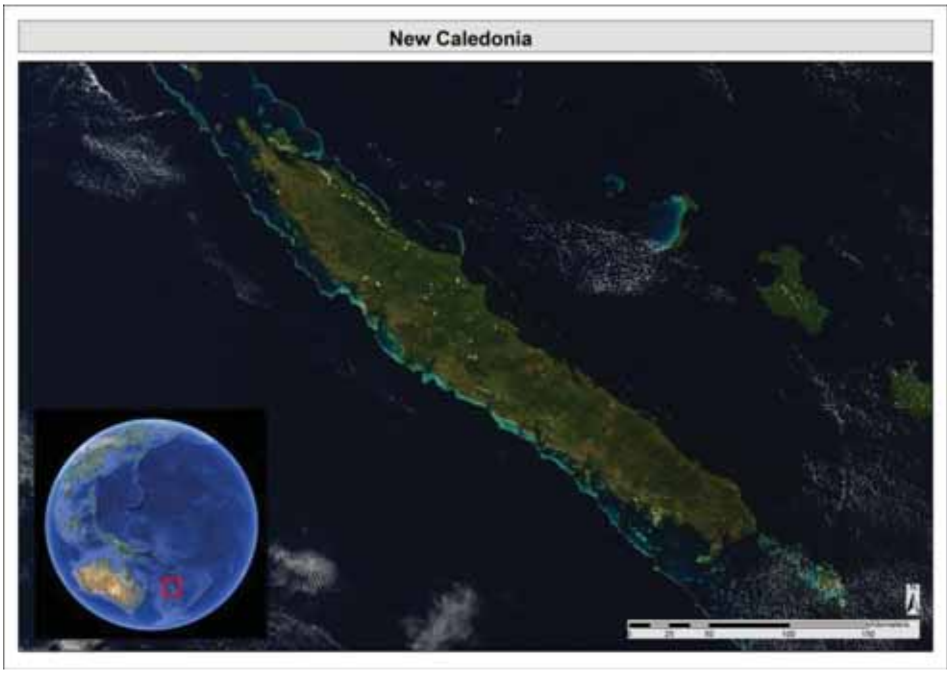

Figure 3: Location of New Caledonia (MODIS Terra Satellite Image, source: NASA).

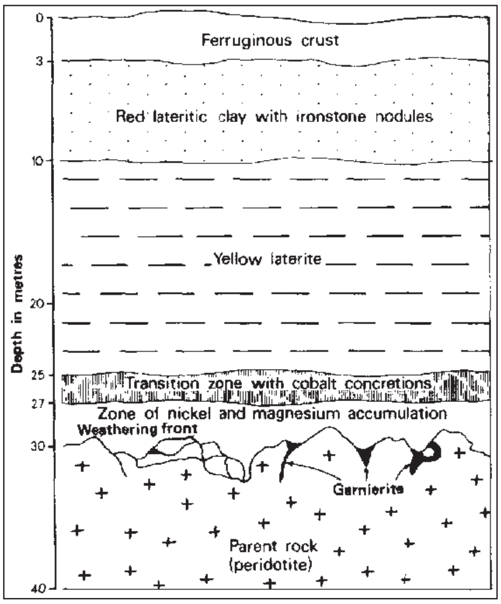

Figure 4: Weathering profile characteristics of hilltop plateaux on ultrabasic massifs in New Caledonia (after Paris, 1981).

Climate

The territory has a tropical climate with two seasons, determined by the position of the inter-tropical convergence zone (ITCZ). The hot and humid period from mid-November until mid-April is characterised by the high frequency of tropical depressions and cyclones, average temperatures range from 25°C to 27°C. During the cooler period from mid-May to mid-September the average temperatures range from 20°C to 23°C (Ministère des Outre-Mer, 2012). Rainfall is highly seasonal and is influenced by the central mountain chain and southeast trade winds. The frequent tropical depressions and cyclones during the wet season cause heavy rainfall and strong winds, the amount of precipitation however varies according to elevation and wind exposure (Dumas et al., 2010). The east coast receives an annual precipitation of up to 4000 mm/year, while the annual precipitation on the west coast ranges between 1000-2000 mm/year (Stevenson et al., 2001).

Environment

New Caledonia was separated from the continent of Gondwana about 75 million years ago. This had an effect of isolating the fauna and flora, allowing it to evolve in a unique way and resulting in one of the highest rates of endemism in the world (Bui-Duyet, 2011). According to Pascal et al. (2008) about 90% of the flora on the island are endemic. Most of the soils are derived from ultramafic rocks, which have high contents of chromium and nickel and can thus be toxic to vegetation. Over the years, the native vegetation has however adapted to these acidic soil conditions, resulting in 3380 endemic species on less than 20,000 km² (Futura Environnement, 2004). Additionally, the island has a high rate of endemic animals, currently 3121 wildlife species are recorded, including 316 endemic species (ENDEMIA, 2008).

Economy

New Caledonia's economy is mainly driven by the mining sector and financial transfers from Metropolitan France and the European Union. Having about 25 % of the world's nickel resources, mining is the main economic resource. Only 0.32 % of the land is suitable for cultivation, agriculture only contributes a very small part to the gross domestic product (GDP) (David et al., 2010; Ministère des Outre-Mer, 2012).

Study area

The study area, Poro, is located in the mountain chain on the east coast of New Caledonia. It was chosen because both, the natural pressures as well as the anthropogenic pressures, which contribute to the erosion process, can be found here. The size of the area is approximately 30 km². The site is characterized by steep slopes facing the sea and red lateritic soils, which are covered by dense forest and shrubland. While land cover changes were assessed over the entire area, shown in the inset in Figure 5, potential soil erodibility was analysed in a small watershed within this area. This small watershed, called Denise, is located on the mine Française operated by the "Centre de Formation des Mines et des Carrières"[16] (CFTMC). It covers an area of 30.4 ha (0.304 km²) and is divided into four sub-watersheds. Within this study the watershed is however treated as a whole.

[16] Training Centre for Mining and Quarry

Figure 5: Location of the study area Poro, New Caledonia.

3.2 Data description

3.2.1 Satellite imagery

Images used for this study were acquired by RapidEye satellites on October 20th, 2011 and January 18th, 2012, see Appendix A. RapidEye satellites acquire images by a constellation of five satellites with identical sensors, meaning that images obtained from two different sensors will be identical in characteristics. The satellites were launched in August 2008 and operate at an altitude of 630 km. RapidEye provides high resolution and multispectral images, which are collected in five distinct bands of the electromagnetic spectrum, as seen in Table 2 and Figure 6. The spatial resolution of the images is 6.5 m, and 5 m after pre-processing. The satellites have a daily revisit time[17] for off-nadir[18] and 5.5 days at nadir[19] (RapidEye AG, 2011).

[17] The amount of time it takes the satellite to capture the same location on the ground again.
[18] The point the sensor is pointing to, which is however not perpendicular below the satellite.

Band	*Wavelength (nm)*
Blue	440-510
Green	520-590
Red	630-685
Red Edge	690-730
Near-Infrared	760-850

Table 2: RapidEye's spectral bands

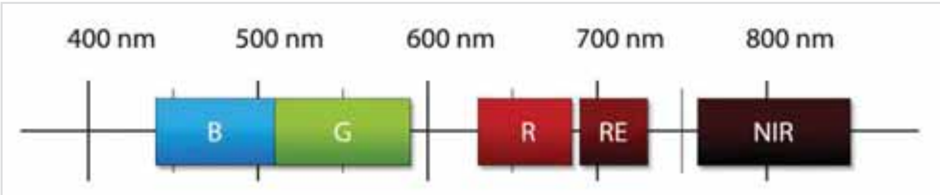

Figure 6: Spectral range of the five RapidEye bands showing the visible to the near infrared (NIR) (RapidEye AG, 2011).

Details of the obtained images are presented in Table 3.

Acquisition date	October 10 2011	January 18 2012
Acquisition time	00:14:50	00:03:02
Cloud cover (%)	8	7
Sun elevation (°)	77.2	75.13
Sun azimuth (°)	30.5	90.8
View angle	-16.45	12.76
Orbital direction	Descending	Descending

Table 3: Metadata of the two RapidEye images

Pre-processing

The image acquisition by remote sensing is disturbed by several factors, such as characteristics of the sensor, atmospheric and weather conditions, solar angle and the Earth's surface. Before the obtained images can be used for further analysis, pre-processing is required to reduce these data distortions and improve the quality of the images. Pre-processing usually consists of two steps: radiometric and geometric corrections (Natural Resources Canada, 2008).

Radiometric correction

Radiometric correction helps to minimise variations in illumination, sensor characteristics, viewing geometry or atmospheric conditions within the image. Some areas within the image might receive more sunlight due to different solar illumination conditions causing

[19] A point on the ground the satellite is pointing at, which is perpendicular below the satellite.

variations in reflectance. Additionally, electromagnetic waves are influenced by suspended particles within the atmosphere causing scattering and absorption. This leads to changes within the direction and spectral distribution of the electromagnetic energy. In order to avoid false interpretation of the images, corrections are required (Chen X. et al., 2005; Song et al., 2001; Yang and Lo, 2000). Atmospheric correction is however not always required. It can be omitted when for example classifying single date images and comparing them using a post-classification change detection approach (Song et al., 2001).

Geometric corrections

Geometric corrections minimise distortions caused by the curvature of the Earth, its rotation or the topography of the terrain. The aim is to obtain a "geometric representation of the imagery [which is] as close as possible to the real world" (Natural Resources Canada, 2008). Geometric correction is an important pre-processing step in rough terrain, such as in New Caledonia, to avoid relief displacement. Otherwise, the effects of terrain and shadow might lead to problems such as misclassifications. A part of the study area is seen in the images displayed in Figure 7, the image on the left is not geometrically corrected, while the one on the right is. This illustrates the influence of shadow due to the rugged terrain.

Figure 7: FORMOSAT-2 image of June 2011 without geometric correction (left) and a RapidEye image of October 2011 with a geometric correction (right).

RapidEye images are provided at two processing levels: RapidEye Basic (Level 1B) are sensor level products, which are geometrically uncorrected. The second level, RapidEye Ortho (Level 3A) are orthorectified images which are radiometrically and geometrically corrected in a cartographic map projection (RapidEye AG, 2011). The applied RapidEye images of this study were pre-processed by AAM Pty Limited in Brisbane, Australia and delivered on a Level 3A.

Orthorectification, the correction of terrain displacement, has been corrected using a digital terrain model (DTM)[20] supplied by IRD and digital terrain elevation data obtained from the Shuttle Radar Terrain Mission (SRTM). A total of 10 ground control points (GCP), old aerial photography and vector data were used during the orthorectification process and an accuracy of 1 pixel or less was achieved. Due to different atmospheric and weather conditions (presence of cloud cover, haze and shadows), variations in colour or reflectivity occur between the two images. By pre-processing their effects were reduced to the best possible.

The image obtained in October 2011 had a viewing angle of -16.45°, while the image obtained in January 2012 had a viewing angle of 12.76°. A visualisation of this difference is given in Figure 8. When performing the image classification, this difference needs to be taken into account as “the detected spectral reflectance of the Earth’s surface materials varies as a function of the angles at which they are illuminated by the Sun and viewed by the sensor. Consequences might be errors in the classification” (Barnsley et al., 1997: 1937).

[20] A digital model of the topography of the Earth’s surface

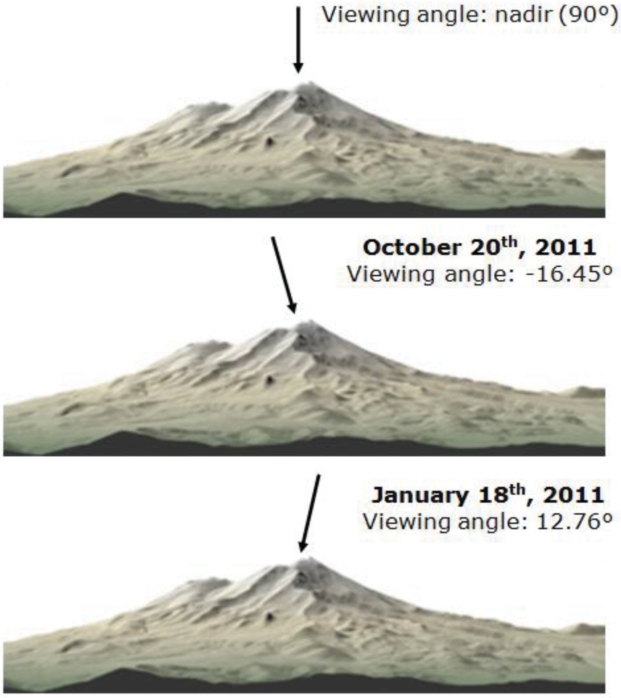

Figure 8: View angle of the satellite in October 2011 and January 2012.

3.2.2 Ancillary data

The following ancillary data was used within this research:

Data	Data type	Acquisition date	Geographic extent	Resolution / scale	Source
Digital Elevation Model (DEM)	Raster	2011	Houailou / Poro	10 metre	IRD
Geological map	Vector	2011/2012	Watershed Poro		IRD
Field measurements: - Rainfall - Water flow - Sediment load	Excel sheet	02/01/2009-12/06/2012	Watershed Poro		IRSTEA
Aerial photographs	Raster	2008	Houailou / Poro	0.5 metre	IRD
Preliminary land cover map 2010	Raster	2010	Houailou / Poro	7.7 metre	IRD
Watershed extent	Shapefile	2012	Watershed Poro		IRD

Table 4: List of ancillary data used.

3.2.3 Software used

The following software programs were applied within this research:

Software	Usage
ENVI 4.8	To perform image processing
ERDAS IMAGINE 2011	To perform image processing
ArcGIS 10	Data preparation, analysis and map
R	To model soil erodibility

Table 5: List of software used.

4 Methodology

The overall research can be split into several phases, as seen in the overview diagram (Figure 9). The first phase included a literature review on the applied techniques, as well as the formulation of the research problem and research objectives. The second phase included the field work, during which data for the image classification were collected. This phase was followed by the actual image classification and the land cover change detection. During the final phase potential soil erodibility was modelled and results were compared to the results of the change detection.

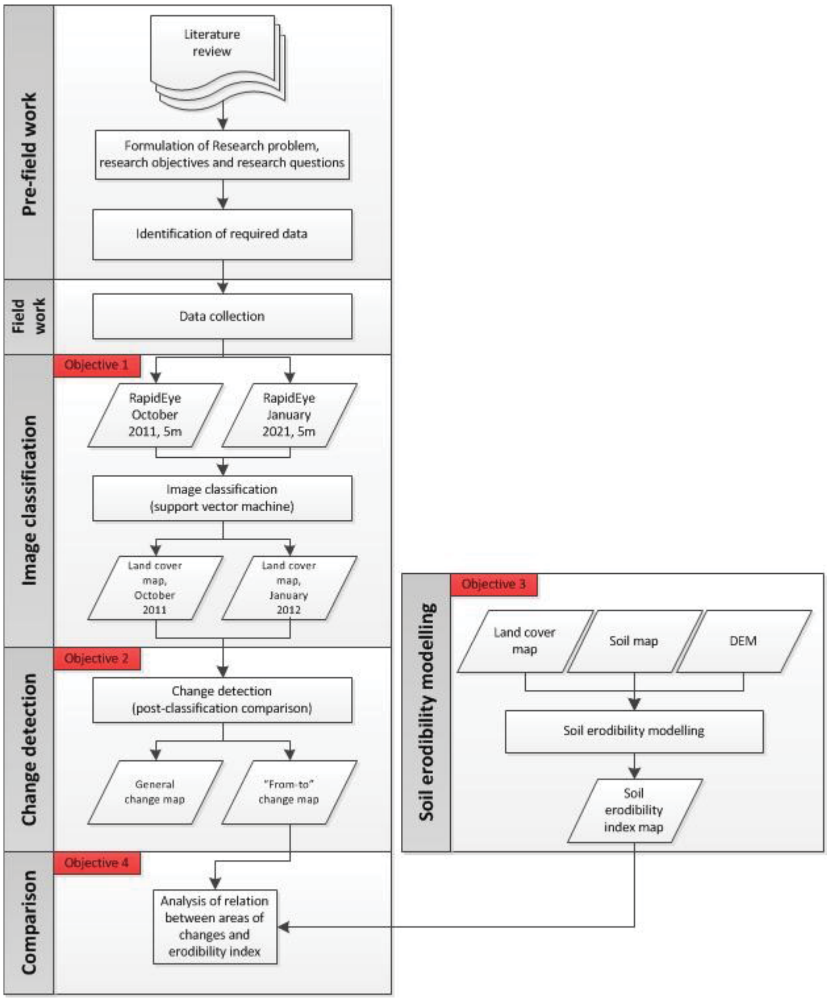

Figure 9: Flowchart of the research process.

4.1 Land cover classification

Before performing the actual land cover classification several steps were necessary. Pre-processing of the satellite images was not required anymore, as this had already been completed (as mentioned in sub-section 3.2.1).

Extraction of the study area
The original RapidEye images cover a larger area than needed. In order to reduce the processing time, the extent of the two images was cropped to the extent of an aerial photograph of 2010 of the study area, seen in Appendix B.

Masking of irrelevant features
The ocean was considered irrelevant for the aim of the study as it focuses on terrestrial land cover changes. Since the ocean might have led to spectral confusion, it was masked. For the creation of the mask, it was necessary to determine a threshold in order to differentiate between water and land. In a first attempt, the Normalized Difference Vegetation Index (NDVI) was calculated in ENVI 4.8, and its data range used to build a mask for the ocean. Vegetation indices, such as NDVI, are often applied to distinguish between vegetated and non-vegetated land cover classes (Dash et al., 2007). NDVI values range from -1.0 to +1.0, bare soil has low positive values and vegetation high positive values, while water values range in the negative. This approach was however problematic because the coral reefs are clearly visible in the shallow water and resulted in positive NDVI values, while the water, due to its low reflectance, resulted in negative values. Consequently, a mask built on these NDVI values did not cover the entire ocean but resulted in a perforated mask. Therefore, this method was neglected.

In a second attempt, an unsupervised classification was completed on images using the ISODATA classifier implemented in ENVI 4.8. The image was, based on statistics, classified into seven basic categories, which showed a clear distinction between land and water. In a post classification process, the classes representing “land” were merged into one single class, leaving only two classes: land and water. This classification was exported to ERDAS IMAGINE 2011, where a few pixels had to be re-coded due to misclassifications. The final classification was used to create a mask for the ocean and then applied to both images.

Development of a classification system

In the next step, a classification system for the study area was developed, which would allow the analysis of different land covers, such as dense and open forest, dense and sparse shrubland. “A suitable classification system and a sufficient number of training samples are prerequisites for a successful classification” (Lu and Weng, 2007: 825). Several classification systems exist, such as the ones proposed by the Food and Agriculture Organization of the United Nations (FAO) (Jansen and Gregorio, 2002), the United States Geological Survey (USGS) (Anderson et al., 1976) or the CORINE Land Cover (CEC, 1995). These classification systems are however not applicable in the context of New Caledonia. As the island has an exceptionally endemic flora, it was necessary to develop a more suitable bespoke classification system for the study area.

The land cover classes considered in the first approach were proposed by IRD. During field research it became clear that this initial classification system was not detailed enough for the variety of existing land covers and needed improvement. The second classification system was based on a nomenclature for New Caledonia, proposed by the “Observatoire de l’environnement Nouvelle-Calédonie” (OEIL) [21]. Instead of just mapping bare soil, it was decided to map the different soil types as this information was required for future research within the project. The final classification scheme resulted in fourteen soil and land cover types, as seen in Table 6.

Vegetation classes were defined according to the density of tree and shrub layer cover, described in Figure 10. Areas with a tree cover of more than 60% were considered as dense forest, while areas with a tree cover between 20 – 60 % fell into the category open forest, a mix of predominantly forest and little shrub. Areas with shrubland as the most dominant land cover were distinguished into dense and sparse shrubland. Dense shrubland is covered by a dense vegetation cover and smaller trees, while sparse shrubland has a very sparse vegetation and tree cover and bare soil is visible in several parts. The major vegetation type in both shrubland categories is the endemic type “Maquis minier”, a plant mostly found on ultramafic rocks. Fragmented vegetation it is covered by a low growing dense vegetation layer without any trees. The most dominant vegetation type in this class is “Fougère”, a fern like plant. Areas with almost no tree and shrub cover, however a dense grass layer are considered as savannah. Photos of the different soil and land cover types are shown in Appendix C.

[21] Environmental observatory of New Caledonia

Class ID	Class (English)	Class (French)	Description
1	Overburden	Materiaux remaniés (roche et sols nus)	Rocks and soil, which are removed during mining process (not to be confused with mining tailings)
2	Bare rock (bare areas)	Enrochement et scories (roche et sols nus)	Bare surface
3	Dunite (bare areas)	Granulat de dunite (roche et sols nus)	Bare or degraded surface
4	Laterite (bare areas)	Latérites (roche et sols nus)	Bare or degraded surface
5	Ferruginous crust (bare	Horizon ferrugineux, cuirasses (roche et sols	Bare or degraded surface
6	Peridotite (bare areas)	Péridotites (roche et sols nus)	Bare or degraded surface
7	Dense forest	Forêts denses humides de basse et moyenne altitudes sur roches ultramafiques	Moist and evergreen forests with a closed canopy cover on ultramafic rocks
8	Open forest	Formations paraforestières et préforestières (substrat ultramafique)	Mosaic of trees and dense vegetation
9	Dense shrubland	Maquis ligno-herbacé sur roches ultramafiques	Dense cover of evergreen plants (mostly maquis miniers) on ultramafic rocks
10	Fragmented vegetation	Végétation éparse sur substrat ultramafique	Vegetation, such as fern (Fougère), with visible areas of bare rock
11	Sparse shrubland	Végétation clairsemée / Maquis minier	Mosaic of very sparse vegetation and maquis miniers
12	Savannah	Savane	Savannah grassland, trees and shrub generally absent
13	Water	Eau continentales	Rivers and lakes
14	Built up	Zone d'habitation	Settlement

Table 6: Description of the soil and land cover classes in Poro.

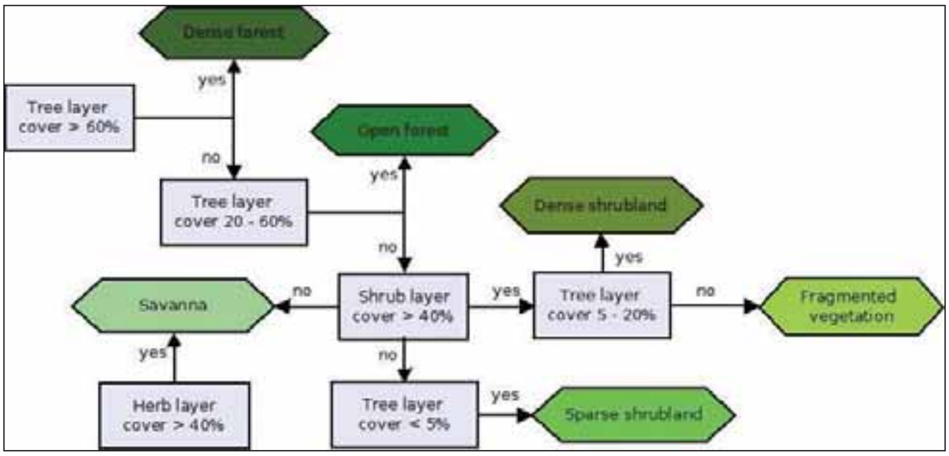

Figure 10: Definition of the land cover classes found in the study area based on vegetation structure.

Training samples selection

IRD provided a set of initial training samples, so called Regions of Interest (ROI), which were originally selected on a FORMATSAT-2 satellite image of 2010. It was however only partly possible to use these points for the classification due to two reasons: first of all, several points selected on the 2010 image were covered by clouds in the images of 2011 and 2012. Second of all, the satellite image of 2010 covered a different area extent than the images of 2011 and 2012, consequently numerous points were not lying within the same extent. Therefore, new points had to be collected.

In ENVI 4.8, on-screen selection of training samples was performed using the point application. With the help of a geologist, Isabelle Rouet, aerial photographs and a preliminary land cover map derived from the FORMOSAT-2 image, new training samples of homogeneous spectral reflectance were selected for each land cover class. Later on, additional points collected during two fieldwork phases were merged with the ROIs and used to improve the classifications.

Due to different phenological conditions, cloud cover and water levels of the river, two sets of ROIs were selected for each image, as seen in Table 7. Several points taken in the image of 2011 were covered by clouds in the image of 2012, additionally points for the class of water were areas of bare soil during the dry season. The amount of ROIs varies between the different classes, for some classes only 25 points were selected, while other classes have more than 100 points. This can be explained by the spatial distribution of the different land cover types over the areas. Some classes are larger in size, or were easier to identify than others, for example training samples for "Savannah" were easier to select than for the soil type "Dunite".

Class	No of pixels	
	2011	2012
Overburden	91	89
Bare rock	61	38
Dunite	27	27
Laterite	108	104
Ferruginous crust	63	107
Peridotite	67	83
Dense forest	125	149
Open forest	153	153
Dense shrubland	109	102
Fragmented vegetation	33	25
Sparse shrubland	98	63
Savanna	182	156
Water	138	87
Built up	37	37
Total	**1292**	**1220**

Table 7: Number of ROIs selected for the image classification.

First classification approach

Because prior knowledge about the study area existed, a supervised classification approach was applied. The images were separately classified using an implemented supervised classification approach in ENVI 4.8. A variety of the available classification methods (Parallelpiped, Minimum Distance, Mahalanobis Distance, Maximum Likelihood and Support Vector Machine) were run and their results compared to one another. The Support Vector Machine (SVM) classification method provided the best results and was therefore selected. An advantage of this classification algorithm is that it can obtain high results with relatively small numbers of training data points (Bishop, 2007; Pal and Mather, 2003). Preliminary land cover classifications were performed on the two images and validated during a first field work in November 2012.

Field work

During field work in November 2012 and December 2012 in the area of Poro, the preliminary land cover maps were validated and field data collection was carried out. Areas, which proved to be difficult to identify on the satellite images and the aerial photo, as well as areas affected by misclassification, were visited in order to gain more knowledge about their land cover. The aim of the field work was to visit as many locations as possible and to compare the results of the classification with the actual land cover on-site. For each land cover class points were taken with a global positioning system (GPS) and information about land cover type and estimation of vegetation cover were collected. Furthermore, photos of each point were taken to document specific features.

Several problems regarding the classification scheme were identified during the first field work, explaining why the initial classification scheme proposed by IRD was discarded and an adapted version of the scheme developed by OEIL was applied. Within the initial classification scheme different soil types were merged into one single class. During field work it became clear that this class had to be distinguished into three different soil types. Additionally, misclassifications were observed between roads and river beds in several locations, cloud cover caused further problems.

Second classification approach

Based on the identified problems in the field, clouds and cloud shadow, and roads were masked by manual digitalization in both images using ENVI 4.8. Additionally, the land cover classes were revised and the class combining several soil types was split into three separate classes, adapting the classification scheme proposed by OEIL.

Once the masking process was finished and the collected GPS points were integrated into the existing ROIs, a supervised classification was performed. Again, two different ROIs were used for the two images. Several algorithms included in ENVI 4.8 were tested and compared, and the most accurate classifier, the SVM classification, was selected. The land cover classification was separately performed on both images and validated again during a second field work period in December 2012. Further field data was collected and used to improve the classification.

Accuracy assessment of the classification

The final classification of the 2011 and 2012 images were first qualitatively evaluated by a local geologist, and then with a quantitative assessment. In most assessment approaches, the dataset is split into two sets, the training set which trains the classifier, and the test sets, which estimates the error rate of the trained classifier (Lu and Weng, 2007). Instead of splitting the dataset into training and validation sets, the accuracy assessment was carried out using a k-fold cross validation using the software R.

This approach was chosen because some classes were very small with only 25 points. Splitting these classes into training and test sets might have led to a reduction of the overall classification result.
In the k-fold cross validation the dataset is randomly split into k-equal size subsamples. One subset is used as validation data, while the remaining subsets are used as training data. This process is repeated k-times on N observations. Within the k-fold cross validation, N equals the observations considered in each fold. The advantage of this approach is that every subsample is being used as validation and training data respectively (Boissieu et al., 2009; Institute of Microbial Technology). A five-fold cross validation with 25 observations per class was applied to the classifications of 2011 and 2012. In this case N equals 25, the smallest amount of selected points of one land cover class. Four datasets were used to train, while one was used to test. This process was repeated five times to obtain a mean accuracy, see Figure 11.

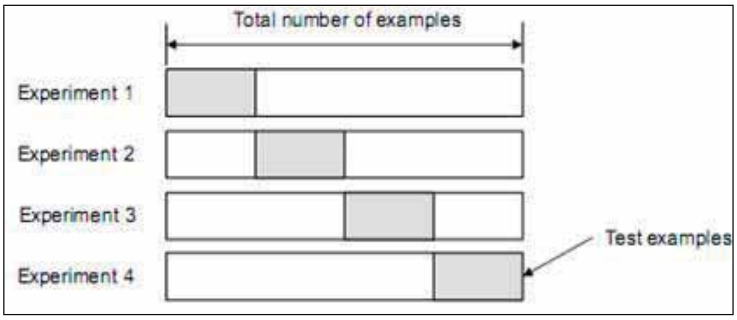

Figure 11: Process of the cross validation (Institute of Microbial Technology).

Potential problems with the land cover classification

Seasonal differences between the images made it difficult to exactly distinguish between sparse and dense vegetation. Furthermore, field data were collected in November and December, when the vegetation's growing stage is again different from the one in January. Additionally, it has to be kept in mind that the viewing angles were different and that atmospheric and weather conditions led to variations in colour and reflectivity in the image. All these factors might influence the overall classification results.

4.2 Land cover change detection

Re-classification of the land cover classes

Prior to performing the change detection on the two classified images, the 14 soil and land cover classes were reclassified. A change detection with 14 categories would result in 196 possible from-to change possibilities, which is cumbersome to analyse. Therefore, the change detection was performed on a broader level and the fourteen classes were reclassified into five major classes, as seen in Table 8.

Analysing changes between different soil types is difficult, consequently all soil classes were merged into the class “Bare soil”. Since the observed vegetation classes differ quite considerably in their density, two classes were created. Dense forest and open forest were merged into the class “dense vegetation”, while the classes of dense and sparse shrubland, fragmented vegetation and savannah were merged into the class “sparse vegetation”. The last two classes “water” and “built up” only changed the code but retained their old name because it was not possible to merge them with any of the other classes.

Original Classification		Re-classification	
Old code	**Class name**	**New code**	**New class name**
1	Overburden	1	Bare soil
2	Bare rock	1	Bare soil
3	Dunite	1	Bare soil
4	Laterite	1	Bare soil
5	Ferruginous crust	1	Bare soil
6	Peridotite	1	Bare soil
7	Dense forest	2	Dense vegetation
8	Open forest	2	Dense vegetation
9	Dense shrubland	3	Sparse vegetation
10	Sparse shrubland	3	Sparse vegetation
11	Fragmented vegetation	3	Sparse vegetation
12	Savannah	3	Sparse vegetation
13	Water	4	Water
14	Built up	5	Built up

Table 8: Reclassification of the original land cover classes.

Application of masks

The cloud cover masks of 2011 and 2012 were combined into one mask and applied to both classifications in order to avoid false changes. Additionally, the same was done with the road masks as these were manually and separately digitized for each image, resulting in a slight displacement between the two masks.

Change detection

The re-classified land cover maps of October 2011 and January 2012 served as input for the change detection process. A first change detection was performed for identifying statistical differences between the two classifications, using ENVI 4.8. The application “Change Detection Statistics” compiles a detailed tabulation of the changes between two classification images. The re-classified image of 2011 presented the initial state, while the re-classified image of 2012 presented the final state. The statistics output provided detailed information about occurred changes between classes in pixel count, percentage as well as in area size (km^2).

The output was exported into statistical software to analyse the changes between the two dates. The information about the direction and the amount the changes between initial and final class is however only available as statistical information. Consequently, a second change detection was performed to allow a spatial analysis of the change directions between the different classes.

In a second approach, the “Matrix union”, implemented in ERDAS IMAGINE 2011, was performed on the two classification files. The user obtains a detailed map, which allows a better understanding of spatial distribution of the changes. Additionally, a more detailed change detection matrix was calculated based on the information obtained from both processes.

Potential problems with the change detection

As mentioned, the two images were acquired during different times of the year, the different phenological conditions might thus have resulted in false changes. Additionally, errors within the classification, for example due to the different viewing angle, need to be kept in mind when analysing the results.

4.3 Modelling soil erodibility with the Revised Universal Soil Loss Equation (RUSLE)

The Revised Universal Soil Loss Equation (RUSLE) was selected from a variety of erosion models to spatialise soil erodibility. Most erosion models require large amounts of input data, which is not always available, especially in a data poor region such as New Caledonia. Previous research on erosion in New Caledonia was conducted using USLE, which provided important information concerning the input parameters, explaining the choice of the model.

The Universal Soil Loss Equation (USLE), an empirical model, developed by Walter H. Wischmeier and Dwight David Smith in the 1960s in the United States, predicts long term average annual rate of soil loss due to sheet and rill erosion. Due to its simplicity and low data requirements, it is one of the most used model in the world (Aksoy and Kavvas, 2005; Merritt et al., 2003). Input parameters require information on rainfall, soil erodibility, topography, land cover, and support practices. The model was later on reviewed and adjusted, resulting in the Revised USLE (RUSLE). The Revised Universal Soil Loss Equation (RUSLE) remains the basic structure of the original model USLE, but incorporates new technologies to calculate the input parameters (Renard et al., 1997).

The RUSLE equation, as seen in Equation 1, is composed of six different factors, which are multiplied to obtain the annual soil loss (A), given in ton per hectare and year per unit area. As the original model is expressed in U.S. imperial units, it was converted to the International system of Units (SI metric system) (Foster et al., 1981).

$$A = R * K * C * LS * P$$ Equation 1

Where:

A: Annual average soil loss [$t.ha^{-1}.yr^{-1}$],
R: Erosivity factor [$MJ.mm.ha^{-1}.h^{-1}$],
K: Soil erodibility factor [$t.ha.h.ha^{-1}.MJ^{-1}.mm^{-1}$],
C: Factor of vegetation cover, [dimensionless],
LS: Slope angle [%] and slope length [m],

P: Factor related to soil conservation practices [dimensionless].

The result is a map, in which soil loss is calculated for each pixel of the grid, expressed in [$t.ha^{-1}.yr^{-1}$]. This is however only feasible when all factors are constant. In the case of the present study, measurements of rainfall vary significantly over the years of measurements (2009–2012) as seen in Appendix D. Due to technical problems only two events were measured in 2010, while there were 20 measurements in 2011. It was consequently decided to exclude the factor R, explaining why soil erodibility was modelled rather than calculating the potential soil loss. Due to lack of information on support management within the study area, the factor P was excluded as well.

When assuming that the layers K, LS and C are constant, it is possible to spatialise potential soil erodibility in the watershed. By combining the factors of soil (factor K), slope length and steepness (factor L and S) and vegetation cover (factor C), according to the RUSLE equation, an index is obtained, which expresses soil erodibility in [$t.ha.h.ha^{-1}.MJ^{-1}.mm^{-1}$].

4.3.1. Definition and calculation of the input parameters

The following sections give a short definition of each input parameter of the RUSLE Equation as well as the way of deriving them for this research, the process is presented in Figure 12.

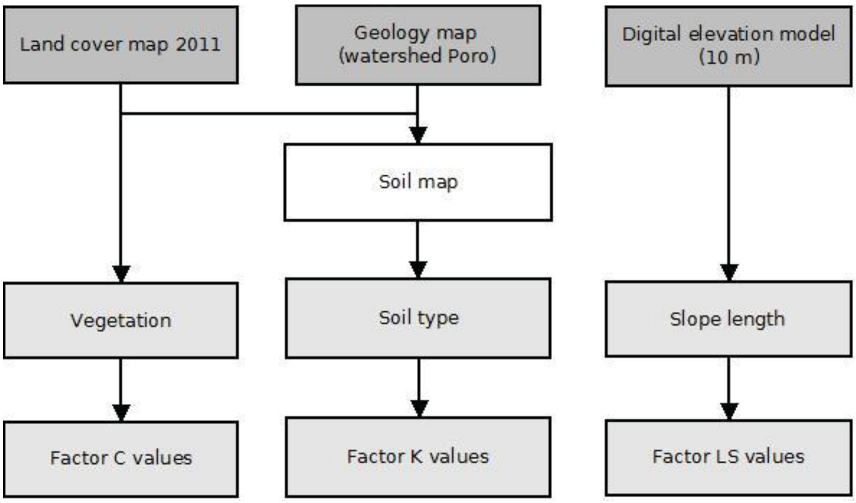

Figure 12: Process of deriving the input parameters for the soil erodibility index.

Definition - Soil erodibility factor (K)

The factor R represents the sensitivity of different soil types to erosion by precipitation, expressed in $t.ha^{-1}$ lost by $MJ.mm.ha^{-1}.h^{-1}$. The factor ranges between 0 to 1, 0 being non-erodible and 1 highly erodible. Soils differ in their resistance to erosion as a result of different texture, structure, soil moisture, organic matter content, as well as permeability (Wischmeier and Smith, 1978). Several methods to estimate the K factor values exist, the approach proposed by Wischmeier and Smith (1978) is considered as the most common one. This approach is based on Equation 2, which can be applied for soils that have a silt content of 70 % or less, and particle sizes ranging from 0.1 – 0.002 mm (Renard et al., 1997). Information on percentages of sand, fine sand and clay, organic matter content, structure of soil and permeability are required to calculate soil erodibility. Soil structure and permeability are defined according to Table 9.

$$K = \left(2.1M^{1.14}10^{-4}(12 - a) + 3.25(b - 2) + 2.5(c - 3)\right)0.1317/100$$

Equation 2

Where:

M: (% silt + % very fine sand) (100 - % clay),
a: Organic matter content (%),
b: Soil structure,
c: Permeability.

Code	Permeability
1	Very slow
2	Slow
3	Slow to moderate
4	Moderate
5	Moderate to rapid
6	Rapid

Code	Soil structure
1	Very fine granular
2	Fine granular
3	Medium to coarse granular
4	Blocky, platy or massive

Table 9: Codes of soil structure and permeability (Wischmeier and Smith, 1978)

Calculation - Soil erodibility factor (K)

As there is no detailed up-to-date soil map for the study area in New Caledonia, the soil erodibility factor K was derived from two maps: a geological map of the watershed and the detailed soil and land cover classification of 2011 with 14 classes.

The geological map was considered to be the more accurate because of its complete validation in 2012, it thus served as the primary data source for the K factor definition in the watershed. Since the geological map does however not cover the entire watershed, missing areas were filled with data derived from the soil and land cover classification. The classification of 2011 was chosen to assess whether soil erodibility contributed to changes in land cover.

Based on the combination of these two maps, different soil types were identified in the watershed, seen in Table 10. These classes were then re-classified into three major soil classes based on tables by L'Huillier et al. (2010). Not all soil classes were however included in the further process due to the following reasons:

- Detailed information was not available for “Peridotite (dominant)”. It was not possible to completely determine the exact soil type in the field as it includes different types, further research is needed.
- Soil types containing no particles smaller than 2 mm are hardly affected by erosion and thus not considered in the model.

Soil type	Soil class
Laterite	Ferrasols, horizon 0 - 15 cm
Plinthosols on peridotite (clay loam)	
Overburden	Ferrasols, horizon 45 - 50 cm
Saprolite	
Ferruginous crust	Altered ferritic and ferralitic soils, horizon 0 - 15 cm
Plinthosols on peridotite (loamy sand)	
Haplic Cambisols	Cambisols / tropical eutrophic brown soils, horizon 0 - 5 cm
Bare rock	Not considered (few or no particles smaller than 2 mm)
Dunite	
Peridotite I	
Peridotite II	Needs to be evaluated in the field

Table 10: Reclassification of soil classes.

The equation proposed by Wischmeier and Smith (1978) requires information on the percentage of clay, silt and sand content, as well as the percentage of organic matter, which were derived from L'Huillier et al. (2010). Soil structure and permeability were empirically determined. Validation of these codes is required, but due to time constraints this was not possible.

Overall, three soil classes were defined, ferrasols, altered ferritic and ferralitic soils, as well as cambisols, and their K-factor values were calculated according to Equation 2. The final K-factor values are presented in Table 11.

Soil		Texture class	K factor value (Wischmeier)
Ferralsols	Horizon 0-15 cm	Clay loam	0.0376
	Horizon 45-50 cm	Sandy clay loam	0.0448
Altered ferritic and ferralitic soils		Loamy sand	0.0208
Cambisols / Tropical eutrophic brown soils, hypermagnesic		Clay	0.0114

Table 11: K-factor values (according to the Wischmeier and Smith approach) and texture classes of the three soil classes.

Based on these values, the spatial distribution of the K factor was computed, resulting in a raster map with a 5m resolution, seen in Figure 13. Classes with a value of zero (0) correspond to soils that are hardly erodible, such as bare rock, or soils that contain only few or no particles smaller than 2 mm. Most of the watershed has a K factor between 0.0376 and 0.0448 $t.ha^{-1}$ / $MJ.mm.ha^{-1}$. h^{-1}. Erodibility occurs in an ascending order: first ferralsols (horizon 45-50 cm) being the most erodible layer with a value of 0.0448, then followed by ferralsols (horizon 0-15 cm) with a value of 0.0376, thirdly ferralsols with a value of 0.0208, and finally cambisols with a value of 0.0114.

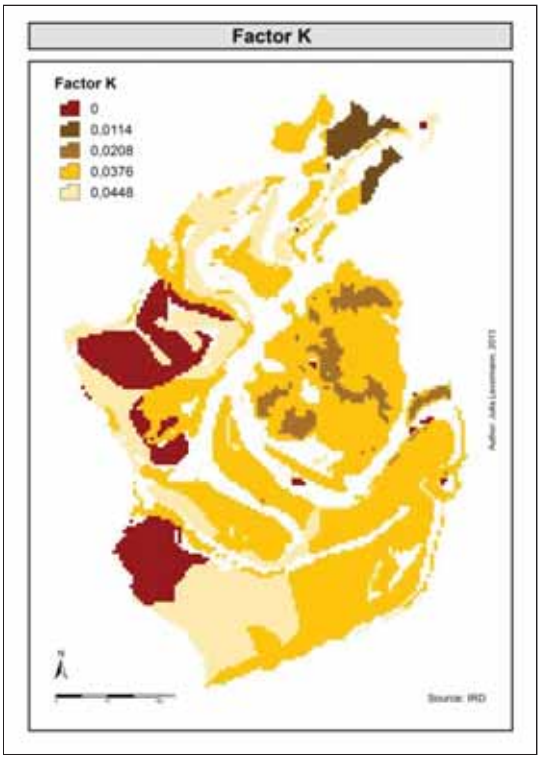

Figure 13: K-factor values in the watershed.

Definition - Cover and management factor (C)
The factor C represents land cover, which limits the impact of rainfall on the soil. The C-factor depends among others on the density of coverage, canopy height, density of the lower strata and the humus coverage. It ranges from 0 to 1, 0 being a completely covered ground, and 1 being bare soil (Mazour and Roose, 2002; Wischmeier and Smith, 1978). Different ways to determine vegetation cover exist, for example by mapping land cover based on digital image classification or the interpretation of aerial photographs. C-factor values are then assigned to each land cover map, either based on previous research or derived from literature. Furthermore, the C-factor value can be calculated as a function of height and percentage of vegetation cover using nomographs, such as the one proposed by Roose (1994) seen in Appendix E.

Calculation – Cover and management factor (C)

The soil and land cover map with 14 classes derived from the supervised classification of the 2011 RapidEye image served as the major source for the definition of the C-factor. Out of the 14 land cover classes, six were vegetation classes:

- Dense forest,
- Open forest,
- Dense shrubland,
- Sparse shrubland,
- Fragmented vegetation, and
- Savannah

Since most of the flora in New Caledonia is endemic, no useful literature was found to determine C-factor values. Thus, values between 0 and 1 were assigned to the different vegetation classes based on previous researches conducted by Bui-Duyet (2011) and Printemps (2007). Areas with sparse or no vegetation cover represent the greatest vulnerability to erosion and consequently have a high C-factor, while areas of dense vegetation cover, such as forests, limit the erosion process and were assigned a low value. Table 12 provides an overview of the land cover classes, the assigned C-factor value and the source on which the value is based.

Class	C-factor value	Source
Dense forest	0.001	Forêt, (Bui-Duyet, 2011)
Savanna	0.04	Savane, (Bui-Duyet, 2011; Printemps, 2007)
Open forest	0.058	Reboisement dense, (Sadiki et al., 2004)
Dense shrubland	0.21	Matorral très dégradé , (Sadiki et al., 2004)
Fragmented vegetation	0.32	Steppes à alfa, (Sadiki et al., 2004)
Sparse shrubland	0.72	(Printemps, 2007)

Table 12: C-factor values.

The spatial distribution of the C-factor is quite heterogeneous, as seen in Figure 14. Vegetation is only found in a small area of the watershed, while bare soil represents most of the area due to the mining activities. Since the protective vegetation cover is missing, these parts have the highest C-factor value. Out of the six different vegetation types identified for the overall study area, only three can be found in the watershed: dense shrubland, fragmented vegetation and sparse shrubland.

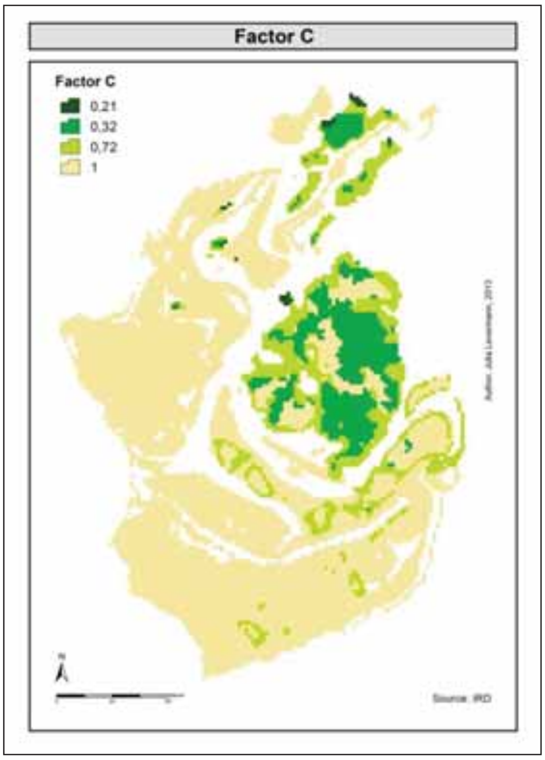

Figure 14: C-factor values in the watershed.

Definition - Slope length and steepness factor (LS)
The factor LS introduces the effect of slope angle and slope length into the model. L characterizes the length of the slope and S its angle. The longer the slope, the greater the amount of cumulative runoff, and the steeper the slope, the higher the velocity of the runoff, which contributes to erosion (McCool et al., 1987).

Calculation - Slope length and steepness factor (LS)
A common approach to derive slope length and slope angle is by applying an Arc Macro Language (AML) script under the software ArcInfo, which was however not available during the research. An alternative approach was chosen, in which the factor LS is calculated based on a recently proposed algorithm developed by Zhang et al. (2013). The layer LS is derived by using their free software, LS-TOOL, which is based on the formulation by McCool et al. (1989), Desmet and Govers (1996) and Remortel et al. (2004). The programme applies an algorithm, which requires a cumulative area threshold, and a DEM in ASCII format as input. A 10 m DEM was used

was input, all other settings retained their default settings. The final raster layer is presented in Figure 15.

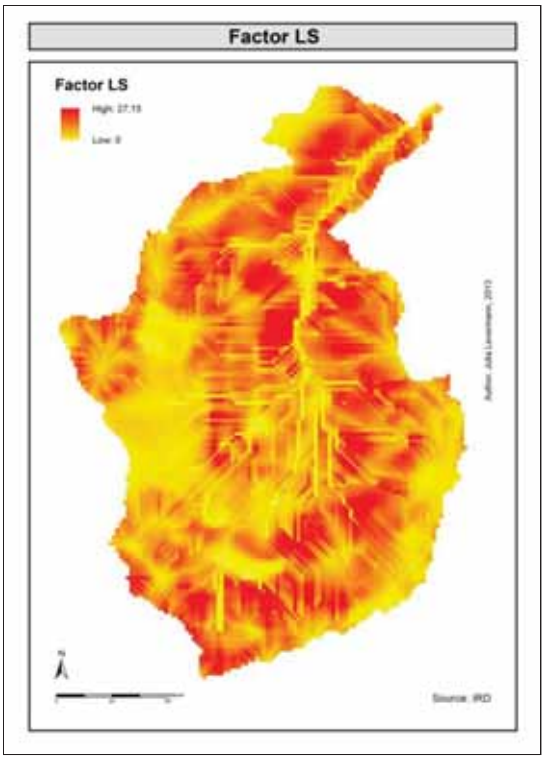

Figure 15: LS-factor values in the watershed.

Calculation of the soil erodibility index

In the last step, the three raster layers of soil, vegetation and slope were multiplied according to Equation 3 to derive a soil erodibility index, expressed in [$t.ha.h.ha^{-1}.MJ^{-1}.mm^{-1}$] for the small watershed.

$$K\ (soil) * C\ (vegetation) * LS\ (slope) = soil\ erodibility\ index$$

Equation 3

5 Results and analysis

5.1 Land cover classification

Spatial distribution of soil and land cover

The supervised classification process, based on the two RapidEye images of October 2011 and January 2012, resulted in two soil and land cover maps with 14 distinguished categories, which are presented in Figure 16 and Figure 17. As seen in the Figures below, the spatial distribution of soil and land cover is similar in both images. The two mines in the north are clearly visible in the maps. These areas are predominantly covered by overburden, bare rock, peridotite, laterite, ferruginous crust and dunite, displayed in yellow and brownish colours. Built up areas, in red, are located at the coast in the north between the two mines. Areas of higher altitude are found towards the central part and are vegetated by open forest, while areas of lower altitude, in the east, are covered by fragmented vegetation. Savannah covers the riparian areas along the Koua River in the south-east. It is apparent that vegetation cover becomes denser towards the south. Dense forest, displayed in dark green, is mostly found on steep slopes in the south-east, an area undisturbed by anthropogenic activities.

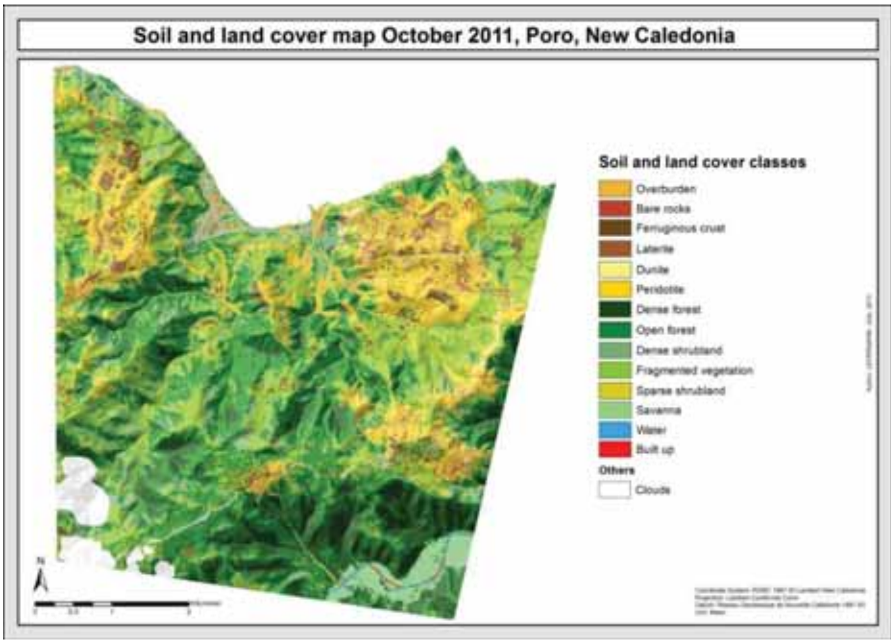

Figure 16: Soil and land cover classification of Poro, October 2011.

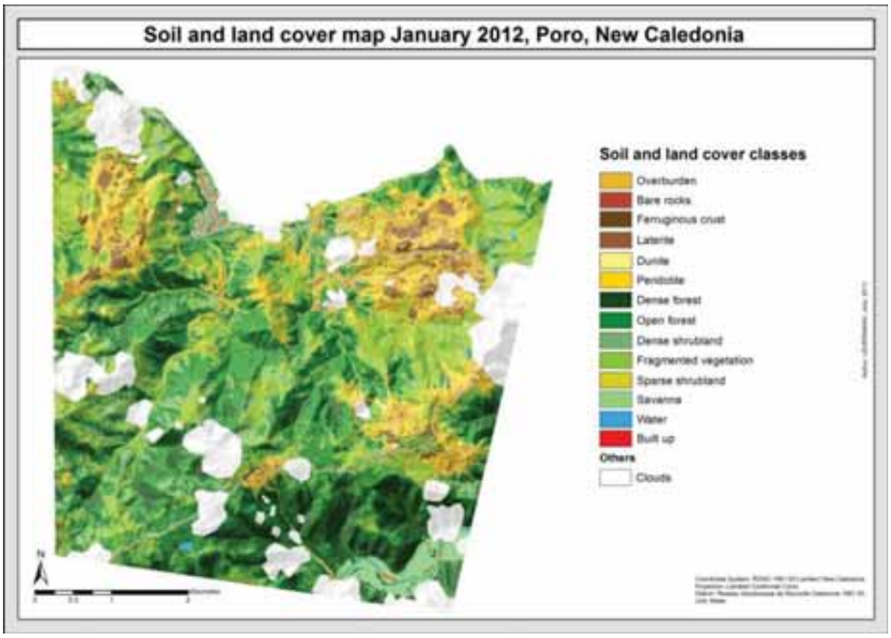

Figure 17: Soil and land cover classification of Poro, January 2012.

Area statistics of land cover classes

Area statistics, which were derived from the land cover maps, are illustrated in Figure 18, and in a more detailed Table 16 in Appendix F. As the second image was acquired during the wet season, it is affected by more cloud cover, the total classified areas of both images consequently differ. While the total classified area of 2011 accounted for 31.02 km², the classified area of 2012 was slightly smaller with 27.68 km². Consequently, Figure 18 does not indicate changes between the two dates.

As shown in Figure 18, the class of “Open forest” was the most dominant land cover class for both dates, representing 28% (2011) and 27% (2012) of the total area. The second major land cover class, “Fragmented vegetation”, covered an area of 6.8 km² in 2011 and 6.2 km² in 2012. Water, built up and dunite were the smallest land cover categories for both dates. Most of the study area was covered by vegetation. In 2011, 25.02 km² of the total area of 31.02 km² was covered by vegetation, and in 2012, 21.86 km² of the total area of 27.68 km² was covered by vegetation. The different soil types only covered small areas each, but considered together as one class of bare soil it covered an area of 5.8 km² and was thereby almost as large as the area of fragmented vegetation.

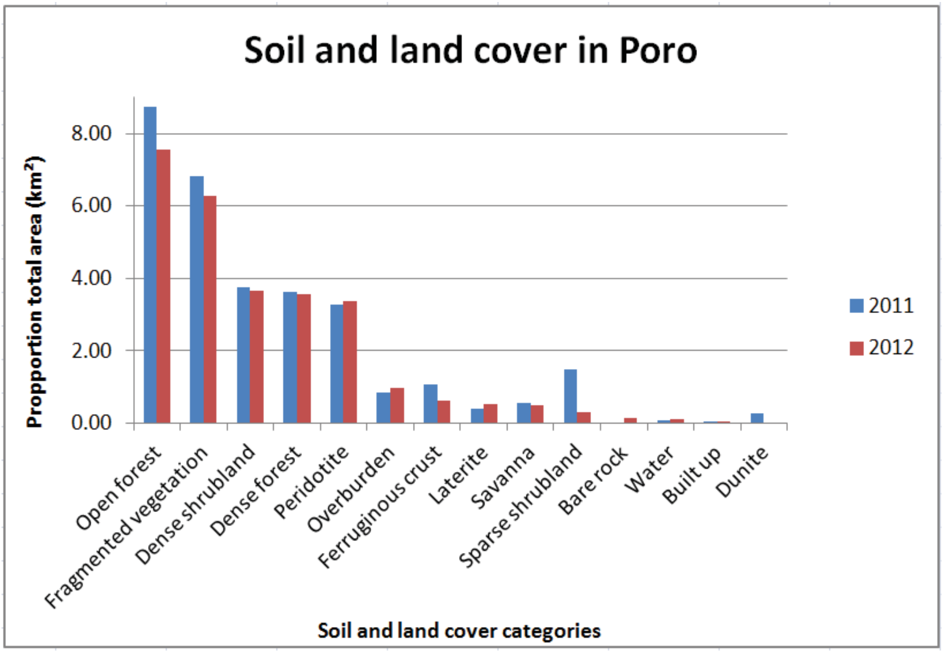

Figure 18: Proportion of land cover classes in 2011 (blue) and 2012 (red) in Poro.

Accuracy assessment

A five-fold cross-validation was performed on the dataset to evaluate the accuracy of the support vector machine classifier. The training, test and overall accuracy are presented in Table 13 the according confusion matrices for 2011 and 2012 can be found in Appendix G. Both images achieved overall accuracies of more than 90 %, according to Ismail and Jusoff (2008) an image classification is acceptable if the accuracy assessment has a level of 85 %. By masking irrelevant features, such as clouds and cloud shadows, significant spectral confusion was avoided. It was possible to distinguish between the 14 soil and land cover categories and no major difficulties occurred due to the large amount of classes. The terrain did not pose any problems as the images were geometrically corrected. Points collected in the mountainous terrain were all correctly classified. The expected problems due to the large amount of land cover classes did not appear. All categories were successfully distinguished. As it was easier to distinguish between bare soil and vegetation during the wet season in 2012 than during the dry season in 2011, the overall accuracy for the classification of 2012 is 93.06 %, while it is 92.25 % for the image of 2011. However, occasional spectral confusion was observed because of seasonal differences between the image acquisition dates and the field data collection.

	Training (%)	Test (%)	Average accuracy (%)	Overall accuracy (%)
2011	93,45 +- 0,7	91,43 +- 1,5	92,97	92,25
2012	92,49 +- 0,7	90,29 +- 1,6	92,53	93,06

Table 13: Accuracy assessment results.

As seen in the confusion matrix in Appendix G, the classes of water and ferruginous crust, as well as ferruginous crust and fragmented vegetation in the classification of 2011 were affected by spectral confusion. Within the classification of 2012, spectral confusion was limited to the categories of dense and open forest. In order to understand why spectral confusions occurred, spectral signatures of the concerned classes were analysed. Figure 19 displays spectral reflectance curves of five different land cover classes. The x-axis corresponds to the wavelength range, while the y-axis displays reflectance in percentage.

As mentioned in sub-section 2.1., land cover types can be distinguished based on their spectral properties as they differ in reflection and absorption at different wavelengths (Liew, 2001; Vrieling, 2006). Consequently, it is easy to distinguish bare soil from dense vegetation as their reflectance is significantly different. As seen in the Figure below, the spectral signature of laterite (bare soil) differs from the one of dense forest (vegetation). While the reflection of dense forest is low within the blue and red bands and peaks in band five (near-infrared, 760-850 nm), the reflectance of laterite increases with increasing wavelength. The spectral reflectance of bare soil depends on its soil composition, while the one of vegetation depends on the content of leaf moisture and the plant's health. Different soil and vegetation types have consequently different spectral reflectance curves (Liew, 2001; Vrieling, 2006). This becomes clear when looking at the spectral properties of different soil types and vegetation densities in Figure 19.

The class fragmented vegetation is made up of the plant "Fougère", which is a fern-like type of vegetation. During the dry season, it turns completely grey, as seen in Figure 35 in Appendix C, and its leaf moisture is low. Its spectral reflectance is consequently different from dense forest but very similar to the one of ferruginous crust. This overlap within spectral reflectance leads to confusion within the two classes and they are misclassified.

Variations in colour and reflectivity due to atmospheric and weather conditions, as well as the viewing angle contribute to this spectral confusion. Although variations in colour and reflectivity have been reduced to the best possible during the image pre-processing, it is highly likely that they have affected the overall results of the image classification.

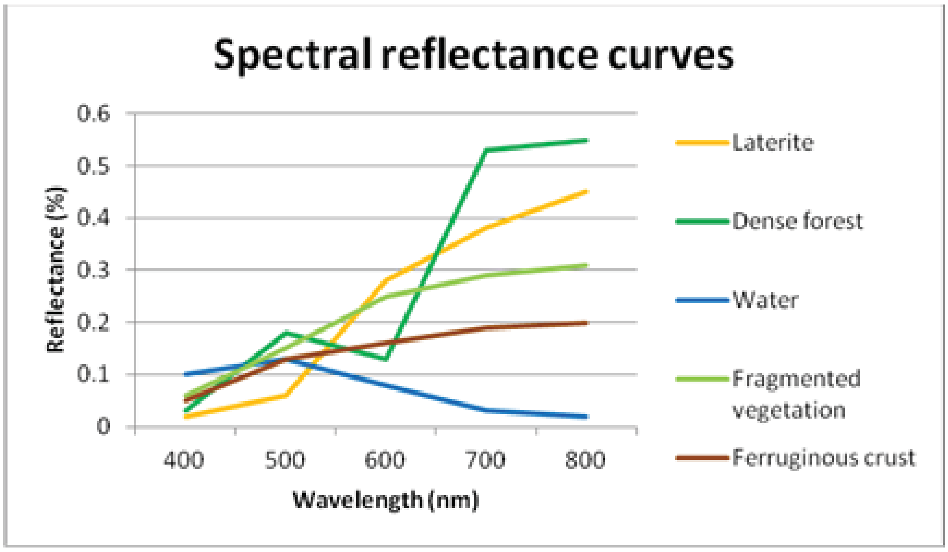

Figure 19: Comparison of spectral profiles.

5.2 Land cover change detection

In the following, the final results of the land cover change detection are presented. Firstly, areas affected by changes in general are quantified, followed by the assessment of change directions and change dynamics.

General land cover changes
The post classification comparison, based on the merged soil and land cover maps presented in Figure 38 in Appendix H, resulted in a map of general changes presented in Figure 20. The spatial distribution shows that changes, displayed in red, occurred over the entire study area.

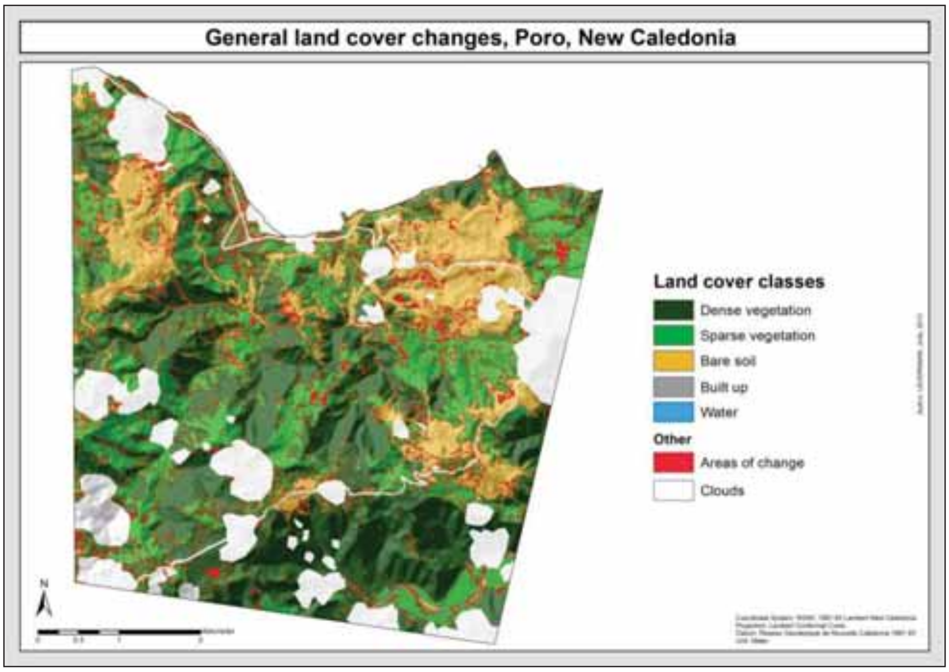

Figure 20: General land cover changes in Poro, New Caledonia.

Area statistics

In the next step, area statistics of the land cover categories were derived from the merged land cover maps. The results are presented in Figure 21, and Table 19 in Appendix I. Figure 21 provides a general comparison of the distribution and size of the different classes over the study area in October 2011 and January 2012, while Table 19 in Appendix I gives more detailed information about net change and growth. Changes including the class of “Built up” were excluded, given that these are very unlikely within such a short period of time.

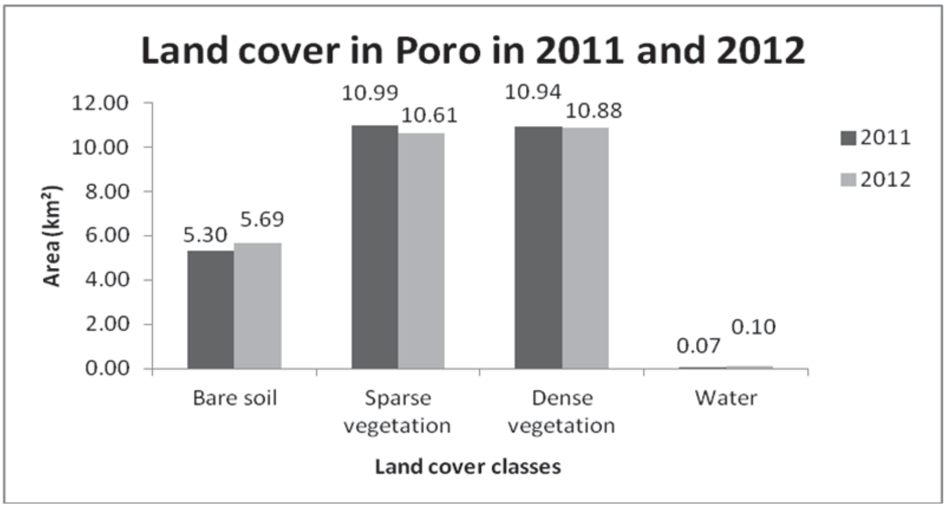

Figure 21: Proportion of different land cover classes in Poro in October 2011 and January 2012. The labels indicate the area in km² for each class.

As it can be seen from Figure above, all land cover classes were affected by change. Dense and sparse vegetation were the dominant land cover types in October 2011 and January 2012 and covered about 80% of the study area together. Both declined over the observed time period by 0.38 km² and 0.06 km² respectively. Nevertheless, they remained the dominant cover types in 2012. While sparse vegetation covered a larger area than dense vegetation in 2011, it was the other way around in 2012. Bare soil and water on the other hand slightly increased. Bare soil furthermore registered the largest increase with 0.39 km², while sparse vegetation was the class that experienced the largest decline with -0.38 km². Water registered the largest growth with almost 43%, as it increased from 0.07 to 0.10 km².

Change detection matrix

Figure 21 and Table 18 quantify the extent of land cover change between October 2011 and January 2012. However, they do not provide detailed information about the direction and dynamics of the observed changes. Only looking at net changes can lead to false conclusions as it does not consider inter-class changes. A class might have only registered a small net change, but this does not mean that no significant change dynamics occurred. It might have registered a loss in one location and experienced a gain somewhere else, neutralizing the loss. As these change dynamics are not apparent from the land cover statistics, it is important to analyse change directions and dynamics by establishing a change matrix. The results are presented in Figure 22, and Table 20 in the Appendix J. As mentioned above, the class of built up areas was excluded, the remaining four classes resulted in 16 possible change combinations. Changes within one land cover were not considered in the analysis and changes between dense vegetation and water were not observed, resulting in ten possible “from-to” change combinations.

The detailed “from-to” change combinations, in km^2, are given in Figure 22. Sparse vegetation, which covered about 40% of the study area in 2011, is the most dynamic classes. It experienced gains and losses of 3.6 km^2. While it lost almost 2 km^2 to bare soil and dense vegetation, it also gained 1.58 km^2 from the same two classes, resulting in a final area of 10.6 km^2. A decline in sparse vegetation was predominantly observed in areas close to the mines in the north of the study area. Furthermore, the steepness of the slopes must have contributed to the decline, as changes were often found in areas with steep gradients. Dense vegetation and bare soil on the other hand were more stable and only registered gains and losses of about 1.8 km^2 each. Bare soil, which registered the largest overall increase from October to January, lost an area of 0.71 km^2, mostly to sparse vegetation. In other locations it however gained 1.11 km^2 from other land cover classes. Changes from bare soil to sparse vegetation were registered all over the study area. Dense vegetation, the second largest land cover class with a total area of 10.94 km^2 in 2011, registered a decrease of -0.06 km^2 until 2012. While it gained 0.87 km^2 from sparse vegetation, it however also lost 0.93 km^2 to the same class, which resulted in an overall decrease of dense vegetation. The change from sparse vegetation into dense vegetation was predominantly found in the south-west of the study area and along the coast, while the degradation from dense to sparse vegetation mainly occurred closer to the mining areas. Areas covered by water accounted for 0.07 km^2 in 2011, but due to gains, such as of bare soil into water, it increased by 0.03 km^2 to 0.1 km^2 in January 2012. Changes from bare soil into water were restricted to the areas of the water bodies in the study area.

Based on the change detection matrix, a simplified “from-to” change detection map (Figure 23) was derived, which only focuses on the conversion to bare soil, to water and to vegetation. Changes were not predominantly located in one area but found all over the study area in Poro. Large parts of stable areas are located in the south-east, which is covered by dense forest. Areas of vegetation reduction on the other hand were mostly located close to the mines, while areas of vegetation increase were predominantly found in the central part.

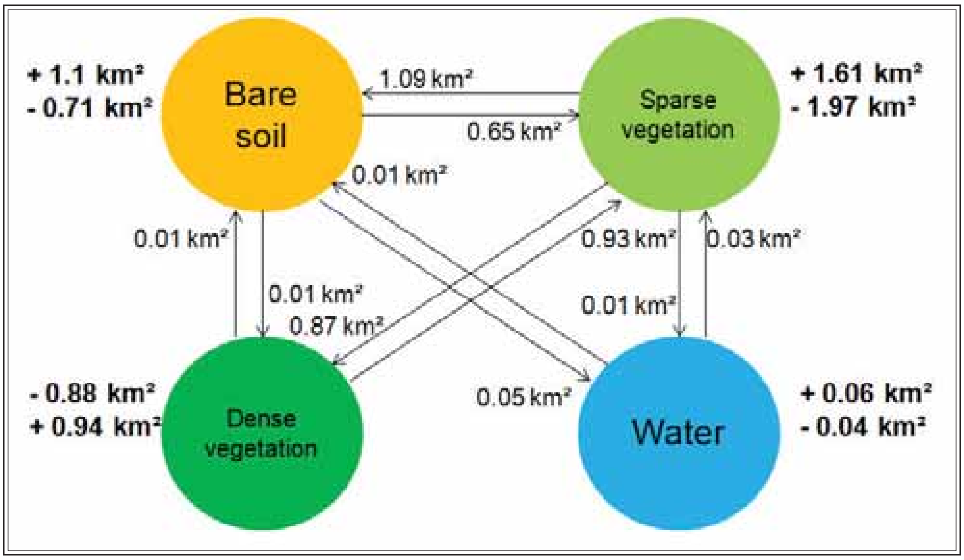

Figure 22: Change matrix of land cover changes between October 2011 and January 2012, units in km².

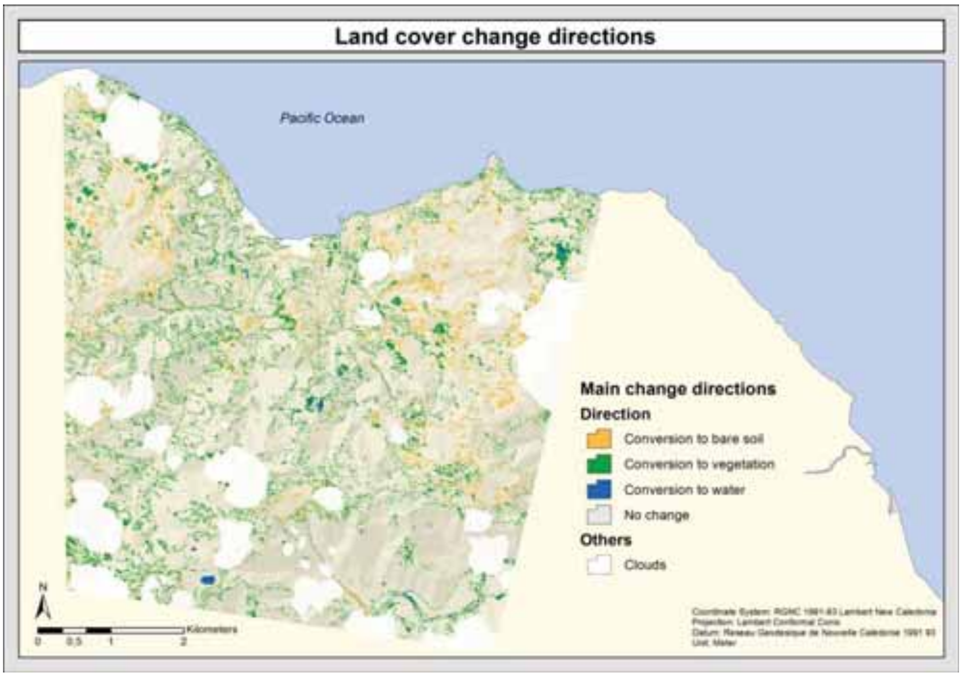

Figure 23: Main land cover changes in the study area.

Assessment of the observed land cover changes

In order to fully exploit information about change directions and dynamics, external factors, which might have affected the change detection procedure and results, need to be taken into consideration. As it is likely that external factors introduced errors into the overall results, it is necessary to analyse the nature of the observed changes. Not all observed changes are logical, such as the change from water to bare soil and vegetation, thus changes were grouped into two categories:

- Actual land cover changes, and
- Detected changes, which are due to external factors.

As expected, the different acquisition dates of the imagery affected the results of the change detection. The phenology of vegetation and water levels in rivers were visibly different between the two images. The transitions from bare soil to sparse and dense vegetation, as well as the change from sparse to dense vegetation, are considered as consequences of different phenological conditions. Changes from bare soil to water are furthermore results of seasonal differences between the two dates, an example is presented in Figure 24. These changes should therefore not be regarded as real land cover changes as they are annually occurring changes.

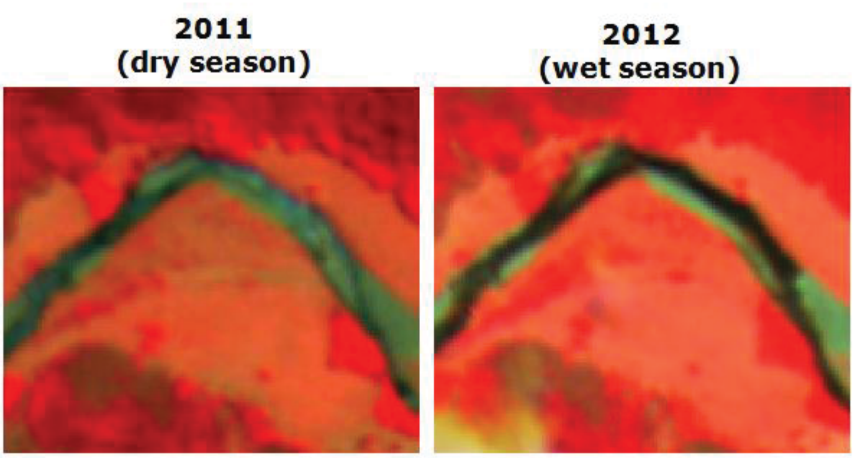

Figure 24: Example of the seasonal change from bare soil to water in the Koua River (displayed in false colour composite).

The changes from bare soil to sparse vegetation, and sparse to dense vegetation however also often followed a systematic pattern, occurring along the edge of the particular two classes. During the analysis a shift of one pixel between the two images was observed, an error which might have occurred during the image registration process (Foody, 2002). Consequently, the observed changes might as well have occurred because of this registration error. The change from bare soil to sparse vegetation might in addition be related to the observed misclassifications. It is difficult to determine the exact factor which caused this change, but in any case these changes should not be considered as actual land cover changes.

According to the change matrix, 1.09 km^2 of sparse vegetation changed into bare soil in the study area, two examples are given in Figure 25. The images in the top row present the situation of October 2011, while the images in the bottom row present the situation of January 2012. The images are displayed in false colour composite as this makes it easier to detect vegetation (red) and bare soil (green). According to example (1), an erosion scar occurred within the period of October 2011 to January 2012. In example (2) an area of bare soil is clearly visible at the end of a small creek in the second image. Measuring the extent of the erosion scar in example (1) showed that its width stayed the same. Example (1) can consequently be considered as a false land cover change, while example (2) presents an actual change in land cover. This illustrates the difficulty of distinguishing between actual and false land cover changes.

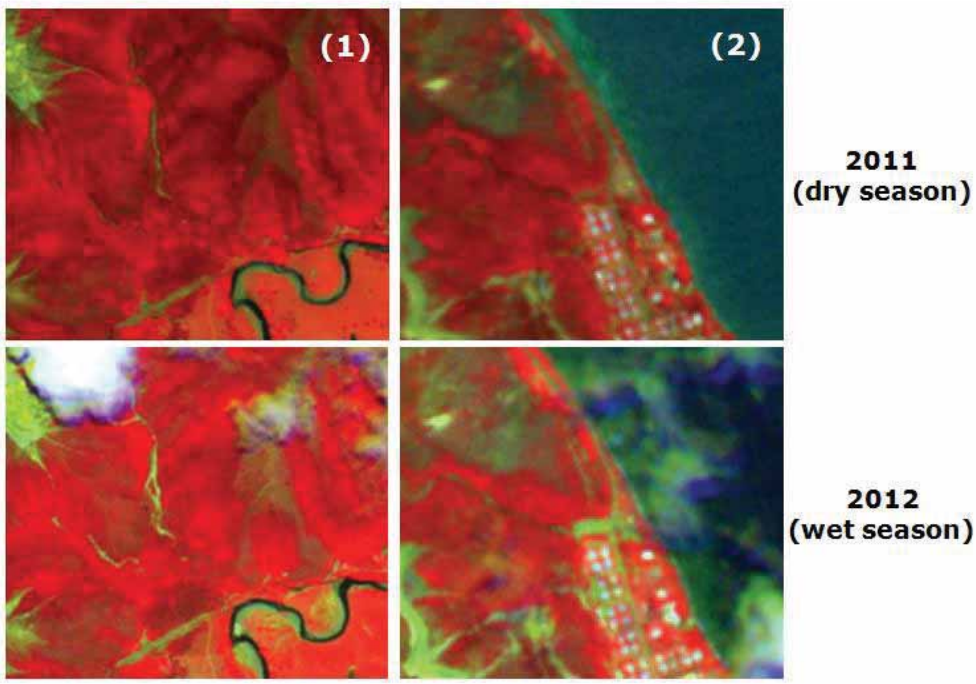

Figure 25: Examples of a (1) false land cover change and (2) actual change between sparse vegetation to bare soil (displayed in false colour composite).

The changes from water to bare soil, water to sparse vegetation and sparse vegetation to water are highly unlikely and most likely occurred due to errors within the classification.

Table 14 classifies the land cover changes into the two categories of actual and false changes. This table should be interpreted with caution as it is difficult to finally determine the driver of each land cover change. The change from sparse vegetation to bare soil for example can be classified either as an actual land cover changes that occurred due to natural or anthropogenic drivers, but on the other hand it might as well be a consequence of the different viewing angles between the images. The table remains very theoretical and requires further research and validation.

Category	From-to	Possible explanations
Actual land cover changes	Sparse vegetation to bare soil	Natural pressure (trop. depression)
		Human activities (mining)
	Dense vegetation to bare soil	Natural pressure (trop. depression)
		Human activities (mining)
	Dense vegetation to sparse vegetation	Natural pressure (trop. depression)
		Human activities (mining)
"False" land cover changes	Sparse vegetation to bare soil	Viewing geometry
		Atmospheric composition
		Time of the year (sun angle)
	Dense vegetation to sparse	Accuracy of image classification
	Bare soil to sparse vegetation	Seasonal differences (vegetation phenology)
		Accuracy of image georeferencing
		Accuracy of image classification
	Bare soil to dense vegetation	Seasonal differences (phenology)
		Accuracy of image classification
	Bare soil to water	Seasonal differences (water level)
	Water to bare soil	Accuracy of the image classification
	Water to sparse vegetation	Accuracy of the image classification
	Sparse vegetation to water	Accuracy of the image classification
	Sparse vegetation to dense vegetation	Seasonal differences (phenology)
		Accuracy of image georeferencing

Table 14: Factors that might have affected the change detection results.

5.3. Soil erodibility modelling

Soil erodibility was estimated by taking into account soil type, vegetation cover and slope. As seen in Figure 26, the watershed can be divided into four classes of soil erodibility: none, low, medium and high.

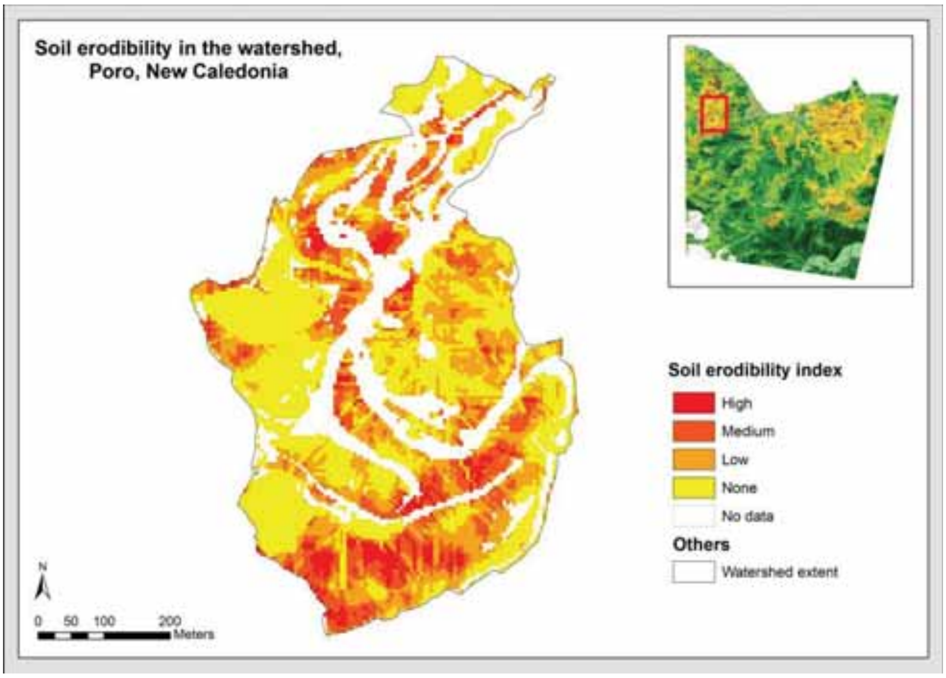

Figure 26: Soil erodibility in the watershed in Poro.

For certain areas it was not possible to determine the exact soil type, these areas correspond to “no data” areas and are displayed in white. Areas which are the least sensible to soil erodibility, displayed in yellow, correspond to classes, such as dunite and peridotite, where no erosion occurs as their particle sizes are bigger than 2 mm. They are therefore assigned a value of KCLS = 0. Low erodibility, displayed in light orange, occurs in areas with sparse vegetation cover on moderately steep slopes and soil types, such as cambisols, ferruginous crust and plinthosols. These soils have high silt contents and are therefore more resistant to erosion. Areas displayed in dark orange and red correspond to medium and high erodibility. Here, areas of sparse or no vegetation cover coincide with steep slopes and soils such as laterite and saprolite. These soils have higher silt amounts compared to the other soil types in the watershed and are thus more vulnerable to erosion (Morgan, 2005). This map has not been calibrated with field measurements and should only be regarded as a qualitative assessment.

The watershed was affected by three types of land cover changes: bare soil to water, bare soil to sparse vegetation and sparse vegetation to bare soil, as seen in Figure 27. Bare soil to sparse vegetation can be considered as a natural change, which occurs when the wet season sets in. The change from bare soil to sparse vegetation occurred either because of phenological changes or is observed due to misclassification. It can be assumed that soil erodibility did not have influence on these two changes. It is however highly likely that soil erodibility contributed to the change from sparse vegetation to bare soil. But given the uncertainties regarding the change detection and soil erodibility modelling, it is difficult to determine whether soil erodibility contributed to this change.

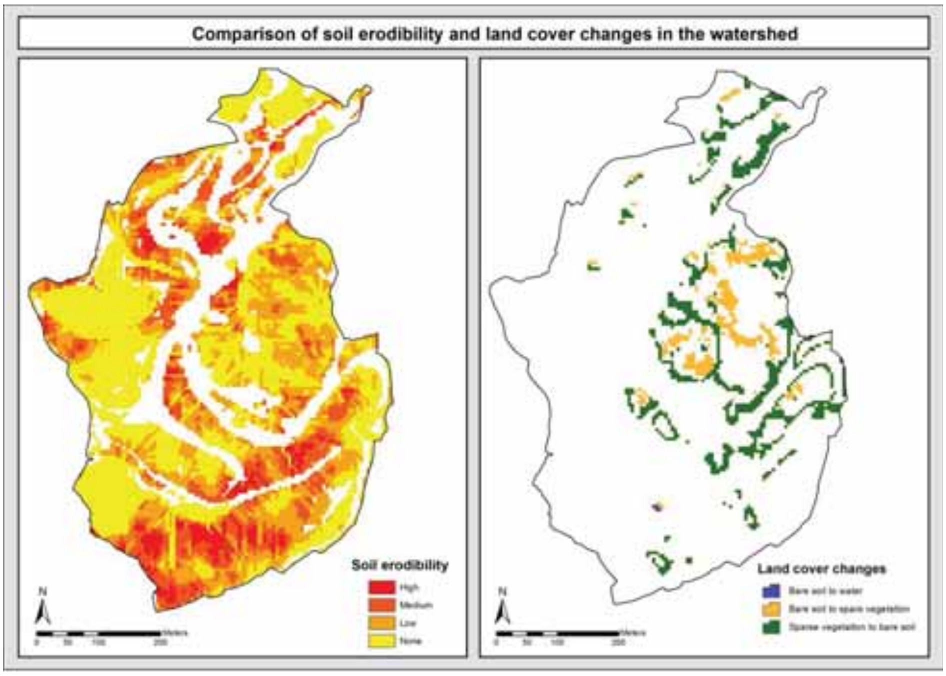

Figure 27: Comparison of soil erodibility index with observed land cover changes in the watershed.

6 Discussion

The image classification and change detection have two main findings. First, the major land cover in October 2011 and January 2012 in the study area is open forest (vegetation). Second, all land cover classes were affected by changes, while vegetation experienced a reduction in its coverage by 0.44 km^2, bare soil and water increased in the study area by 0.39 km^2 and 0.3 km^2, respectively.

Given the natural conditions and human pressures in the study area, extreme rainfall events and nickel mining were initially considered as the driving forces of the observed land cover changes. As nickel ore is being extracted by surface mining, which requires the removal of vegetation in order to access the deposits, it seemed reasonable to regard it as the main driver of the change from sparse and dense vegetation to bare soil (United Nations, 2003). Additionally, high amounts of precipitation, generated by frequent cyclones and tropical depressions during the early wet season, often result in extensive flooding and the disruption of vegetation cover in New Caledonia (Terry et al., 2008). Soils are still dry during the beginning of the wet season and have poor absorption abilities. In situations of severe rainfall, soils are unable to absorb the amount of rainfall quickly enough, often resulting in flash floods and landslides, which contribute to the removal of bare soil and sparse vegetation (Morgan, 2005). Flash floods occur when rainfall exceeds the infiltration rates or soils capacity and are “a major source of erosion” (Foody et al., 2004: 49).

The observed results of this study are partially similar to previous studies by Latifovic et al. (2005); Schulz et al. (2008); Wasige et al. (2013); Zomer et al. (2001), who analysed land cover changes in Canada, Chile, Kagera Basin of Lake Victoria, Africa and in Nepal and have reported about reductions of natural vegetation and the expansion of bare areas. Tovar et al. (2013) analysed land cover changes in the tropical Andes and observed an overall reduction in vegetation cover due to the expansion of mining and agriculture. Townsend et al. (2009) reported that the process of surface mining results in severe land cover alterations, ecologically as well as hydrologically.

No study on land cover changes was however found which particularly mentioned rainfall as its driver. When assessing the relation between rainfall and land cover changes, previous research focused on flash floods, or mass movements, such as landslides, that were either triggered by extreme rainfall and caused changes in land cover (Blaschke et al., 2000), or were the consequence of land cover changes (Alcántara-Ayala et al., 2006). Alcántara-Ayala et al. (2006) analysed landslides related to changes in land cover and stated that land cover changes might be considered either as the cause or the effect of landslides. While they concluded that the observed landslides in their study area in Mexico are a consequence of vegetation cover reduction, Blaschke et al. (2000) identified landslides as the driver of vegetation cover reduction, which are often consequences of the combination of extreme rainfall and steep slopes.

According to Lambin et al. (2001) and Shrestha (2011), agriculture, such as shifting cultivation, and deforestation are regarded as the primary drivers of land cover changes in tropical environments. Arable land in New Caledonia however only makes up 0.32 % of the land use (Central Intelligence Agency, 2009). Other studies named population growth and economic development as the major causes of land cover changes (Wasige et al., 2013). Population growth cannot be considered as a driving factor either since it slowed down over the last years (Institut national de la statistique et des études économiques, 2011). Consequently, these drivers were not considered as potential drivers of the observed land cover changes.

In an area, where both the natural and anthropogenic pressures are present, it is not always possible to determine the exact driver of the observed changes in land cover. Consequently, it cannot be differentiated which pressure contributed to which change in this case. The amount of external factors additionally complicated the analysis of the changes. As a result it is difficult to conclude whether the observed changes are actual changes in land cover or were only observed due to the influence of external factors.

A major obstacle when using optical remote sensing in tropical regions is the frequent cloud cover, especially during the wet season (Asner, 2001). According to Coppin et al. (2004) “for most documented studies, the periodicity of the data acquisition seems to have been determined according to the availability of satellite sensor data of acceptable quality”. In the present study, it was important to use images, which frame the rainfall event of December 2011 as close as possible. The closest and most cloud cover free images were the ones obtained in October 2011 and January 2012. Singh (1989), Pons et al. (2002) and Lambin and Strahler (1994) regarded the application of different acquisition dates as major sources of uncertainties to post-classification change detection. In the present study, this has at least two constraints on the process.

First of all, using images from different times of the year implies that each image represents the phenological conditions of its acquisition date. Additionally, the images are likely to be affected by different sun angles. Changes due to seasonal differences and sun angles are considered as changes by the software program and need to be manually separated by the analyst, which is not always easy and time consuming. The problems due to seasonal differences are comparable to the ones by Barreda-Bautista et al. (2011) who experienced similar difficulties when mapping tropical forest cover. As they worked with images acquired during different times of the year, forest was often misinterpreted with non-treed ecosystems during the dry season. According to Barreda-Bautista et al. (2011) using images of different times can be necessary when assessing vegetation cover in tropical regions as cloud-free satellite imagery is often difficult to obtain during the wet season, and vegetation is often sparse or leaves fall off during the dry season. This however also implies a high error potential when comparing these images.

Secondly, when the first image was acquired towards the end of the dry season, vegetation cover was sparse and the soil dry. The second image was obtained during the wet season in January when vegetation cover was denser and consequently more protective against rainfall. Soils however had a lower infiltration rate as they were more saturated after several rainfalls. Comparing land cover changes based on images obtained in the dry and wet season might lead to different results than assessing land cover changes measured during the wet season. The observed results should thus not be extrapolated over the entire year.

This explains why most research focusing on assessing land cover changes applied images of anniversary dates as this partially reduces the impact of seasonal and sun angles differences (Bayarsaikhan et al., 2009; Prenzel and Treitz, 2004; Zomer et al., 2001), only a few exceptions used images across a season (Pouliot et al., 2009; Zhan et al., 2000). When assessing land cover changes due to strong rainfall it is however necessary to apply images framing the particular event as close as possible to be certain that only changes, which were triggered by this event, are identified. Imagery of anniversary dates are however not an option as they cover too long of a time span and consequently make it too difficult to determine which changes occurred because of the rainfall and which are due to other causes. An alternative is the application of time series. A major advantage of their application is “the fact that the issue of influence of phenology on change detection performance is resolved, because data are collected throughout the growing season. As such, changes inherently linked to seasonality can be separated from other changes" (Coppin et al., 2004: 1569). A significant trade-off of the application of time series is however that this data is presently only available in coarse to moderate spatial resolution (AVHRR, MODIS) and consequently leads to the loss of spatial information (Coppin et al., 2004; Jianya et al., 2008). Consequently, time series are only an option when looking at a larger study area with coarser resolution.

Further constraints to the study are related to the different viewing angles of the sensor, which introduce major uncertainties into the analysis as they lead to different image perspectives (Mas, 2004). Although form and magnitude vary, these factors often result in differences in reflectance. This consequently caused errors in the individual image classification process leading to false changes within the change detection (Barnsley et al., 1997). Changes, which seemed logical and expected at first, such as the change from sparse vegetation to bare soil, became difficult to evaluate after further analysis as they might only be a consequence of the different viewing geometry.

The mentioned misregistration between the two images is another limitation to the study. "Perfect co-registration of multi-temporal images is impossible as there is always residual error in rectification models" (Verbyla and Boles, 2000: 3553), but according to Aguirre-Gutiérrez et al. (2012) "slight errors [...] can be overcome by applying correction rules for the size and width of the changed patches".

Given the limitations and uncertainties related to the results, it is difficult to make a sound statement about the impact of rainfall on the observed changes and whether the changes can actually be considered as actual changes in land cover.

As mentioned, according to MacLeod and Congalton (1998), four aspects are important when performing a change detection: detecting whether changes have occurred, determine their nature, and assess extent as well as spatial pattern of the observed change. In this case, it is difficult to determine the exact nature of the changes due to the amount of external factors influencing the results. Consequently, the change detection cannot be considered as successful.

Erodibility modelling

According to the soil erodibility index, areas are prone to soil erodibility if they are affected by the combination of soils with high silt contents, sparse or no vegetation cover and steep slopes. Similar findings were reported in the studies by Dumas et al. (2010) Printemps (2007) and Bui-Duyet (2011).

Several studies using RUSLE were conducted in New Caledonia and other tropical regions in order to assess potential soil loss. These studies applied the model in its original form and are consequently not comparable to the results of the present studies, the ways of deriving the input parameters are however similar. Soil information, the K factor values, were derived based on the nomograph by Wischmeier and Smith (1978), the obtained values are compatible to studies conducted in other parts of New Caledonia (Dumas et al., 2010) and Haiti (Delusca, 1998; Durosier, 1990). The cover and management factor C is based on the land cover classification of the RapidEye image of October 2011, a common approach in previous erosion research (Erencin, 2004; Mati et al., 2000; Meusburger et al., 2010b). The derived C-factor values are similar to the ones obtained by Printemps (2007) and Bui-Duyet (2011).

It is questionable in whether high soil erodibility can be considered as a driver of the observed land cover changes. Most studies focused on the consequences of land cover changes on soil erosion (Cebecauer and Hofierka, 2008; Koirala, 2010; Paiboonvorachat and Oyana, 2011; Quan et al., 2011) and not the other way around. Only Bakker et al. (2005) focused on the soil erosion as a driver on land use changes.

This study faced several limitations and uncertainties, which are related to the data sources, which were used to derive the different input parameters. Finding suitable indices for each input parameter was a major difficulty due to the rare soil types and endemic vegetation. Mati and Veihe (2001) reported similar difficulties when deriving factors for the input parameters from USLE guide tables.

Finding a suitable erodibility index in tropical conditions was a major problem as most of the existing indices were developed for soils in temperate regions (Dumas et al., 2010). According to Vanelslande et al. (1987), the nomograph used to derive K-factor values proposed by Wischmeier and Smith (1978) is not always applicable to tropical soils. Soils in New Caledonia are of ultrabasic origin and only little soil research has been conducted on the islands. Due to time constraints the collection of soil samples and their detailed analysis was not possible. Consequently, it was difficult to derive representative K factor values. In order to obtain information on the different soil types in the watershed, it was necessary to merge two maps. As only one of these maps was validated, the error potential of the derived K-factor values is high.

The same problem was observed when deriving C-factor values. Nomographs, such as the one proposed by Roose (1994), were not applicable because of the endemic flora in New Caledonia. Thus, C factor values were based on previous research performed by Bui-Duyet (2011) and Printemps (2007). Additionally, it has to be kept in mind that the classification of 2011 was used to derive a map for C-factor values. Different C factor values apply during the different seasons of the year, resulting in different soil erodibility indices in the wet or dry season. The obtained results can consequently not be extrapolated over the entire year. Furthermore, assigning C-factor values to vegetation classes derived from image classifications implies that areas affected by misclassifications were assigned wrong values and thus caused wrong overall results.

A common approach to derive slope length and slope angle is an Arc Macro Language (AML) script under ArcInfo developed by Remortel et al. (2004). As the software ArcInfo was not available during the research, an alternative approach had to be selected. In this case, slope length and slope angle are combined in the factor LS, which is calculated based on a recently proposed algorithm developed by (Zhang et al., 2013). To what extent this approach presents advantages and disadvantages when conducting soil erosion assessments is unknown as the software was just recently published.
Another limitation concerns the factor P, the effect of support practices. Due to lack of information on it, this factor was not included. This seems to be a common problem, as several other studies faced a lack of information as well and consequently excluded this factor (Beskow et al., 2009; Cohen et al., 2005). According to (Knijff et al., 2000), this alters the model as the management practices is one of the most important factors affecting erosion.

According to Lu et al. (2004a) “uncertainties regarding data sources may introduce larger uncertainties in soil erosion estimates”. This highlights why it is difficult to estimate how reliable the results of the soil erodibility index are and whether they can be related to the observed changes in land cover.

7 Conclusion & recommendations

Conclusion

This study showed that the application of remote sensing data is helpful to extract information on land cover in New Caledonia. While the northern part of the study area is mostly covered by bare soil due to the mining industry, the southern part is covered by dense vegetation cover as it is undisturbed from human activities. The optical remote sensing based approach has however clear implications for detecting changes in land cover after extreme rainfall when using images across two seasons. Areas affected by change were identified, but the results are significantly affected by external factors, such as seasonal differences between the two images, the different viewing geometry as well as errors related to the image classification process. Seasonal differences are considered as the most constraining factor when assessing changes over the dry and wet season. As the analyst will always face problems due to phenology, it can be consequently be concluded that optical remote sensing is an inadequate approach for detecting land cover changes. Given that the erosive force is particularly strong in the beginning of the wet season due to the combination of the frequent occurrence of extreme rainfall events, sparse vegetation cover and dry soils, there is a pressing need to develop more efficient and accurate methods to effectively detect land cover changes after a particular event and across seasons.

Soil erodibility can successfully be modelled based on the Revised Universal Soil Loss Equation when assuming that the input parameters remain constant. Areas, in which soils of high silt contents coincide with sparse or no vegetation cover and steep slopes are especially prone to soil erodibility. But due to the listed uncertainties concerning the data sources and the missing calibration, it is difficult to estimate how reliable the results of the soil erodibility map are. The generated soil erodibility index can however be regarded as a first step towards an assessment of soil erosion risk in the watershed as it provides a preliminary understanding of which areas might potentially be affected by erosion. Given the limitations and uncertainties regarding the change detection results and the soil erodibility modelling, it is difficult to make a sound statement about their relation. Consequently, it is questionable to which extent soil erodibility contributed to the observed land cover changes.

Recommendations

Although cloud cover poses a major problem in tropical regions, a possible future approach could be to assess changes after a rainfall event based on two images obtained at the very beginning of the wet season. Another approach includes the application of time series, even though this is only possible on coarser resolution and should consequently address a larger area as explained in chapter six.

Several studies applying either USLE or RUSLE were conducted in the southern Pacific Ocean, such as in New Caledonia, Tahiti, Fiji and Vanuatu. A major drawback of these studies is the missing validation of the results. By including the rainfall factor R in the model, the obtained results can be compared with actual measurements on suspended sediment load in the water, which can be regarded as a validation of the model. A future objective is the modelling of potential soil loss by including the rainfall factor R in the model. Rainfall data can be either obtained from the meteorological station in the neighbour village Houaïlou or from the Tropical Rainfall Measurement Mission (TRMM), which is available for free online.

References

AGUIRRE-GUTIÉRREZ, J., SEIJMONSBERGEN, A. C. & DUIVENVOORDEN, J. F. 2012. Optimizing land cover classification accuracy for change detection, a combined pixel-based and object-based approach in a mountainous area in Mexico. *Applied Geography,* 34**,** 29-37.

AKSOY, H. & KAVVAS, M. L. 2005. A review of hillslope and watershed scale erosion and sediment transport models. *CATENA,* 64**,** 247-271.

ALCÁNTARA-AYALA, I., ESTEBAN-CHÁVEZ, O. & PARROT, J. F. 2006. Landsliding related to land-cover change: A diachronic analysis of hillslope instability distribution in the Sierra Norte, Puebla, Mexico. *CATENA,* 65**,** 152-165.

ALI, S. H. G., A.S., 2006. The ecology and economy of indigenous resistance: divergent perspectives on mining in New Caledonia. *The Contemporary Pacific* 18**,** 361-392.

ANDERSON, J. R., HARDY, E. E., ROACH, J. T. & WINTER, R. E. 1976. A land use and land cover classification system for use with remote sensor data. *U.S. Geological Survey Professional Paper 964***,** 28.

ASNER, G. P. 2001. Cloud cover in Landsat observations of the Brazilian Amazon. *International Journal of Remote Sensing,* 22**,** 3855-3862.

BABAN, S. M. J. & YUSOF, K. W. 2001. Modelling soil erosion in tropical environments using remote sensing and geographical information systems. *Hydrological Sciences Journal-Journal Des Sciences Hydrologiques,* 46**,** 191-198.

BAKKER, M. M., GOVERS, G., KOSMAS, C., VANACKER, V., OOST, K. & ROUNSEVELL, M. 2005. Soil erosion as a driver of land-use change. *Agriculture, ecosystems and environment.,* 105**,** 467-481.

BARNSLEY, M. J., ALLISON, D. & LEWIS, P. 1997. On the information content of multiple view angle (MVA) images. *International Journal of Remote Sensing,* 18**,** 1937-1960.

BARREDA-BAUTISTA, B. D. L., LOPEZ-CALOCA, A. A., COUTURIER, S. & SILVAN-CARDENAS, J. L. 2011. Tropical Dry Forests in the Global Picture: The Challenge of Remote Sensing-Based Change Detection in Tropical Dry Environments. *In:* CARAYANNIS, E. (ed.) *Planet Earth 2011: Global Warming Challenges and Opportunities for Policy and Practice.* InTech.

BAYARSAIKHAN, U., BOLDGIV, B., KIM, K.-R., PARK, K.-A. & LEE, D. 2009. Change detection and classification of land cover at Hustai National Park in Mongolia. *International Journal of Applied Earth Observation and Geoinformation,* 11**,** 273-280.

BESKOW, S., MELLO, C. R., NORTON, L. D., CURI, N., VIOLA, M. R. & AVANZI, J. C. 2009. Soil erosion prediction in the Grande River Basin, Brazil using distributed modeling. *CATENA,* 79**,** 49-59.

BISHOP, C. 2007. *Pattern Recognition and Machine Learning (Information Science and Statistics)*, Springer.

BLANCO-CANQUI, H. & LAL, R. 2008. *Principles of Soil Conservation and Management*, Springer.

BLASCHKE, P. M., TRUSTRUM, N. A. & HICKS, D. L. 2000. Impacts of mass movement erosion on land productivity: a review. *Progress in Physical Geography,* 24**,** 21-52.

BOISSIEU, F. D., GODIN, C., GUILHAMAT, B., DAVID, D., SERVIERE, C. & BAUDOIS, D. 2009. Tactile texture recognition with a 3-axial force MEMS integrated artificial finger. *Robotics: Science and Systems,* V**,** 49-56.

BRUZZONE, L., COSSU, R. & VERNAZZA, G. 2002. Combining parametric and non-parametric algorithms for a partially unsupervised classification of multitemporal remote-sensing images. *Information Fusion,* 3**,** 289-297.

BUI-DUYET, D. 2011. *Cartographie de l'aléa érosion - Application du modèle USLE (Universal Soil Loss Equation) assistée d'un SIG à l'ensemble de la Grande Terre de Nouvelle-Calédonie.* Master's thesis, Université d'Orléans.

CEBECAUER, T. & HOFIERKA, J. 2008. The consequences of land-cover changes on soil erosion distribution in Slovakia. *Geomorphology,* 98**,** 187-198.

CEC 1995. CORINE - Guide Technique. Commission of the European Communities, Brussels

CENTRAL INTELLIGENCE AGENCY. 2009. *The World Factbook 2009* [Online]. Washington, DC: Central Intelligence Agency. Available: https://www.cia.gov/library/publications/the-world-factbook/geos/nc.html [Accessed April 2nd 2013].

CHABANET, P., GUILLEMOT, N., KULBICKI, M., VIGLIOLA, L. & SARRAMEGNA, S. 2010. Baseline study of the spatio-temporal patterns of reef fish assemblages prior to a major mining project in New Caledonia (South Pacific). *Marine Pollution Bulletin,* 61**,** 598-611.

CHEN X., VIERLING, L. & DEERING, D. 2005. A simple and effective radiometric correction method to improve landscape change detection across sensors and across time. *Remote Sensing of Environment,* 98**,** 63-79.

CIHLAR, J. 2000. Land cover mapping of large areas from satellites: status and research priorities. *International Journal of Remote Sensing,* 21**,** 1093-1114.

CIHLAR, J., XIAO, Q., CHEN, J., BEAUBIEN, J., FUNG, K. & LATIFOVIC, R. 1998. Classification by progressive generalization: A new automated methodology for remote sensing multichannel data. *International Journal of Remote Sensing,* 19**,** 2685-2704.

CNRT 2009. Revue d'offre: Bassin versant. Nouméa, Nouvelle-Calédonie.

COHEN, M. J., SHEPHERD, K. D. & WALSH, M. G. 2005. Empirical reformulation of the universal soil loss equation for erosion risk assessment in a tropical watershed. *Geoderma,* 124**,** 235-252.

COPPIN, P., JONCKHEERE, I., NACKAERTS, K., MUYS, B. & LAMBIN, E. 2004. Digital change detection methods in ecosystem monitoring; a review. *International Journal of Remote Sensing,* 25**,** 1565-1596.

COPPIN, P. R. & BAUER, M. E. 1996. Change Detection in Forest Ecosystems with Remote Sensing Digital Imagery. *Remote Sensing Reviews,* 13**,** 207-234.

CYR, L., BONN, F. & PESANT, A. 1995. Vegetation indices derived from remote sensing for an estimation of soil protection against water erosion. *Ecological Modelling,* 79**,** 277-285.

DASH, J., MATHUR, A., FOODY, G. M., CURRAN, P. J., CHIPMAN, J. W. & LILLESAND, T. M. 2007. Land cover classification using multi-temporal MERIS vegetation indices. *International Journal of Remote Sensing,* 28**,** 1137-1159.

DAVID, G., LEOPOLD, M., DUMAS, P. S., FERRARIS, J., HERRENSCHMIDT, J. B. & FONTENELLE, G. 2010. Integrated coastal zone management perspectives to ensure the sustainability of coral reefs in New Caledonia. *Marine Pollution Bulletin,* 61**,** 323-334.

DE ASIS, A. M. & OMASA, K. 2007. Estimation of vegetation parameter for modeling soil erosion using linear Spectral Mixture Analysis of Landsat ETM data. *ISPRS Journal of Photogrammetry and Remote Sensing,* 62**,** 309-324.

DE JONG, S. M. 1994. *Applications of Reflective Remote Sensing for Land Degradation Studies in a Mediterranean Environment,* Utrecht, Netherlands, KNAG/Faculty of Geosciences, Utrecht University.

DE JONG, S. M., PARACCHINI, M. L., BERTOLO, F., FOLVING, S., MEGIER, J. & DE ROO, A. P. J. 1999. Regional assessment of soil erosion using the distributed model SEMMED and remotely sensed data. *CATENA,* 37**,** 291-308.

DEER, J. P. 1995. Digital change detection techniques: civilian and military applications. *International Symposium on Spectral Sensing Research.*

DELUSCA, K. 1998. *Estimation de l'érosion hydrique des sols à l'aide de l'Équation Universelle de Perte de Sol, assistée d'un*

Système d'Information Géographique: Le cas du bassin versant de la ravine Balan, Haïti. Master's thesis, Université de Moncton.

DESMET, P. J. J. & GOVERS, G. 1996. A GIS Procedure for Automatically Calculating the USLE LS Factor On Topographically Complex Landscapes Units. *Journal of Soil and Water Conservation,* 81**,** 427-433.

DHAKAL, A. S., T. AMADA, MASAMU, A. & SHARMA, R. R. 2002. Detection of areas associated with flood and erosion caused by a heavy rainfall using multitemporal Landsat TM data. Bethesda, MD, ETATS-UNIS: American Society for Photogrammetry and Remote Sensing.

DIRECTION DES TECHNOLOGIES ET SERVICES DE L'INFORMATION 2008. Classification de l'occupation du sol de la Nouvelle-Calédonie par approche objet V1.0 - 2008. Nouméa, New Caledonia.

DUMAS, P., PRINTEMPS, J., MANGEAS, M. & LUNEAU, G. 2010. Developing erosion models for integrated coastal zone management: A case study of The New Caledonia west coast. *Marine Pollution Bulletin,* 61**,** 519-529.

DUROSIER, J. S. 1990. *Assessment of land degradation and its consequences. A case study of the Bouyaha River watershed, Haïti.* Master's thesis, International Institute for Aerospace Survey and Earth Sciences.

EL-KAWY, O. R. A., RØD, J. K., ISMAIL, H. A. & SULIMAN, A. S. 2011. Land use and land cover change detection in the western Nile delta of Egypt using remote sensing data. *Applied Geography,* 31**,** 483-494.

ENDEMIA. 2008. *Faune et Flore de Nouvelle-Calédonie* [Online]. Available: http://www.endemia.nc/ [Accessed April 03 2013].

ERENCIN, Z. 2004. C-Factor mapping using Remote Sensing and GIS : a case study of Lom Sak / Lom Kao, Thailand. Gießen: Universitätsbibliothek.

ESWARAN, H., LAL, R. & REICH, P. 2001. Land degradation: an overview. *In:* BRIDGES, E. M., HANNAM, I. D., OLDEMAN, L. R., F.W.T, P. D. V., SCHERR, S. J. & S, S. (eds.) *Response to land degradation.* Enfield, NH, USA: Science Publishers Inc.

FAO 1977. Assessing soil degradation. *FAO Soil Bull. no. 34*.

FOOD AND AGRICULTURAL ORGANISATION. 2000. *Land Cover Classification System (LCCS)* [Online]. Available: http://www.fao.org/DOCREP/003/X0596E/X0596E00.HTM [Accessed December 10 2012].

FOODY, G. M. 1996. Approaches for the production and evaluation of fuzzy land cover classifications from remotely-sensed data. *International Journal of Remote Sensing,* 17**,** 1317-1340.

FOODY, G. M. 2002. Status of land cover classification accuracy assessment. *Remote Sensing of Environment,* 80**,** 185-201.

FOODY, G. M., GHONEIM, E. M. & ARNELL, N. W. 2004. Predicting locations sensitive to flash flooding in an arid environment. *Journal of Hydrology,* 292**,** 48-58.

FOSTER, G. R., MCCOOL, D. K., RENARD, K. G. & MOLDENHAUER, W. C. 1981. Conversion of the universal soil loss equation to SI metric units. *Journal of Soil and Water Conservation,* 36**,** 355-359.

FUTURA ENVIRONNEMENT. 2004. *La faune et la flore de Nouvelle-Calédonie* [Online]. Available: http://www.futura-sciences.com/fr/doc/t/zoologie-1/r/nouvelle-caledonie/d/la-faune-et-la-flore-de-nouvelle-caledonie_468/c3/221/p2/ [Accessed April 01 2013].

GALLEGO, F. J. 2004. Remote sensing and land cover area estimation. *International Journal of Remote Sensing,* 25**,** 3019-3047.

GAY, M., CHERET, V. & DENUX, J. P. 2002. Apport de la télédétection dans l'identification du risque d'érosion. *La Houille Blanche***,** 81-86.

GOEL, M. K., JAIN, S. K. & AGARWAL, P. K. 2002. Assessment of sediment deposition rate in Bargi Reservoir using digital image processing. *Hydrological Sciences Journal-Journal Des Sciences Hydrologiques,* 47**,** S81-S92.

GONG, P. & HOWARTH, P. J. 1990. Land cover to land use conversion: a knowledge-based approach. *Annual Conference of American Society of Photogrammetry and Remote Sensing.* Denver, Colorado, United States.

GUILLON, J. H. & LAWRENCE, L. J. 1973. The opaque minerals of the ultramafic rocks of New Caledonia. *Mineralium Deposita,* 8**,** 115-126.

HAUT-COMMISSARIAT DE LA RÉPUBLIQUE EN NOUVELLE-CALÉDONIE. 2011. *La Nouvelle Calédonie* [Online]. Available: http://www.nouvelle-caledonie.gouv.fr/site/La-Nouvelle-Caledonie/Presentation [Accessed April 04 2013].

HIRATA, M., KOGAB, N., SHINJO, H., FUJITA, H., GINTZBURGER, G. & MIYAZAKI, A. 2001. Vegetation classification by satellite image processing in a dry area of north-eastern Syria. *International Journal of Remote Sensing,* 22**,** 507-516.

HUANG, C. 2002. An assessment of support vector machines for land cover classification. *International Journal of Remote Sensing,* 23**,** 725-749.

HUIPING, Z., HONG, J. & QINGHUA, H. 2011. Landscape and Water Quality Change Detection in Urban Wetland: A Post-classification Comparison Method with IKONOS Data. *Procedia Environmental Sciences,* 10, Part B, 1726-1731.

INSTITUT NATIONAL DE LA STATISTIQUE ET DES ÉTUDES ÉCONOMIQUES. 2011. *Recensement de la population en Nouvelle-Calédonie en 2009* [Online]. [Accessed April 17th 2013].

INSTITUTE OF MICROBIAL TECHNOLOGY. *Evaluation of Bioinformatics Methods* [Online]. Available: http://www.imtech.res.in/raghava/gpsr/Evaluation_Bioinformatics_Methods.htm [Accessed March 13th 2013].

ISMAIL, M. H. & JUSOFF, K. 2008. Satellite data classification accuracy assessment based from reference dataset. *International Journal of Computer and Information Science and Engineering*, 96-102.

JAIN, A. K., DUIN, W. & MAO, J. C. 2000. Statistical Pattern Recognition: A Review. *IEEE Transactions on Pattern Analysis and Machine Intelligence,* 22, 4-37.

JANSEN, L. J. M. & GREGORIO, A. D. 2002. Parametric land cover and land-use classifications as tools for environmental change detection. *Agriculture, Ecosystems & Environment,* 91, 89-100.

JENSEN, J. R. 1996. *Digital Image Processing, third edition.*, Prentice Hall, Upper Saddle River, NJ, USA.

JENSEN, J. R. & TOLL, D. L. 1982. Detecting residential land-use development at the urban fringe. *Photogrammetric Engineering and Remote Sensing,* 48.

JETTEN, V., DE ROO, A. & FAVIS-MORTLOCK, D. 1999. Evaluation of field-scale and catchment-scale soil erosion models. *CATENA,* 37, 521-541.

JETTEN, V., GOVERS, G. & HESSEL, R. 2003. Erosion models: quality of spatial predictions. *Hydrological Processes,* 17, 887-900.

JIANYA, G., HAIGANG, S., GUORUI, M. & QIMING, Z. A Review of Multi-Temporal Remote Sensing Data Change Detection Algorithms. ISPRS Congress Beijing 2008, 2008 Bejing. 757-762.

KINNELL, P. I. A. & RISSE, L. M. 1998. Empirical modelling rainfall erosion through runoff and sediment concentration. *Soil Science Society of America Journal,* 62, 1667-1672.

KNIJFF, J. M. V. D., JONES, R. J. A. & MONTANARELLA, L. 2000. Soil erosion risk assessment in Italy. European Soil Bureau. European Commission.

KOIRALA, S. 2010. *Land use and land cover change and its impact on soil erosion process in Begnas Tal Rupa Tal watershed using geospatial tools, Kaski district, Nepal.* Master's thesis, Universidade Nova de Lisboa.

KOTSIANTIS, S. B. 2013. Decision trees: a recent overview. *Artificial Intelligence Review,* 39, 261-283.

L'HUILLIER, L., JAFFRÉ, T. & WULFF, A. 2010. *Mines et Environnement en Nouvelle-Calédonie: les milieux sur substrats ultramafiques et leur restauration,* Nouméa, Nouvelle-Calédonie, Éditions IAC.

LAL, R. 1994. *Soil erosion research methods*, CRC Press.

LAL, R. 2004. Soil carbon sequestration impacts on global climate change and food security. *Science,* 304, 1623-1627.

LAMBIN, E. F. & EHRLICH, D. 1997. Land-cover changes in sub-saharan Africa (1982–1991): Application of a change index based on remotely sensed surface temperature and vegetation indices at a continental scale. *Remote Sensing of Environment,* 61, 181-200.

LAMBIN, E. F. & STRAHLER, A. H. 1994. Change-vector analysis in multitemporal space: A tool to detect and categorize land-cover change processes using high temporal-resolution satellite data. *Remote Sensing of Environment,* 48, 231-244.

LAMBIN, E. F., TURNER, B. L., GEIST, H. J., AGBOLA, S. B., ANGELSEN, A., BRUCE, J. W., COOMES, O. T., DIRZO, R., FISCHER, G., FOLKE, C., GEORGE, P. S., HOMEWOOD, K., IMBERNON, J., LEEMANS, R., LI, X., MORAN, E. F., MORTIMORE, M., RAMAKRISHNAN, P. S., RICHARDS, J. F., SKÅNES, H., STEFFEN, W., STONE, G. D., SVEDIN, U., VELDKAMP, T. A., VOGEL, C. & XU, J. 2001. The causes of land-use and land-cover change: moving beyond the myths. *Global Environmental Change,* 11, 261-269.

LATIFOVIC, R., FYTAS, K., CHEN, J. & PARASZCZAK, J. 2005. Assessing land cover change resulting from large surface mining development. *International Journal of Applied Earth Observation and Geoinformation,* 7, 29-48.

LIEW, S. C. 2001. *Optical Remote Sensing* [Online]. CRISP. Available: http://www.crisp.nus.edu.sg/~research/tutorial/optical.htm [Accessed May 21 2013].

LILLESAND, T. M. & KIEFER, R. W. 1994. *Remote Sensing and Image Interpretation*, Wiley & Sons.

LILLESAND, T. M. & KIEFER, R. W. 2004. *Remote sensing and image interpretation,* Hoboken, NJ, John Wiley & Sons.

LIU, J. G., MASON, P., HILTON, F. & LEE, H. 2004. Detection of rapid erosion in SE Spain: A GIS approach based on ERS SAR coherence imagery. *Photogrammetric Engineering and Remote Sensing,* 70, 1179-1185.

LU, D., BATISTELLA, M. & MORAN, E. 2004a. Multitemporal spectral mixture analysis for Amazonian land-cover change detection. *Canadian Journal of Remote Sensing,* 30, 87-100.

LU, D., MAUSEL, P., BRONDIZIO, E. & MORAN, E. 2004b. Change detection techniques. *International Journal of Remote Sensing,* 25**,** 2365-2401.

LU, D. & WENG, Q. 2007. A survey of image classification methods and techniques for improving classification performance. *International Journal of Remote Sensing,* 28**,** 823-870.

LUNETTA, R. S. 1998. Applications, project formulation, and analytical approach. *Remote Sensing Change Detection: Environmental Monitoring Methods and Applications.* Chelsea, MI, USA: Ann Arbor Press.

LUNETTA, R. S., KNIGHT, J. F., EDIRIWICKREMA, J., LYON, J. G. & WORTHY, L. D. 2006. Land-cover change detection using multi-temporal MODIS NDVI data. *Remote Sensing of Environment,* 105**,** 142-154.

MACLEOD, R. D. & CONGALTON, R. G. 1998. A quantitative comparison of changedetection algorithms for monitoring eelgrass from remotely sensed data. *Photogrammetric Engineering and Remote Sensing,* 64**,** 207–216.

MANYATSI, A. M. & NTSHANGASE, N. 2008. Mapping of soil erosion using remotely sensed data in Zombodze South, Swaziland. *Physics and Chemistry of the Earth, Parts A/B/C,* 33**,** 800-806.

MARQUES, M. J., BIENES, R., JIMÉNEZ, L. & PÉREZ-RODRÍGUEZ, R. 2007. Effect of vegetal cover on runoff and soil erosion under light intensity events. Rainfall simulation over USLE plots. *Science of The Total Environment,* 378**,** 161-165.

MAS, J. F. 1999. Monitoring land-cover changes: A comparison of change detection techniques. *International Journal of Remote Sensing,* 20**,** 139-152.

MAS, J. F. 2004. Mapping land use/cover in a tropical coastal area using satellite sensor data, GIS and artificial neural networks. *Estuarine, Coastal and Shelf Science,* 59**,** 219-230.

MATI, B. M., MORGAN, R. P. C., GICHUKI, F. N., QUINTON, J. N., BREWER, T. R. & LINIGER, H. P. 2000. Assessment of erosion hazard with the USLE and GIS: A case study of the Upper Ewaso Ng'iro North basin of Kenya. *International Journal of Applied Earth Observation and Geoinformation,* 2**,** 78-86.

MATI, B. M. & VEIHE, A. 2001. Application of the USLE in a Savannah Environment: Comparative Experiences from East and West Africa. *Singapore Journal of Tropical Geography,* 22**,** 138-155.

MAZOUR, M. & ROOSE, E. 2002. Influence de la couverture végétale sur le ruissellement et l’érosion des sols sur parcelles d’érosion dans les bassins versants du Nord-Ouest de l’Algérie. *Bull Réseau Erosion,* 21**,** 320-330.

MCCOOL, D. K., BROWN, L. C., FOSTER, G. R., MUTCHLER, C. K. & MEYER, L. D. 1987. Revised slope steepness factor for the Universal Soil Loss Equation. *Trans. ASCE,* 30.

MCCOOL, D. K., FOSTER, G. R., MUTCHLER, C. K. & MEYER, L. D. 1989. Revised slope length factor for the Universal Soil Loss Equation. *Trans. ASCE,* 32**,** 1571-1576.

MERRITT, W. S., LETCHER, R. A. & JAKEMAN, A. J. 2003. A review of erosion and sediment transport models. *Environmenal Modelling & Software,* 18.

MET OFFICE. 2013. *UK climate - Averages - Southampton.* [Online]. Met office. Available: http://www.metoffice.gov.uk/public/weather/climate/?tab=climateTables [Accessed April 14th 2013].

MÉTEO FRANCE. 2011. *Record de précipitation en Nouvelle Calédonie à Noël* [Online]. Nouméa, New Caledonia: Méteo France. Available: http://france.meteofrance.com/france/actu/archives/2011/2011?page_id=14728&document_id=26195&portlet_id=78025 [Accessed December 16th 2012].

MEUSBURGER, K., BÄNNINGER, D. & ALEWELL, C. 2010a. Estimating vegetation parameter for soil erosion assessment in an alpine catchment by means of QuickBird imagery. *International Journal of Applied Earth Observation and Geoinformation,* 12**,** 201-207.

MEUSBURGER, K., KONZ, N., SCHAUB, M. & ALEWELL, C. 2010b. Soil erosion modelled with USLE and PESERA using QuickBird derived vegetation parameters in an alpine catchment. *International Journal of Applied Earth Observation and Geoinformation,* 12**,** 208-215.

MEYERS, N. 1990. The biodiversity challenge: expanded hotspots analysis. *Environmentalist,* 10**,** 243-256.

MINISTÈRE DES OUTRE-MER. 2012. *Nouvelle-Calédonie* [Online]. Available: http://www.outre-mer.gouv.fr/?presentation-nouvelle-caledonie.html [Accessed August 21 2012].

MORGAN, R. P. C. 1995. *Soil erosion and conservation,* Essex, U.K., Longman Group.

MORGAN, R. P. C. 2005. *Soil erosion and conservation*, Blackwell Science Ltd.

MORGAN, R. P. C., QUINTON, J. N., SMITH, R. E., GOVERS, G., POESEN, J. W. A., AUERSWALD, K., CHISCI, G., TORRI, D. & STYCZEN, M. E. 1998. The European Soil Erosion Model (EUROSEM): a dynamic approach for predicting sediment transport from fields and small catchments. *Earth Surface Processes and Landforms,* 23**,** 527-544.

NASA. 2013. *Landsat 7* [Online]. Available: http://landsat.gsfc.nasa.gov/about/L7_td.html [Accessed May 20th 2013].

NATURAL RESOURCES CANADA. 2008. *Pre-Processing* [Online]. The Government of Canada and Natural Resources Canada. Available: http://www.nrcan.gc.ca/earth-sciences/geography-boundary/remote-sensing/fundamentals/2321 [Accessed May 22 2013].

NEARING, M. A., JETTEN, V., BAFFAUT, C., CERDAN, O., COUTURIER, A., HERNANDEZ, M., LE BISSONNAIS, Y., NICHOLS, M. H., NUNES, J. P., RENSCHLER, C. S., SOUCHERE, V. & VAN OOST, K. 2005. Modeling response of soil erosion and runoff to changes in precipitation and cover. *CATENA,* 61**,** 131-154.

NEARING, M. A., LANE, L. J. & LOPES, V. L. 1994. Modeling soil erosion. *In:* LAL, R. (ed.) *Soil Erosion Research Methods.* CRC Press.

O'NEAL, M. R., NEARING, M. A., VINING, R. C., SOUTHWORTH, J. & PFEIFER, R. A. 2005. Climate change impacts on soil erosion in Midwest United States with changes in crop management. *CATENA,* 61.

OTUKEI, J. R. & BLASCHKE, T. 2010. Land cover change assessment using decision trees, support vector machines and maximum likelihood classification algorithms. *International Journal of Applied Earth Observation and Geoinformation,* 12, Supplement 1**,** S27-S31.

OUYANG, W., SKIDMORE, A. K., HAO, F. & WANG, T. 2010. Soil erosion dynamics response to landscape pattern. *Science of The Total Environment,* 408**,** 1358-1366.

OXFORD UNIVERSITY PRESS. 2012. *Oxford Dictionaries* [Online]. Available: http://oxforddictionaries.com/definition/english/endemic?q=endemic [Accessed September 4th 2012].

PAIBOONVORACHAT, C. & OYANA, T. J. 2011. Land-cover changes and potential impacts on soil erosion in the Nan watershed, Thailand. *International Journal of Remote Sensing,* 32**,** 6587-6609.

PAL, M. & MATHER, P. M. 2003. An assessment of the effectiveness of decision tree methods for land cover classification. *Remote Sensing of Environment,* 86**,** 554-565.

PASCAL, M., DE FORGES, B. R., LE GUYADER, H. & SIMBERLOFF, D. 2008. Mining and other threats to the New Caledonia biodiversity hotspot. *Conservation Biology,* 22**,** 498-499.

PIMENTEL, D., HARVEY, C., RESOSUDARMO, P., SINCLAIR, K., KURZ, D., MCNAIR, M., CRIST, S., SHPRITZ, L., FITTON, L., SAFFOURI, R. & BLAIR, R. 1995. Environmental and economic costs of soil erosion and conservation benefits. *Science* 267, 1117-1123.

PONS, X., SERRA, P. & SAURÍ, D. A rigorous protocol for post-classification land cover and land use change detection. *In:* BENES, T., ed. Geoinformation for European-wide integration. Proceedings of the 22nd Symposium of the European Association of Remote Sensing Laboratories, 4-6 June 2002 Prague, Czech Republic.

POULIOT, D., LATIFOVIC, R., FERNANDES, R. & OLTHOF, I. 2009. Evaluation of annual forest disturbance monitoring using a static decision tree approach and 250 m MODIS data. *Remote Sensing of Environment,* 113, 1749-1759.

PRENZEL, B. & TREITZ, P. 2004. Remote sensing change detection for a watershed in north Sulawesi, Indonesia. *Progress in Planning,* 61, 349-363.

PRINTEMPS, J. 2007. *Estimation et spatialisation de l'érosion hydrique des sols en Nouvelle-Calédonie - Utilisation de l'équation universelle de perte de sol assistée d'un SIG sur les communes de Voh,*

Koné et Pouembout. Master's thesis, Université Joseph Fourier.

PROCTOR, J. 2003. Vegetation and soil and plant chemistry on ultramafic rocks in the tropical Far East. *Perspectives in Plant Ecology, Evolution and Systematics,* 6, 105-124.

QUAN, B., RÖMKENS, M. J. M., LI, R., WANG, F. & CHEN, J. 2011. Effect of land use and land cover change on soil erosion and the spatio-temporal variation in Liupan Mountain Region, southern Ningxia, China. *Frontiers of Environmental Science & Engineering in China,* 5, 564-572.

RAMSEY, R. D. 2008. Introduction to Remote Sensing, 4th Edition - by James B. Campbell. *Geographical Research,* 46, 472-473.

RAPIDEYE AG. 2011. *HIGH-RESOLUTION SATELLITE IMAGERY* [Online]. Available: http://www.rapideye.com/products/index.htm [Accessed April 21nd 2013].

REMORTEL, R. D. V., MAICHLE, R. W. & HICKEY, R. J. 2004. Computing the LS factor for the Revised Universal Soil Loss Equation through array-based slope processing of digital elevation data using a C++ executable. *Computers & Geosciences,* 30, 1043-1053.

RENARD, K. G., FOSTER, G. R., WEESIES, G. A., MCCOOL, D. K. & YODER, D. C. 1997. *Predicting Soil Erosion by Water: A Guide to Conservation Planning with the Revised Universal Soil Loss Equation (RUSLE)*, U.S. Department of Agriculture. Agricultural Handbook No. 537

RENARD, K. G. & FREIMUND, V. A. 1993. RUSLE model description and database sensitivity. *Journal of Environmental Quality,* 22**,** 458-466.

RICHARDS, J. A. & JIA, X. 2006. *Remote Sensing Digital Image Analysis: An Introduction*, Springer Verlag.

ROOSE, E. 1994. Introduction à la Gestion Conservatoire de l'Eau, de la biomasse et de la fertilité des Sols (GCES). *Bulletin Pédologique de la FAO n°70*.

ROUET, I. 2009. *Caractérisation et éléments de quantification d'aléas naturels liés à l'évolution des versants dans les massifs ultrabasiques de Nouvelle-Calédonie* M.Env.Sc. thesis, Université de la Nouvelle-Calédonie.

ROUET, I., D. GAY, M. ALLENBACH, N. SELMAOUI, A.G AUSSEIL, M. MANGEAS, J. MAURA, P. DUMAS & LILLE, D. 2009. Tools for soil erosion mapping and hazard assessment: application to New Caledonia, SW Pacific. *MODSIM conference.* Cairns, Australia.

SAADAT, H., ADAMOWSKI, J., BONNELL, R., SHARIFI, F., NAMDAR, M. & ALE-EBRAHIM, S. 2011. Land use and land cover classification over a large area in Iran based on single date analysis of satellite imagery. *ISPRS Journal of Photogrammetry and Remote Sensing,* 66**,** 608-619.

SAN MIGUEL-AYANZ, J. & BIGING, G. S. 1997. Comparison of single-stage and multi-stage classification approaches for cover type mapping with TM and SPOT data. *Remote Sensing of Environment,* 59**,** 92-104.

SAVY, C. B., MAHLETTE; LEFEUVRE, JEAN-CHRISTOPHE 2011. Mining and nature in New Caledonia. *Mining and mining policy in the Pacific: history, challenges & perspectives.* Nouméa, Nouvelle-Calédonie.

SCHOWENGERDT, R. A. 2006. *Remote Sensing: Models and Methods for Image Processing*, Academic Press.

SCHULZ, J. J., CAYUELA, L., ECHEVERRIA, C., SALAS, J. & BENAYAS, J. M. R. 2008. Monitoring land cover changes of the dryland forest landscape of Central Chile (1975-2008). *Applied Geography***,** 436-447.

SHALABY, A. & TATEISHI, R. 2007. Remote sensing and GIS for mapping and monitoring land cover and land-use changes in the Northwestern coastal zone of Egypt. *Applied Geography,* 27**,** 28-41.

SHAO, Y. & LUNETTA, R. S. 2012. Comparison of support vector machine, neural network, and CART algorithms for the land-cover classification using limited training data points. *ISPRS Journal of Photogrammetry and Remote Sensing,* 70**,** 78-87.

SHRESTHA, D. P. 2011. Factors controlling land degradation. ITC, Enschede, Netherlands.

SINGH, A. 1989. Review Article Digital change detection techniques using remotely-sensed data. *International Journal of Remote Sensing,* 10**,** 989-1003.

SONG, C., WOODCOCK, C. E., SETO, K. C., LENNEY, M. P. & MACOMBER, S. A. 2001. Classification and Change Detection Using Landsat TM Data: When and How to Correct Atmospheric Effects? *Remote Sensing of Environment,* 75**,** 230-244.

SPREP. 2012. *PEIN Country Profile and Virtual Environment Library* [Online]. Samoa Available: http://www.sprep.org/New-Caledonia/new-caledonia-pein [Accessed August 14th 2012].

SRIVASTAVA, P. K., HAN, D., RICO-RAMIREZ, M. A., BRAY, M. & ISLAM, T. 2012. Selection of classification techniques for land use/land cover change investigation. *Advances in Space Research,* 50**,** 1250-1265.

STEVENSON, J., DODSON, J. & PROSSER, J. 2001. A late Quaternary record of environmental change and human impact from Plum Swamp, New Caledonia. *Palaeogeography, Palaeoclimatology, Palaeoecology,* 168**,** 97-123.

SZUSTER, B. W., CHEN, Q. & BORGER, M. 2011. A comparison of classification techniques to support land cover and land use analysis in tropical coastal zones. *Applied Geography,* 31**,** 525-532.

TERRY, J. P., KOSTASCHUK, R. A. & WOTLING, G. 2008. Features of tropical cyclone-induced flood peaks on Grande Terre, New Caledonia. *Water and Environment Journal,* 22**,** 177-183.

THÉAU, J. 2012. Change Detection. *In:* KRESSE, W. & DANKO, D. M. (eds.) *Springer Handbook of Geographic Information.* Springer Berlin Heidelberg.

THIAM, A. K. 2003. The causes and spatial pattern of land degradation risk in southern Mauritania using multitemporal AVHRR-NDVI imagery and field data. *Land Degradation & Development,* 14**,** 133-142.

TOVAR, C., SEIJMONSBERGEN, A. C. & DUIVENVOORDEN, J. F. 2013. Monitoring land use and land cover change in mountain regions: An example in the Jalca grasslands of the Peruvian Andes. *Landscape and Urban Planning,* 112**,** 40-49.

TOWNSEND, P. A., HELMERS, D. P., KINGDON, C. C., MCNEIL, B. E., DE BEURS, K. M. & ESHLEMAN, K. N. 2009. Changes in the extent of surface mining and reclamation in the Central Appalachians detected using a 1976–2006 Landsat time series. *Remote Sensing of Environment,* 113**,** 62-72.

TOY, T. J., FOSTER, G. R. & RENARD, K. G. 2002. *Soil Erosion: Process, Prediction, Measurement, and Control,* Hoboken, NJ, John Wiley & Sons.

TRANAP, H. 2004. *Cartographie des zones dégradées par l'ancienne exploitation minière en Nouvelle-Calédonie.* Diplôme d'Étude Universitaire Scientifique et Technique, Université de la Nouvelle-Calédonie.

UNITED NATIONS. 2003. *Mining activities in New Caledonia* [Online]. Available: http://www.unescap.org/drpad/vc/conference/bg_nc_147_man.htm [Accessed August 14th 2012].

UNIVERSITÉ DE LA NOUVELLE-CALÉDONIE 2010. Le réseau d'observation « Fonctionnement des petits bassins versants miniers » - Programme CNRT 2010 - 2014. Nouméa, New Caledonia.

UNIVERSITÉ DE LA NOUVELLE-CALÉDONIE 2012a. Le réseau d'observation « Fonctionnement des petits bassins versants miniers » - Programme CNRT 2010 - 2014.

UNIVERSITÉ DE LA NOUVELLE-CALÉDONIE. 2012b. *Projet CNRT "Fonctionnement des petits bassins versants miniers"* [Online]. Available: http://portail-scientifique.univ-nc.nc/index.php?option=com_content&view=article&catid=74&id=145&Itemid=31&lang=fr [Accessed August 25th 2012].

VAN LIER, O. R., LUTHER, J. E., LECKIE, D. G. & BOWERS, W. W. 2011. Development of large-area land cover and forest change indicators using multi-sensor Landsat imagery: Application to the Humber River Basin, Canada. *International Journal of Applied Earth Observation and Geoinformation,* 13**,** 819-829.

VANELSLANDE, A., LAL, R. & GABRIELS, D. 1987. The erodibility of some Nigerian soils: A comparison of rainfall simulator results with estimates obtained from the Wischmeier nomogram. *Hydrological Processes,* 1**,** 255-265.

VERBYLA, D. L. & BOLES, S. H. 2000. Bias in land cover change estimates due to misregistration. *International Journal of Remote Sensing,* 21**,** 3553-3560.

VRIELING, A. 2006. Satellite remote sensing for water erosion assessment: A review. *CATENA,* 65**,** 2-18.

VRIELING, A., DE JONG, S. M., STERK, G. & RODRIGUES, S. C. 2008. Timing of erosion and satellite data: A multi-resolution approach to soil erosion risk mapping. *International Journal of Applied Earth Observation and Geoinformation,* 10**,** 267-281.

WANG, G., GERTNER, G., SINGH, V., SHINKAREVA, S., PARYSOW, P. & ANDERSON, A. 2002. Spatial and temporal prediction and uncertainty of soil loss using the revised universal soil loss

equation: a case study of the rainfall–runoff erosivity R factor. *Ecological Modelling,* 153**,** 143-155.
WASIGE, J. E., GROEN, T. A., SMALING, E. & JETTEN, V. 2013. Monitoring basin-scale land cover changes in Kagera Basin of Lake Victoria using ancillary data and remote sensing. *International Journal of Applied Earth Observation and Geoinformation,* 21**,** 32-42.
WEISMILLER, R. A., KRISTOF, S. J., SCHOLZ, D. K., ANUTA, P. E. & MOMEN, S. A. 1977. Change detection in coastal zone environments. *Photogrammetr ic Engineering and Remote Sensing,* 43**,** 1533–1539.
WISCHMEIER, W. H. & SMITH, D. D. 1978. *Predicting rainfall-erosion losses: A guide to conservation planning.* , U.S. Department of Agriculture. Agricultural Handbook No. 537.
XU, Y., ZHOU, Q. & LI, S. 2005. An analysis on spatial–temporal distribution of rainfall erosivity in Guizhou Province. *Bulletin of Soil and Water Conservation,* 4.
YANG, X. & LO, C. P. 2000. Relative radiometric normalization performance for change detection from multi date satellite images. *Photogrammetric Engineering and Remote Sensing,* 66**,** 967-980.
ZANOTTA, D. C. & HAERTEL, V. 2012. Gradual land cover change detection based on multitemporal fraction images. *Pattern Recognition,* 45**,** 2927-2937.
ZHAN, X., DEFRIES, R., TOWNSHEND, J. R. G., DIMICELI, C., HANSEN, M., HUANG, C. & SOHLBERG, R. 2000. The 250 m global land cover change product from the Moderate Resolution Imaging Spectroradiometer of NASA's Earth Observing System. *International Journal of Remote Sensing,* 21**,** 1433-1460.
ZHANG, H., YANG, Q., LI, R., LIU, Q., MOORE, D., HE, P., RITSEMA, C. J. & GEISSEN, V. 2013. Extension of a GIS procedure for calculating the RUSLE equation LS factor. *Computers & Geosciences,* 52**,** 177-188.
ZHONGMING, W., LEES, B. G., FENG, J., WANNING, L. & HAIJING, S. 2010. Stratified vegetation cover index: A new way to assess vegetation impact on soil erosion. *CATENA,* 83**,** 87-93.
ZHOU, P., LUUKKANEN, O., TOKOLA, T. & NIEMINEN, J. 2008. Effect of vegetation cover on soil erosion in a mountainous watershed. *CATENA,* 75**,** 319-325.
ZOMER, R., USTIN, S. & CARPENTER, C. 2001. Land cover change along tropical and subtropical riparian corridors within the Makalu Barun National Park and Conservation Area, Nepal. *Mountain Research and Development,* 21**,** 175-183.

Appendix A: RapidEye images

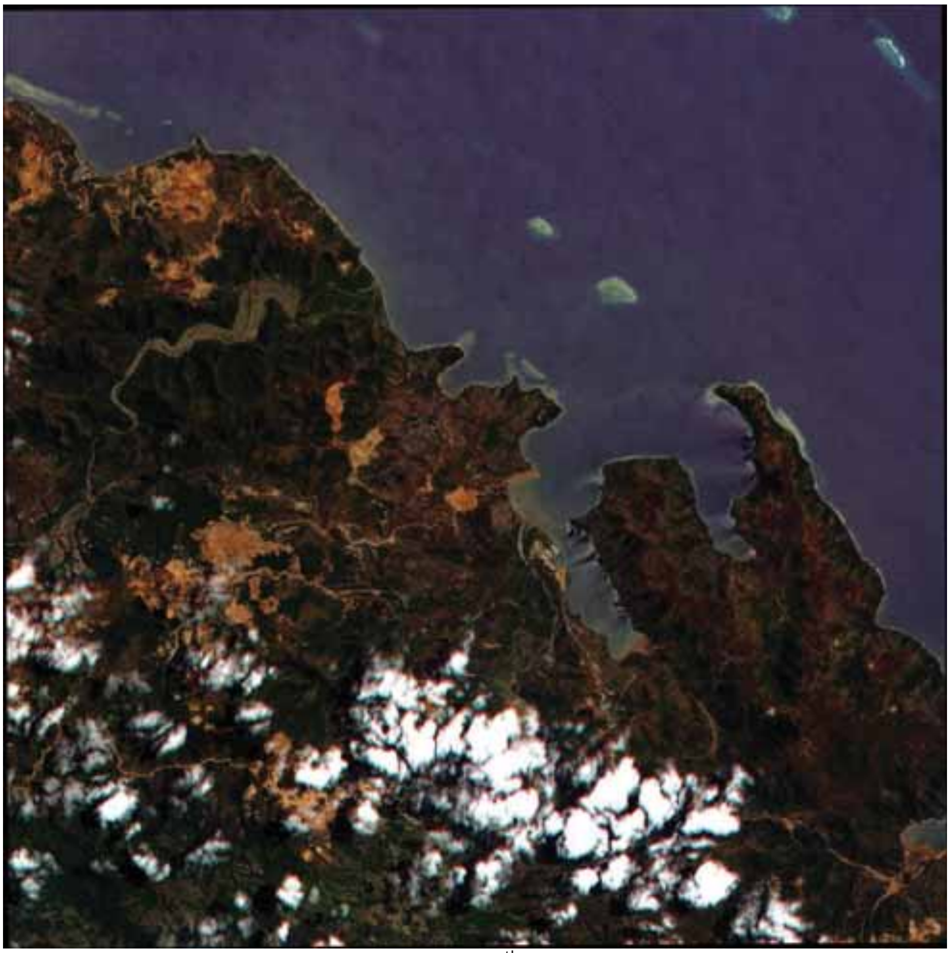

Figure 28: RapidEye image of October 20th, 2011.

Figure 29: RapidEye image of January 18th, 2012.

Appendix B: Aerial photograph

Figure 30: Aerial photograph of the study area Poro

Appendix C: Soil and land cover classes

Figure 31: Bare rock (left) and overburden (right)

Figure 32: Laterite (left) and Peridotite (right)

Figure 33: Ferruginous crust (left) and dense forest (right)

Figure 34: Open forest (left) and dense shrubland (right)

Figure 35: Sparse shrubland (left) and fragmented vegetation (right)

Figure 36: Savannah (left) and built up (right)

Appendix D: Rainfall measurements

Year	2009	2010	2011	2012
No of episodes	8	2	20	10
Precipitation [mm]	736	220	1359.5	449
Runoff depth [mm]	171	36.2	423.4	106.1
Precipitation / runoff [%]	23	16	31	24
Runoff volume [m3]	51984	11004.8	128713.6	32254.4
Sediment flux [t]	43.77	13.08	580.43	31.23
R_{Brown} [$MJ.mm.ha^{-1}.h^{-1}$]	8336	2324	30617	4928

Table 15: Rainfall measurements from the watershed Denise in Poro between the years 2009 to 2012.

Appendix E: Vegetation nomograph

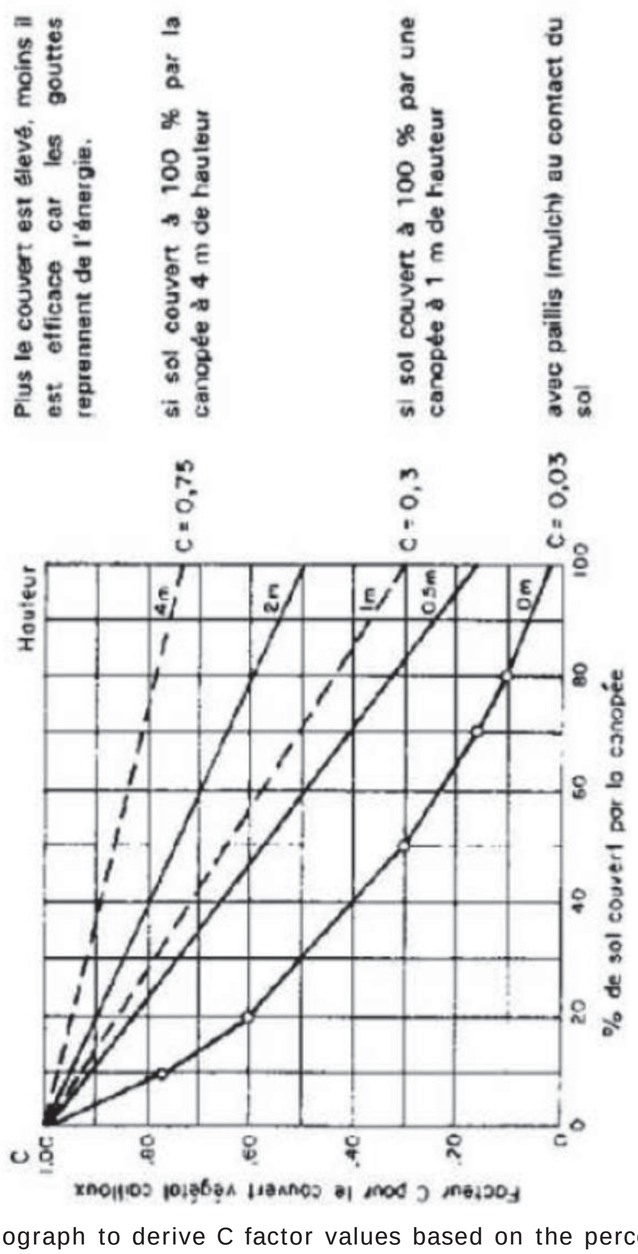

Figure 37: Nomograph to derive C factor values based on the percentage of soil covered by vegetation and vegetation height (according to Roose (1994)).

Appendix F: Land cover statistics for 2011 and 2012

Land-cover classes	Area in 2011		Area in 2012	
	(km²)	(%)	(km²)	(%)
Total	**31.02**	**100**	**27.68**	**100**
Open forest	8.73	28.1	7.56	27.3
Fragmented vegetation	6.83	22	6.28	22.7
Dense shrubland	3.76	12.1	3.65	13.2
Dense forest	3.64	11.7	3.56	12.9
Peridotite	3.27	10.5	3.37	12.2
Sparse shrubland	1.49	4.8	0.3	1.1
Ferruginous crust	1.06	3.4	0.61	2.2
Overburden	0.86	2.8	0.97	3.5
Savannah	0.57	1.8	0.51	1.8
Laterites	0.4	1.3	0.54	2
Dunite	0.26	0.8	0.02	0.1
Water	0.09	0.3	0.1	0.4
Built up	0.05	0.2	0.05	0.2
Bare rock	0.01	0	0.16	0.6

Table 16: Soil and land cover statistics derived from the land cover classifications of the RapidEye images of October 2011 and January 2012.

Appendix G: Confusion matrix

Class	(1)	(2)	(3)	(4)	(5)	(6)	(7)	(8)	(9)	(10)	(11)	(12)	(13)	(14)	
Water (1)	101	0	0	0	0	0	0	0	0	0	0	0	0	0	
Bare rock (2)	2	56	0	0	0	0	0	0	0	0	1	0	0	0	
Dense forest (3)	0	0	123	7	0	0	0	0	0	0	0	0	0	0	
Open forest (4)	2	0	2	141	0	0	0	0	0	0	0	0	0	0	
Dunite (5)	0	0	0	0	27	0	0	0	0	0	0	0	0	0	
Ferruginous crust (6)	14	0	0	0	0	43	0	0	0	0	0	0	0	0	
Laterite (7)	0	0	0	0	0	0	108	0	0	0	0	0	0	0	
Fragmented vegetation (8)	4	0	0	0	0	20	0	33	22	0	0	0	0	0	
Sparse shrubland (9)	11	0	0	0	0	0	0	0	87	0	0	0	0	0	
Dense shrubland (10)	4	0	0	0	0	0	0	0	0	97	0	0	1	0	
Overburden (11)	0	3	0	2	0	0	0	0	0	0	90	0	0	0	
Peridotite (12)	0	2	0	0	0	0	0	0	0	0	1	67	0	0	
Savanah (13)	0	0	0	2	0	0	0	0	0	1	0	0	181	0	
Built up (14)	0	0	0	0	0	0	0	0	0	0	0	0	0	37	
Total	138	61	125	153	27	63	108	33	109	98	91	67	182	37	**1292**
Number correct	101	56	123	141	27	43	108	33	87	97	90	67	181	37	
Accuracy	73%	92%	98%	92%	100%	68%	100%	100%	80%	99%	99%	100%	99%	100%	
Overall accuracy	92.25%														
Average accuracy	92.97%														

Table 17: Confusion matrix of 2011, derived from 5-fold cross validation.

Class	(1)	(2)	(3)	(4)	(5)	(6)	(7)	(8)	(9)	(10)	(11)	(12)	(13)	(14)	
Water (1)	78	0	0	0	0	0	0	1	0	0	0	0	0	0	
Bare rock (2)	0	38	0	0	0	0	0	0	0	0	0	2	0	0	
Dense forest (3)	0	0	133	15	0	0	0	0	0	0	0	0	0	0	
Open forest (4)	1	0	11	128	0	0	0	0	0	0	0	0	0	0	
Dunite (5)	0	0	0	0	25	0	0	0	0	0	0	0	0	0	
Ferruginous crust (6)	0	0	0	0	0	107	0	0	0	0	0	0	0	0	
Laterite (7)	0	0	0	0	0	0	104	0	0	0	0	2	0	0	
Fragmented vegetation (8)	4	0	0	0	0	0	0	18	6	0	0	2	0	0	
Sparse shrubland (9)	1	0	0	0	0	0	0	3	87	0	0	0	0	0	
Dense shrubland (10)	1	0	0	4	0	0	0	0	9	63	0	1	0	0	
Overburden (11)	0	0	0	0	2	0	0	0	0	0	89	4	0	0	
Peridotite (12)	0	0	0	0	0	0	0	3	0	0	0	67	0	1	
Savanah (13)	0	0	5	5	0	0	0	0	0	0	0	0	156	1	
Built up (14)	0	0	0	0	0	0	0	0	0	0	0	0	0	34	
Total	87	38	149	153	27	107	104	25	102	63	89	83	156	37	**1220**
Number correct	78	38	133	128	25	107	104	18	87	63	89	67	156	34	
Accuracy	90%	100%	89%	84%	93%	100%	100%	72%	85%	100%	100%	81%	100%	92%	
Overall accuracy	93.06%														
Average accuracy	92.53%														

Table 18: Confusion matrix of 2012, derived from 5-fold cross validation

Appendix H: Merged land cover maps

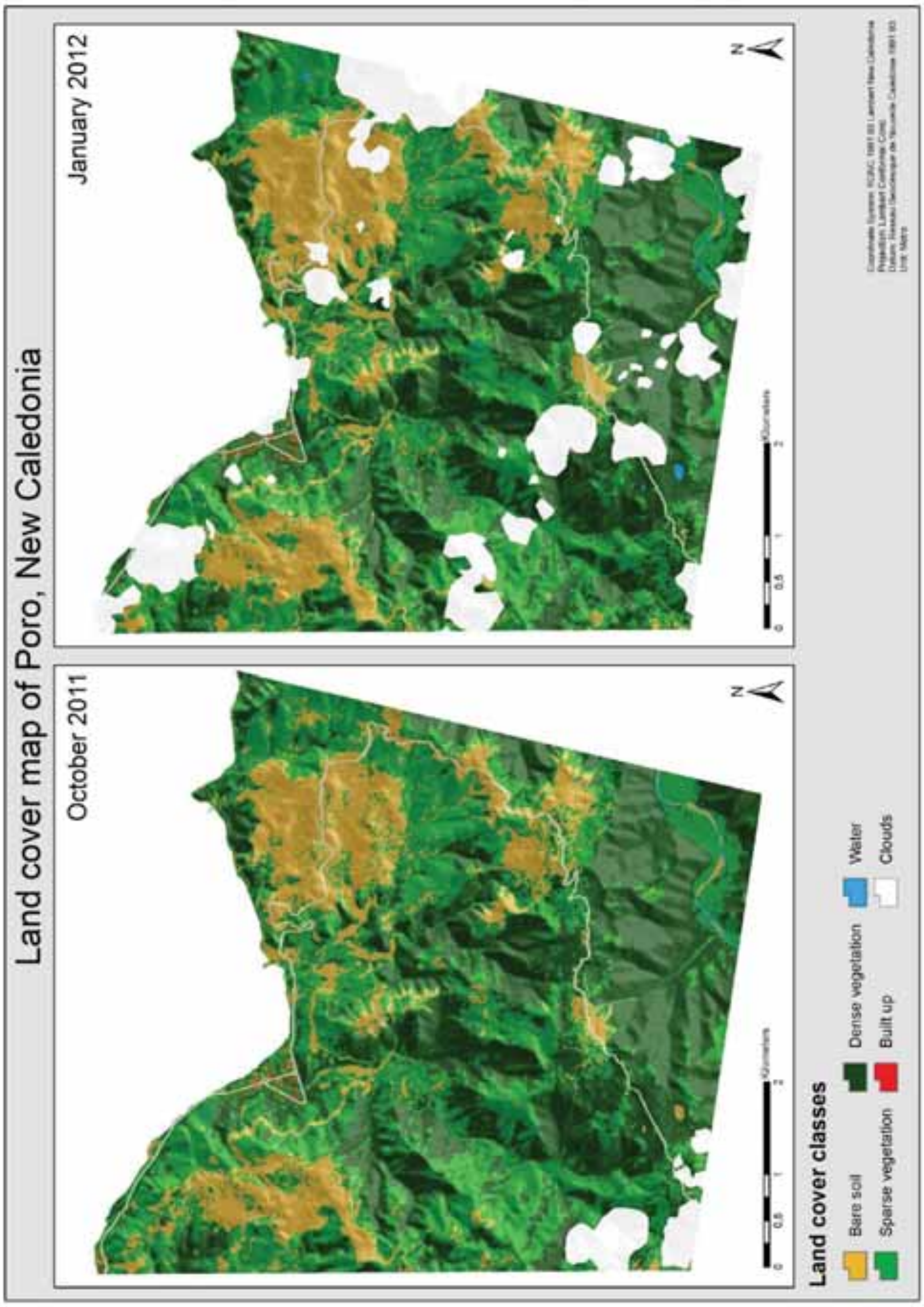

Figure 38: Land cover maps of October 2011 and January 2012 with five classes.

Appendix I: Net changes between 2011 and 2012

Land cover class	Year	Area (km²)	Area (%)	Net change (km²)	Growth (%)
Bare soil	2011	5,30	19,39	0,39	7,36
	2012	5,69	20,82		
Sparse vegetation	2011	10,99	40,20	-0,38	-3,46
	2012	10,61	38,82		
Dense vegetation	2011	10,94	40,01	-0,06	-0,55
	2012	10,88	39,81		
Water	2011	0,07	0,26	0,03	42,86
	2012	0,10	0,37		

Table 19: Distribution, net change and growth for the five land cover classes in 2011 and 2012.

Appendix J: Change detection matrix

Land cover January 2012	Land cover October 2011					
Area (km²)	Bare soil	Sparse vegetation	Dense vegetation	Water	Gain	Total
Bare soil	4,58	1,09	0,01	0,01	1,11	**5,69**
Sparse vegetation	0,65	9,00	0,93	0,03	1,61	**10,61**
Dense vegetation	0,01	0,87	10,00	0,00	0,88	**10,88**
Water	0,05	0,01	0,00	0,03	0,06	**0,09**
Loss	0,71	1,97	0,94	0,04		
Total	**5,29**	**10,97**	**10,94**	**0,07**		

Table 20: Change detection matrix, the initial situation of October 2011 is presented in the column, while the rows display the final situation of January 2012.